# Organic Light-Emitting Devices (OLEDs) and their Optically Detected Magnetic Resonance (ODMR)

by

Gang Li

A dissertation submitted to the graduate faculty in partial fulfillment of the requirements for the degree of DOCTOR OF PHILOSOPHY

Major: Condensed Matter Physics

Program of Study Committee:
Joseph Shinar, Major Professor
John Hill
Vikram Dalal
Kai-Ming Ho
Paul Canfield

Iowa State University

Ames, Iowa

2003

# Graduate College

# Iowa State University

This is to certify that the doctoral dissertation of

Gang Li

has met the dissertation requirements of Iowa State University

Major Professor

For the Major Program

# **Table of Contents**

Chaj	pter	1. Introduction to Organic Light-Emitting Devices (OLEDs)	1
]	[.	General Background	1
)	II.	OLED Device Physics	22
]	III.	Optimization of OLED performance	. 31
]	IV.	Fabrication of OLEDs	38
]	Refe	rences	39
Cha	pter	2. Introduction to Optically Detected Magnetic Resonance (ODMR)	43.
	I.	Background	43
	II.	Spin-dependent Decay Channels in $\pi$ -conjugated Materials	45
	III.	The Spin ½ Polaron Resonance	48
	IV.	The Spin 1 Triplet Resonance	51
	V.	Frequency resolved ODMR (FR-ODMR)	56
	VI.	Description of ODMR Experimental Apparatus	58
	VII.	Description of Dissertation Organization	62
		erences	62
Chapter 3. Magnetic Resonance Studies of Tris-(8-hydroxyquinoline)			64
Alu	Aluminum -Based Organic Light-Emitting Devices  Abstract		64
	I.	Introduction	65
	II.	Experimental Methods	67
	III.	Results	68
	IV.	Discussion	70
	V.	Summary and Concluding Remarks	75
	Acl	cnowledgements	76
		Perences	76

Fig	ures	80
Chapte	r 4. Electroluminescence (EL)-Detected Magnetic Resonance Studies of	
Pt octa	ethyl porphyrin (PtOEP)-based Phosphorescent Organic Light-Emitting	
Devices		
Ab	stract	89
I.	Introduction	90
II.	Experimental Procedure	92
III.	Results and Discussion	93
IV.	Summary and Conclusions	103
Ac	knowledgements	104
Re	Ferences	104
Fig	ures	109
Chapte	er 5. A Combinatorial Study of Exciplex Formation at Organic/Organic	
Interfaces in Organic Light-Emitting Devices		
Ab	stract	116
I.	Introduction	117
II.	Experimental Procedure	118
III.	Results and Discussion	120
IV.	Summary and Conclusions	124
Ac	knowledgements	124
Re	ferences	124
Fig	gures	127
Chapter 6. General Conclusions		
I.	General Discussion	132
· II	Recommendation for Future Research	134
Acknowledgements		

# Chapter 1. Introduction to Organic Light-Emitting Devices (OLEDs)

#### I. General Background

Organic Light-Emitting Devices (OLEDs), both small molecular and polymeric have been studied extensively since the first efficient small molecule OLED was reported by Tang and VanSlyke in 1987 <sup>1</sup>. Burroughes' report on conjugated polymer-based OLEDs <sup>2</sup> led to another track in OLED development. These developments have resulted in full color, highly efficient (up to ~20% external efficiency 60 lm/W power efficiency<sup>3</sup> for green emitters), and highly bright (>140 000 Cd/m<sup>2</sup> DC <sup>4</sup>, ~2000 000 Cd/m<sup>2</sup> AC <sup>5</sup>), stable (> 40 000 hr at 5 mA/cm<sup>2</sup>) devices <sup>6</sup>. OLEDs are Lambertian emitters, which intrinsically eliminates the view angle problem of liquid crystal displays (LCDs). Thus OLEDs are beginning to compete with the current dominant LCDs in information display. Numerous companies are now active in this field, including large companies such as Pioneer, Toyota, Estman Kodak, Philipps, DuPont, Samsung, Sony, Toshiba, and Osram, and small companies like Cambridge Display Technology (CDT), Universal Display Corporation (UDC), and eMagin. The first small molecular display for vehicular stereos was introduced in 1998, <sup>7</sup> and polymer OLED displays have begun to appear in commercial products.

Although displays are the major application for OLEDs at present, they are also candidates for next generation solid-state lighting. In this case the light source needs to be white in most cases. Organic transistors, organic solar cells, etc. are also being developed vigorously.

#### 1. Historical Background

The first electroluminescence (EL) from organic solids was reported in 1963 by Pope and coworkers <sup>9</sup>. The material used was single crystal anthracene. Following studies on anthracene OLEDs using powdered graphite electrodes yielded high quantum efficiency devices <sup>10</sup> (external quantum efficiency ~ 4-6%). These achievements did not stimulate interest in industry due to the high driving voltage of the devices (~100 V), which was due to the ~ 100 µm thickness of the anthracene crystals.

On the other hand, Vincett <sup>11</sup> used vacuum sublimation to deposit amorphous thin films of anthracene. The voltage dropped, demonstrating that vacuum sublimation is a viable method of producing small molecular organic EL devices, since it yields uniform thin films deposited over a large area. However, in the early single layer devices, the recombination zone was close to the injection contact and the external quantum efficiency was less than 0.1%.

The breakthrough was achieved by Tang and Van Slyke in 1987,<sup>1</sup> who described a double-layered hetero-structure EL device with good efficiency (external ~1%) and low operation voltage (~10 V). This breakthrough showed the potential of organic materials as an efficient emissive technology applicable to displays and stimulated the worldwide extensive studies on OLEDs.

Following the success in fabricating small molecular OLEDs, in 1990, Friend and coworkers <sup>2</sup> described the first polymer LED, in which the luminescent poly-(para-phenlene vinylene) (PPV) was fabricated by spin-casting a precursor polymer onto indium tin oxide (ITO)-coated glass and then thermally converted to PPV. Unlike molecular film, where there is only a weak Van der Waals attraction between molecules, the polymer chain is held

together by strong covalent bonds. Also, in polymer film, the chains are typically entangled, which further increases the mechanical strength of the film. The molecular weight of polymer is too large to be thermally evaporated, thus the standard deposition method is spin casting, for which high vacuum is not needed as in small molecular OLED fabrication.

Progress in OLED technology has been very rapid. Figure 1.1 <sup>12</sup> shows the progress of inorganic and OLEDs over time. As clearly seen, the pace of OLED improvement has been very impressive.

OLEDs have some very attractive advantages in large area displays. Emissive like the phosphorescent screen of a cathode-ray-tube (CRT) but thinner than an LCD, it has the potential of creating a whole new breed of portable displays. Because it is emissive, OLED provides full angle viewing. The efficiency of OLEDs is now also high. Current commercial product including multi-color passive matrix displays for car stereo panels, available from Pioneer Corp. <sup>7</sup>, and an alphanumeric cellular phone with blue-green OLED display from Motorola. Full color passive and active matrix high resolution OLED-based displays are being developed intensively and prototypes include Kodak and Sanyo's 15-inch full-color active matrix display <sup>13</sup> (Figure 1.2). OLED are also promising for flexible displays, but they require flexible coatings which will product the devices from oxygen and water. <sup>14</sup>

# 2. Inorganic vs. Organic Semiconductors

Inorganic semiconductors are generally characterized by the strong covalent bonding between the atoms in the lattice. For facile charge transport, a strong exchange interaction between overlapping atomic orbitals in a close-packed structure is required. The mobility of carriers is high in inorganic semiconductors (~1000 cm²/V-s). Due to the band-like nature of

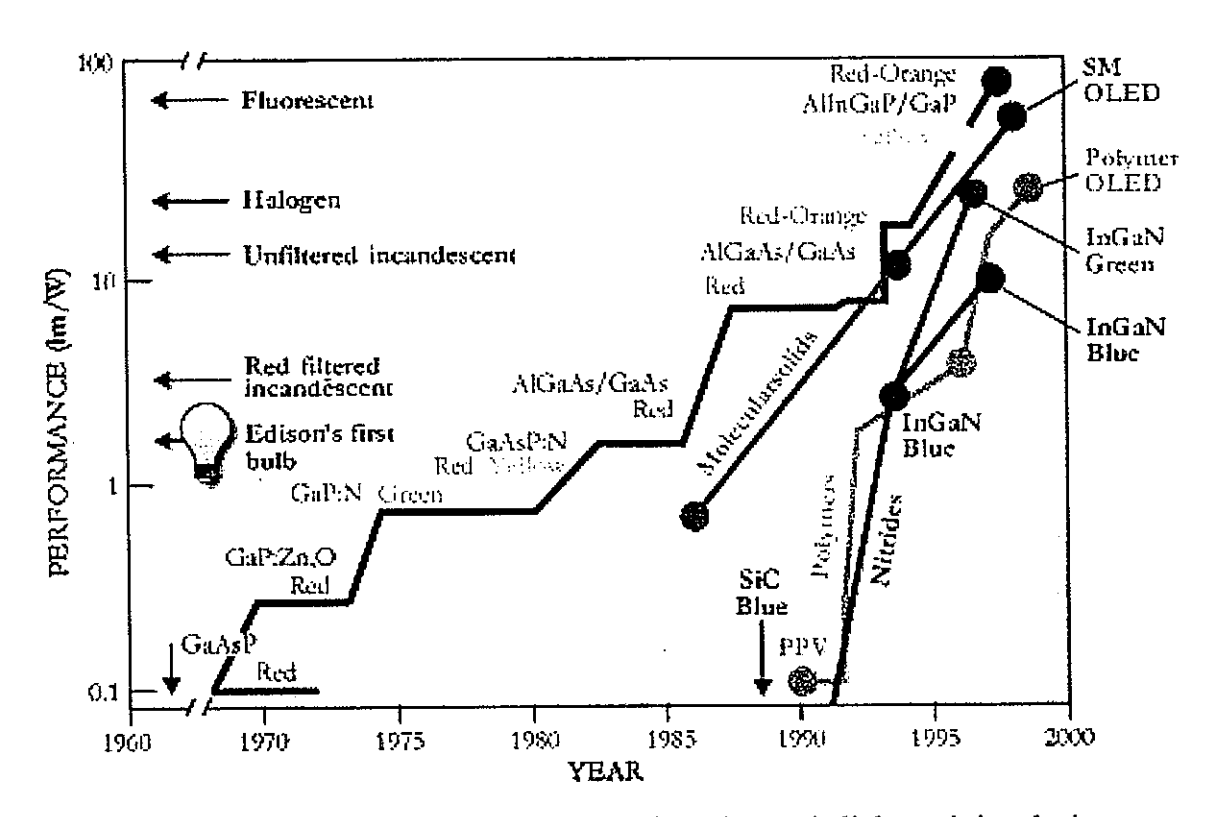


Figure 1.1. Comparison of progresses in inorganic and organic light-emitting devices

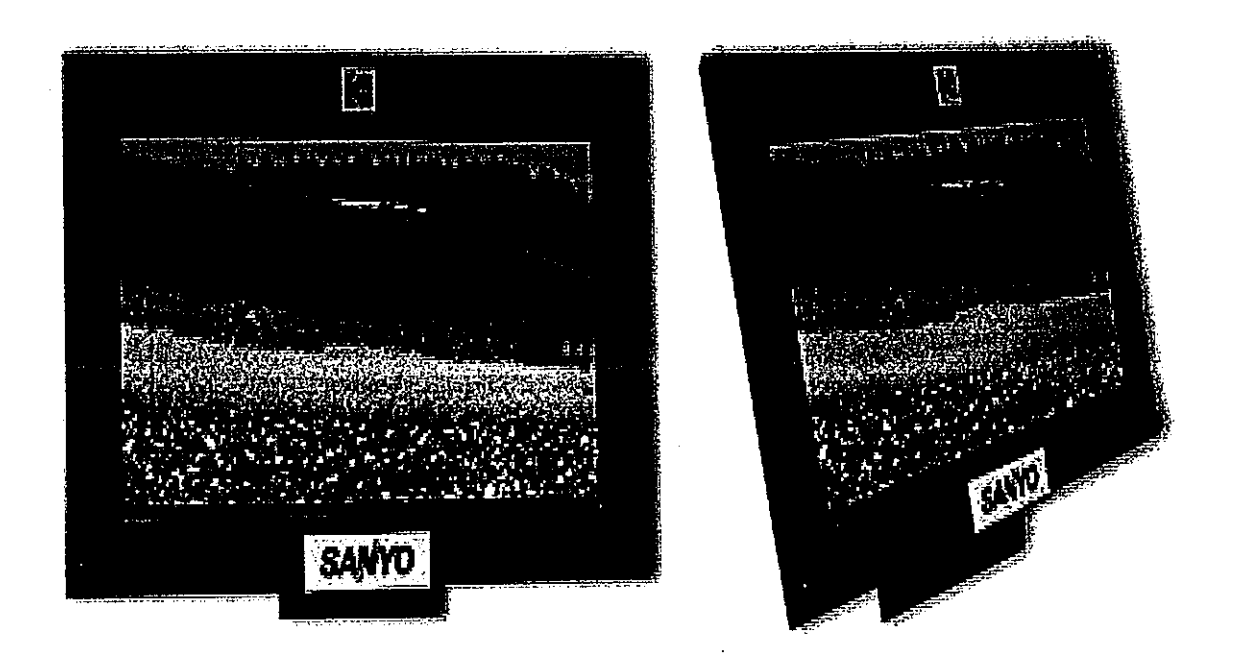


Figure 1.2. Kodak-Sanyo 15" Active-Matrix OLED display

their electronic structure and the recombination of electrons and holes may result in interband emission of light. Dielectric charge screening is more efficient in inorganic semiconductors, where typically  $\epsilon_r \sim 10$ . In turn, polarization energies are small and the resulting electron-hole binding energies are small, 4.9 meV in GaAs. Hence the bound electron-hole pairs, called Mott-Wannier excitons thermally dissociate at temperatures well below room temperature, where kT = 25 m eV.

Organic semiconductors are molecular semiconductors, which are characteristically wide gap, with low carrier mobility and low melting point. Most organic semiconductors should really be designated as insulators. They are called semiconductors because their dark electric conductivity increases exponentially with temperature and some other properties are similar to those of inorganic semiconductors. Semi-conducting or conducting properties in organic materials usually derive from the presence of extended  $\pi$  orbitals formed by overlapping  $p_z$ orbitals. Thus the term  $\pi$ -conjugated material is often used. The intermolecular separation is large in organic materials so that the molecular energy levels are relatively less disturbed. Organic materials are characterized by charge localization to a single molecule, their dielectric constant is low ( $\epsilon_r$ ~3), and polarization energies are as large as 1 eV. The binding energy of excitons is large (~1 eV), and hence the excitons are localized Frenkel excitons. Because the mean free path of the carriers is of the order of the intermolecular distance, the conduction and valence bands are not well defined. The transport properties of thin organic films are dominated by carrier hopping from site to site in the disordered organic film. The carrier mobility is much lower in organic materials, typically  $10^{-6}-10^{-4}~\mathrm{cm^2/V-s}$ .

Light emission from organic semiconductors is due to exciton decay. If the spins of the recombining carriers are uncorrelated, then simple spin statistics mandate that of the resulting

excitons, 75% will be triplet excitons (TEs) and 25% will be singlet excitons (SEs). In inorganic semiconductors, since the exciton binding energy is small, the exciton is relatively delocalized, the exchange interaction between the electro and the hole is small, and the singlet and triplet wavefunctions are almost identical. In fluorescent organic semiconductors, only the SEs radiate, hence the upper limit of the internal quantum efficiency is 25% in fluorescent OLEDs, while it is 100% for inorganic semiconductors. Fortunately, phosphorescence, i.e., the radiative decay of TEs, can also be achieved to get nearly 100% internal efficiency in OLEDs.

The optical energy gaps of organic semiconductors are ~1.5 to 3.5 eV, thus their emission spectra span the visible region. Because the interaction between organic molecules is the weak Van der Waals interactions rather than strong covalent bonding, no strong chemical bonds need to be broken at the interfaces or surfaces of molecular materials, and there need not be any surface or impurity states within the semiconductor gap. Hence, from a device point of view, the interface requirements are greatly relaxed and relatively simple fabrication techniques can be used very successfully to fabricate multilayer device structures. This renders organic semiconductor device fabrication much easier and cheaper than inorganic. In particular, large-area, or bulk fabrication of organic semiconductor devices is feasible, in contrast to the difficulties encountered in crystalline inorganic semiconductor technology.

High mechanical flexibility of organic thin films allows for compatibility with a large number of substrates, including flexible substrates. Due to the strong covalent or ionic bonds between atoms, the growth of crystalline inorganic thin films requires a close lattice match to the underlying substrate. This limits the combination s of inorganic materials. The intermolecular Van der Waals interaction enables growth of crystalline organic solids with

substantial lattice mismatch, which results in a large number of organic hetero-interfaces being possible.

Unlike inorganic semiconductor devices, which use crystalline structure, the thin organic layers of OLEDs are typically amorphous. The amorphous structure leads to a reduction in quenching of the radiative decays from internal conversion processes present in strongly coupled, crystalline organic systems, since many phonon modes are associated with the crystal lattice. Consequently the radiative recombination efficiency of Frenkel excitons increases.

Organic materials also have unique optical and electrical properties. For example, they normally have large Franck-Condon shift, which makes them transparent to their own emission. This largely eliminates self-absorption in OLEDs and has enabled the development of transparent OLEDs.

# 3. Molecular structure and electronic processes in organic materials

# (1). $\pi$ -conjugated materials

Chemically, organic semiconductors are  $\pi$ -conjugated materials, i.e., materials in which single and double (in most cases) or single and triple bonds alternate throughout the molecule or polymer backbone.

Carbon-carbon double bonds are formed in a process called  $sp^2$  hybridization. In this hybridization, the s orbital combines with only two of the three p orbitals. Three  $sp^2$  hybrid orbitals result, and one p orbital remains unchanged. The three  $sp^2$  orbitals lie in a plane at an angle of  $120^\circ$  to each other, with the remaining p orbital perpendicular to the  $sp^2$  plane. (See Figure 1.3a)

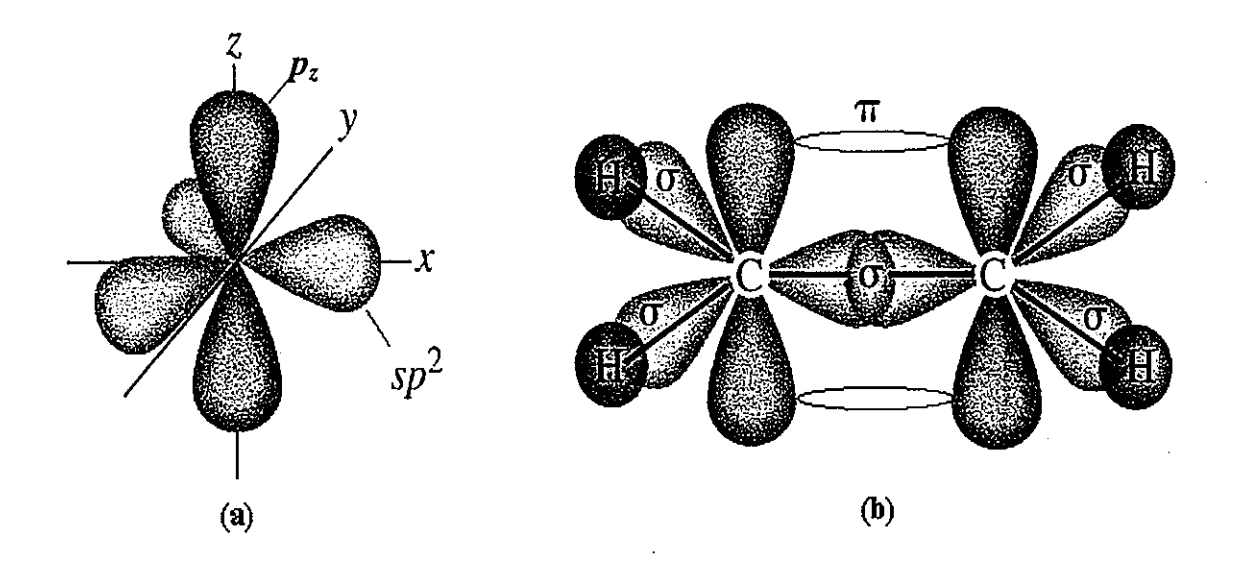


Figure 1.3. (a).  $sp^2 + p_z$  orbitals (b) Orbitals in ethylene (C<sub>2</sub>H<sub>4</sub>).

When two  $sp^2$ -hybridized carbons approach each other, they form a  $\sigma$  bond by  $sp^2$ - $sp^2$  overlap. At the same time, the un-hybridized p orbitals approach with the correct geometry for sideways overlap, leading to the formation of  $\pi$  bond (Figure I-3 (a)). The  $\pi$  bond has regions of electron density on either side of a line between nuclei but has no electron density directly between nuclei. The C=C double bond in ethylene is both shorter and stronger than the single bond in ethane because it results to the sharing of four electrons rather than two. Ethylene (C<sub>2</sub>H<sub>4</sub>, Figure 1.3 (b)) has a C=C bond length of 133 pm and a strength of 611kJ/mol. C=C bond is considerably less than twice as strong as a single bond because the overlap in the  $\pi$  part is not as effective as the overlap in the  $\sigma$  part.

Figure 1.4 shows the six  $\pi$  molecular orbitals of benzene, which virtually exists in all organic materials of interesting. The carbon atom in the benzene molecule has three sp<sup>2</sup>

orbitals with the inter-bond angle of  $120^{\circ}$  on the same molecular plane for sigma-bond formation and a  $2p_z$  orbital perpendicular to the molecular plane. In the ground state ( $\psi_1$ , bonding), the lone  $2p_z$  orbitals overlap to form a  $\pi$ -orbital and the electron charge density in the  $\pi$ -orbitals is symmetrically distributed to form two streamer-type layers stretching around the ring. Therefore, the number of nodal planes in which the  $\pi$ -electron density is zero, is zero. The  $\sigma$ -orbitals are symmetrical around the bond axis giving localized C-C and C-H bonds.

The electrons occupying the  $\sigma$ -orbitals are localized, and concentrated mainly along the

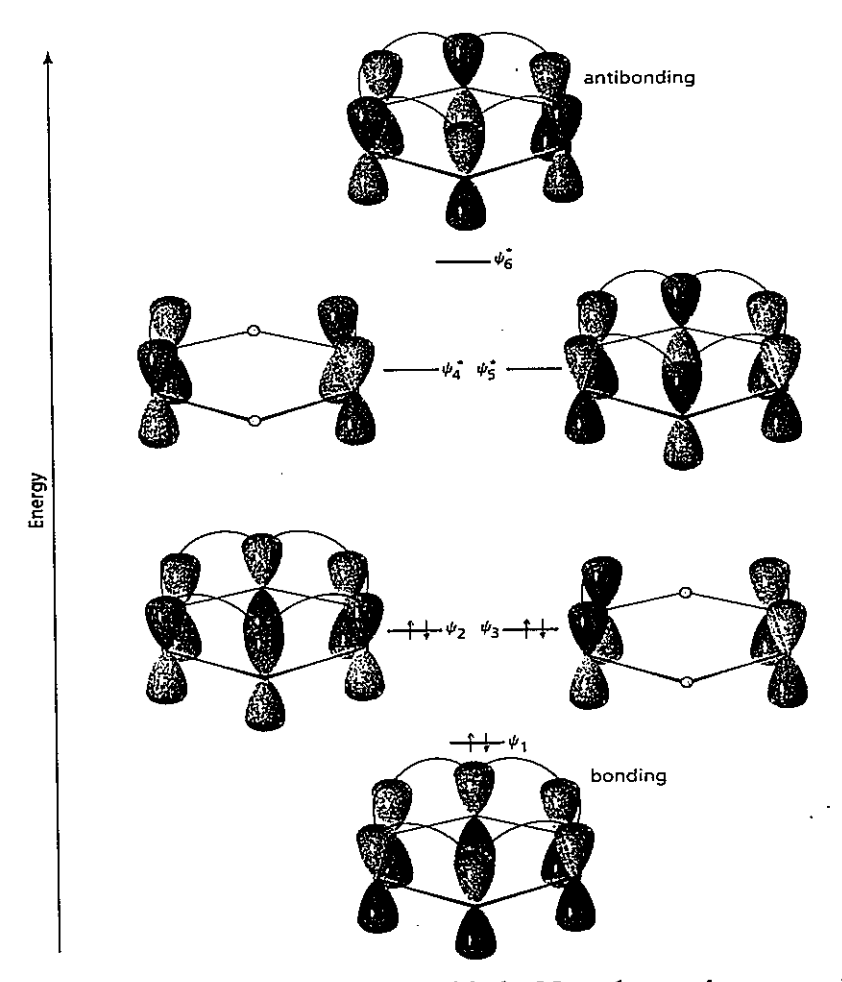


Figure 1.4. The six benzene  $\pi$  molecular orbitals. Note that as the energy increases, the number of nodal plane increase from 0 in bonding case to 3 in antibonding case.

line joining the two nuclei and are localized. But the electrons occupying the  $\pi$ -orbitals are delocalized over all the atoms so they can move freely inside the molecule. Through such mobile  $\pi$ -electrons, charges can easily propagate from one part of the molecule to another. These  $\pi$ -electrons are consequently responsible for the semiconducting properties of  $\pi$ -conjugated materials.

In any organic molecule, the number of molecular orbitals (MOs) is the sum of the number of atomic orbitals. If a MO has lower energy than the starting atomic orbitals, it is called bonding; if it is higher, it is called antibonding.

In the important case of benzene, there are six  $\pi$ -MO's. In Figure 1.4, if the adjacent porbitals are of the same color, they form bonding orbitals; otherwise, they form antibonding orbital, and there is a node in between with  $\pi$ -electron density being zero. The lowest-energy  $\pi$  MO has no node between nuclei and is bonding. The  $\pi$  MO of the next lowest energy,  $\psi_2$ . and  $\psi_3$ , has two nodes (one nodal palne) between nuclei and is also bonding. Above $\psi_2$ , and  $\psi$ <sub>3</sub> are two antibonding  $\pi$  MOs,  $\psi_4^*$  and  $\psi_5^*$ , each has four nodes (two nodal planes) between nuclei. The highest-energy MO,  $\psi_6^*$  has six nodes (three nodal planes) and is also antibonding,  $\psi_2$  and  $\psi_3$ , and  $\psi_4^*$  and  $\psi_5^*$ , are degenerate. In the ground state, the six p electrons of benzene occupy the three bonding  $\pi$ -orbitals and are delocalized over the entire conjugated system, leading to the observed 150 kJ/mol stabilization of benzene. $\psi_2$  and  $\psi_3$  are called the highest occupied molecular orbitals (HOMOs) and  $\psi_4^*$ ,  $\psi_5^*$  are called the lowest unoccupied molecular orbitals (LUMOs). The HOMO corresponds to the top of the valence band in inorganic semiconductors and the LUMO corresponds to the bottom of the conduction band. Both are very important in the study of organic semiconductors and OLEDs.

And similar to amorphous inorganic semiconductors, the amorphous nature of the organic layers in OLEDs results in highly localized electronic states with a random but relatively broad density-of-states (DOS) distribution of energy. The primary contribution to the energy disorder is the interaction of the charge with all of the dipoles in the surrounding medium. In the amorphous structure, each molecule is randomly oriented, and experiences a different environment. Thus the intermolecular orbital overlap varies, which affects the transport behavior. In polymers, topological defects, either intrinsic (e.g. kinks, torsional conformations, cross-link with neighboring chains, etc.) or external (e.g., H, O, Cl, or F atoms) can interrupt the conjugation in the otherwise long polymer chain. Thus conjugated polymers are actually an assembly of conjugated segments with random length, which is the major source of energetic disorder. In molecular glasses, estimates of the energy disorder have been made by charge mobility measurements, which shows they are in the range of ~0.1 eV, comparable to the bandwidth.

## (2) Excitations in $\pi$ -conjugated materials

One of the first theoretical work on excitations of  $\pi$ -conjugated materials was by Su, Schrieffer and Heeger (SSH) <sup>17</sup> on the simplest conjugated polymer possible – transpolyacetylene with a degenerate ground state since the infinite chain of it has two equivalent structures with the same energy. They found that the bond alternation defect is not localized at a single carbon site, but is spread over some 10 to 15 carbon sites. The soliton was invoked as the fundamental excitation in this long chain polymer, and the delocalization is crucial to the energetics of the stabilization of the soliton. In the SSH model, the soliton has associated with it an energy level that lies at mid-gap and is of nonbonding  $p_z$  character.

In polymers with a nondegenerate ground state, such as PPV, the two alternative senses of bond alternation do not have the same energy. Then the soliton is not a stable excitation <sup>18</sup> since the high-energy form can only exist over a finite length of the chain. The charged excitations are now termed polarons or bipolarons and represent localized charges with an accompanying local distortion. Polarons and bipolarons may be considered as equivalent to a confined soliton pair and the two nonbonding mid-gap soliton states form bonding and nonbonding combinations, and produce two gap states symmetrically displaced about mid-gap. These levels can be occupied by 0, 1, 2, 3, and 4 electrons, giving a positive bipolaron

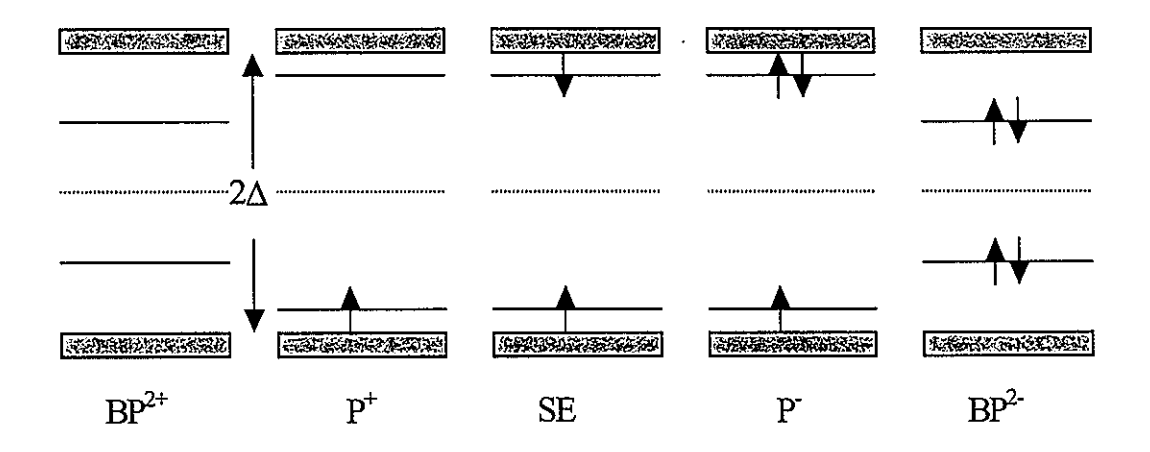


Figure 1.5. Polaron, bipolaron, and singlet exciton (SE) energy levels in a nondegenerate ground state polymer with energy gap  $2\Delta$ . The soliton energy level is in the middle of the gap.

(BP<sup>2+</sup>), positive polaron (P<sup>+</sup>), polaron exciton, negative polaron (P<sup>-</sup>) and negative bipolaron (BP<sup>2-</sup>), respectively. A schematic figure of these excitations is shown in Figure 1.5.

Like an electron, a polaron is a spin 1/2 species; bipolarons are spinless. A bipolron has a greater degree of relaxation than a polaron and this stabilizes the coalescence of two like-

charged polarons to form a bipolaron.

Physically, polaron formation is driven by the electron-phonon interaction, which is particularly effective in organic materials since they have both strongly coupled intramoleclular phonons and many low energy intermolecular modes. At low temperature, the phonons dress the mobile electrons and holes forming large polarons and leading to an increase in their effective mass. As T increases, the phonon interaction leads to narrowing of the electron bandwidth, and to the formation of a small polaron, i.e., the electron is localized on a single molecule, which is distorted to accommodate the extra charge. The transition from large to small polaron was found to be well below room temperature even in crystalline compounds with favorable molecular arrangement.<sup>19</sup>

Exciton dynamics are of primary importance in light emitting materials and OLEDs. An exciton is a bound electron-hole pair. If the pair is localized on one molecular unit and typically has a large binding energy (~1 eV), it is a Frenkel exciton. If it extends over many molecular units and typically has a low binding energy (a few meV), it is a Mott-Wannier exciton. The intermediate case, where the exciton extends over a few adjacent molecular units, is called a charge-transfer exciton (CTE).

In inorganic semiconductors the carriers have low effective masses and the materials have a relatively high relative permittivity, so the excitons are usually Mott-Wannier. In organic semiconductors, the carriers have high effective masses, and the permittivity of the materials is relatively low so the excitons are Frenkel excitons.

Due to the large exciton binding energy, the electron-electron exchange interaction must be considered for Frenkel excitons. The result is that SEs and TEs are of different energy, with the SE energy typically 0.4-1.1 eV higher. The TE is considerably more localized than

SE. Calculation by Shuai et al.<sup>20</sup> and Beljonne et al.<sup>21</sup> verifies that the TE in PPV is stabilized by 0.65 eV compared to the SE.

If an exciton extends over two or more identical molecular units, it forms an excimer. An exciplex is formed if the exciton extends over two or more different molecular units.

The systems studied in organic semiconductors normally have significant electronphonon interaction. Thus the exciton is called polaronic exciton and its transportation is more appropriately described by hopping between sites.

## (3) Electronic processes in organic semiconductors

In principle, all the macroscopic properties of a system can be deduced once the wavefunction be obtained by solving the Schrödinger equation. However, in reality, even the simplest molecules are too complex to yield analytical solutions.

The treatment of transitions is generally performed within the framework of the Born-Oppenheimer (BO) approximation, whose use is based on the fact that there is a large disparity between the nuclear and electronic masses. Since the mass of nuclei is much larger than that of the electron, the electrons can be considered to response instantaneously to any change in the configuration of the nuclei. Thus in determining the energy level of molecules, one can fix the nuclear position and solve the electron energies in a static potential.

The B-O approximation results in the Franck-Condon principle in optical transitions. It states that there are no changes in the nuclear coordinates during an electronic transition and the most probable vibronic transitions are vertical, since electronic transitions take place in  $<10^{-15}$  s, as compared with  $10^{-13}$  -  $10^{-12}$  s for nuclear motions. These vertical transitions are also called Franck-Condon transitions.

Following the emission or absorption of a photon, the vibrational state of the molecule relaxes. This leads to a red-shift in the emission spectrum with respect to the absorption spectrum, known as Franck-Condon shift. In organic molecules, the Franck-Condon shift is normally large (up to 1 eV). Consequently, the molecules are transparent to their own emission. As mentioned before, this property can be exploited to make transparent OLED.

In molecular transitions, the electrons of interest are those in the HOMO because they are most likely to participate in electron transfer or optical transitions. We will now consider electronic dipole transitions.

Ignore the rotational wavefunction, the probability of exciting the molecule  $R_{lu}^{\ 2}$  can be expressed as:

$$R_{lu}^{2} \propto \left| \left\langle \psi_{el} \left| \vec{M} \right| \psi_{eu} \right\rangle \right|^{2} \left| \left\langle \chi_{vl} \left| \chi_{vu} \right\rangle \right|^{2} \left| \left\langle \psi_{sl} \left| \psi_{su} \right\rangle \right|^{2}$$

$$(1)$$

The electronic wavefunction is the product of two non-interacting terms:  $\psi_e$  (only depends on the spatial coordinates of the electron), and  $\psi_s$  (only depends on the spin coordinates).  $\chi_v$  is vibrational state wavefunction. l and u denotes the initial and final state for the transition.

The dipole moment operator  $\vec{M}$  appears only in the electronic term because the nuclei cannot respond rapidly enough to optical frequencies and the spin is insensitive to the electric field.

Dipole allowed transitions are those for which the first term in Eq. (1) being nonzero. Since  $\vec{M}$  is a sum of odd operators, this term vanishes unless l and u are of opposite symmetry with respect to the inversion operator. Since the ground-state wavefunction of

most  $\pi$ -conjugated materials is  $IA_g$  state, the dipole allowed transition leads to odd, i.e., u-excited state (1B<sub>u</sub>).

The second term is called Franck-Condon factor. As mentioned before, the electronic transition is vertical. The last term defines spin selection rule. For spin allowed transition, e.g., singlet – singlet, this term is 1. For spin-forbidden transition, i.e., singlet – triplet, it is zero. The actual value of the third term depends on spin-orbital coupling.

In organic semiconductors, excitons are modeled as two-electron systems, with one in a partially filled LUMO and the other in a partially filled HOMO. For a two-electron system, the total spin may be S=0 or S=1.

The S=0 state is singlet state, which is antisymmetric under particle exchange:

$$|S = 0, S_z = 0\rangle = \frac{1}{\sqrt{2}} \left[ \left| \frac{1}{2}, -\frac{1}{2} \right\rangle - \left| -\frac{1}{2}, \frac{1}{2} \right\rangle \right]$$
 (2.1)

The S=1 has three states (triplet states), all symmetric under particle exchange:

$$\begin{vmatrix} S = 1, S_z = 0 \rangle = \frac{1}{\sqrt{2}} \left[ \frac{1}{2}, -\frac{1}{2} \rangle + \left| -\frac{1}{2}, \frac{1}{2} \rangle \right]$$

$$\begin{vmatrix} S = 1, S_z = 1 \rangle = \left| \frac{1}{2}, \frac{1}{2} \rangle \\ \begin{vmatrix} S = 1, S_z = -1 \rangle = \left| -\frac{1}{2}, -\frac{1}{2} \rangle \end{vmatrix}$$

$$(2.2)$$

## Electronic Processes in organic molecules

In most stable molecules, the HOMO is completely filled in the ground state. Thus the ground state wavefunction is spatially symmetric under electron exchange, which determines that the ground state is singlet. So usually only singlet exciton can decay radiatively to ground state.

Figure 1.6 shows the Electronic Processes in molecules in the form of Jabilonski diagram.

Optical absorption of the ground state of an organic molecule normally results in a vibronic excited state, i.e., it includes both an electronic and a vibrational excitation. Then internal conversion where thermal motion of the lattice removes the vibrational excitation

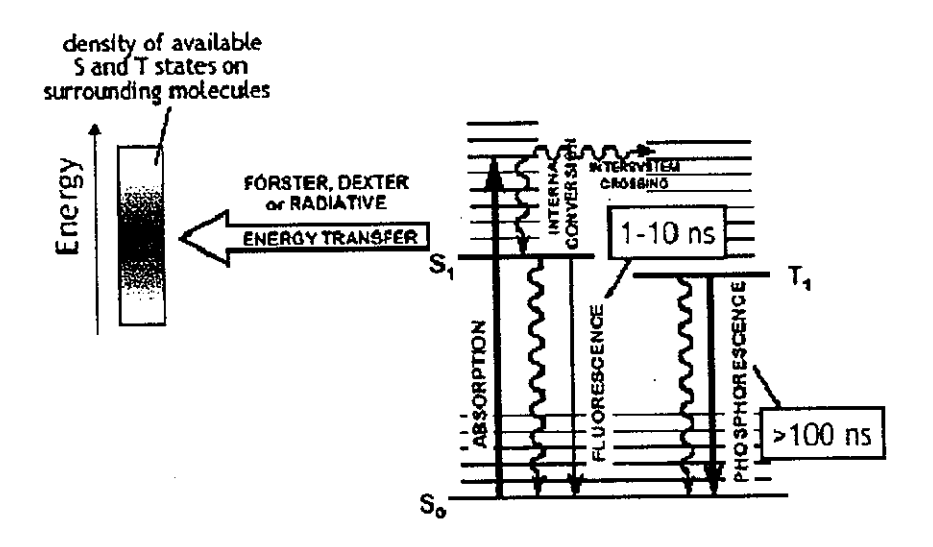


Figure 1.6. Electronic processes in organic molecules. S represent singlet state, and T represents triplet state.

and leads to pure electronic excitation occurs. In general, internal conversion is a non-radiative transition between two states of like multiplicity.

Intersystem crossing (ISC) is a term describing a non-radiative process involving states of different multiplicity. The origin of ISC is an electron-electron interaction that breaks the degeneracy between the singlet and triplet energy levels. It can be shown that the spatial wavefunction which is antisymmetric under exchange of electrons, i.e., the wavefunction of the triplet states, has a lower energy. The ISC rate, from the lowest excited singlet (S<sub>1</sub>) to the

lowest excited triplet  $(T_1)$ , via a highly vibrating level of  $T_1$   $(T_1^*)$ , depends on the spin-orbital coupling.

Fluorescence is the emission which originates from and terminates at the same multiplicity. Since most organic materials' ground state is the singlet state  $S_0$ , fluorescence is the radiative transition from the lowest excited singlet  $S_1$  to  $S_0$ . This process is fast with a time constant which is typically  $\sim 1$  ns.

Phosphorescence is the radiative transition in which the initial and final states differ in the multiplicity. In most cases, it is from the lowest triplet state  $T_1$  to the ground state  $S_0$ . Since it is a spin forbidden transition, the lifetime of this process is relatively long, typically microseconds to milliseconds.

Radiative energy transfer involves the emission of a photon by donor molecule and the subsequent re-absorption of this photon by acceptor molecule. Clearly, it can occur only if the fluorescence spectrum of the donor overlaps the absorption spectrum of the acceptor, and the medium between the two molecules is transparent to the radiation involved.

Förster and Dexter energy transfer are both so-called resonance transfer processes with the necessary conditions being the same as that of a radiative energy transfer. The main difference is that no actual emission or absorption of photons occurs in the process.

The general equation for energy transfer can be expressed as

$$D^* + A \rightarrow D + A^* + h\nu_T \rightarrow D + A + h\nu_A \tag{3}$$

where D is the donor molecule, A is the acceptor molecule, \* means an excited state, and  $h\nu_A$  and  $h\nu_T$  are the optical and thermal energies emitted in the process, respectively. The interaction between D\* and A is expressed by a Hamiltonian H, which could be electrostatic (Coulombic or Förster), or electron exchange (or Dexter).

Fermi 's golden rule expresses the probability of evolution from the initial state  $\Psi_i(D^* + A)$  to the final state  $\Psi_f(D + A^*)$ :

$$P_{da} = 2\pi / \hbar \left| \left\langle \Psi_i \mid H \mid \Psi_f \right\rangle \right|^2 \rho(E) \tag{4}$$

where  $\rho(E)$  is the density of states. We now treat the Förster and Dexter resonant energy transfer processes in some detail.

# 1. Förster energy transfer

This is a dipole-dipole-interaction-facilitated energy transfer. Förster<sup>22</sup> first recognized that if the emission of the donor molecule overlaps with the absorption of the acceptor molecule, then rapid, long-range (<100Å) energy transfer may happen without the emission of a photon.

The dipole-dipole interaction Hamiltonian is

$$H(\vec{R}) = \frac{1}{4\pi\varepsilon_{a}\varepsilon_{a}R^{3}} \left( \vec{\mu}_{d} \bullet \vec{\mu}_{a} - 3\left( \vec{\mu}_{d} \bullet \hat{R}\right) \left( \vec{\mu}_{a} \bullet \hat{R}\right) \right)$$
 (5)

where  $\varepsilon_r$  is the relative dielectric constant,  $\varepsilon_\theta$  is the permittivity of free space,  $\bar{\mu}_d$  and are  $\bar{\mu}_a$  the electric dipole moment operators of the donor and acceptor molecules; and  $\hat{R}$  is the unit vector between the donor and acceptor molecules.

It can be shown that the Förster energy transfer rate can be written as

$$K_{Förster}(R) = \left(\frac{1}{\tau}\right) \left(\frac{R_0}{R}\right)^6 \tag{6}$$

where

$$R_0^6 = \frac{3\hbar^4 c^4}{4\pi\varepsilon_r^2} \frac{\alpha_A}{N_a} \int F_D(E) F_A(E) / E^4 dE \tag{7}$$

 $\tau$  is the observed donor lifetime,  $N_A$  is the number density of acceptor molecules,  $F_D$  is the normalized emission spectrum of the donor,  $F_A$  is the normalized absorption spectrum of the acceptor and  $\alpha_A$  is the total absorption coefficient of the acceptor. Clearly,  $R_0$  is the donor

acceptor distance at which transfer competes equally with the total rate of removal of energy from D by any other means, such as radiative or radiationless decay or hopping away.

Typical values of  $R_0$  range from 30 to 100Å. The energy transfer efficiency can be shown to be

$$\eta_{F\"{o}rster} = \frac{1}{1 + \left(R / R_0\right)^6} \tag{8}$$

Hence, almost all the energy transferred for  $R < R_0$ . Note that 30 - 100 Å corresponds to a minimum acceptor molecule concentration of 0.01% to 0.3%.

#### 2. Dexter energy transfer

Dexter extended the theory of resonance energy transfer to exciton states with electronic dipole-forbidden transitions, i.e. by higher multipole interactions or by electron exchange. In the important case of triplet-triplet energy transfer in which the electron exchange is the dominant interaction, Dexter showed that the transfer rate could be expressed as

$$K_{Dexter}(R) = \frac{2\pi}{\hbar} \left| \beta_{DA}^{2} \right| \int F_{D}(E) F_{A}(E) dE \propto e^{-2R/L}$$
(9)

where  $\beta_{DA}$  is the exchange energy interaction between the molecules, E is the energy,  $F_D(A)$  and  $F_A(E)$  are the normalized phosphorescence spectrum of the donor and the normalized absorption spectrum of the acceptor, respectively, and E is a constant. Due to the electron exchange, the energy transfer is a contact type, and hence it occurs only over a short distance of ~10Å.

In Förster dipole-dipole energy transfer, due to the spin selection role  $\Delta S = 0$ , the spin of both D and A must be conserved. Thus the allowed transitions are:

$${}^{1}D^{*} + {}^{1}A \rightarrow {}^{1}D + {}^{1}A^{*}$$
 (10.1)

$${}^{1}D^{*} + {}^{3}A \rightarrow {}^{1}D + {}^{3}A^{*}$$
 (10.2)

Note that since the ground state of most organic molecules is a singlet state, the second transition is rare. In addition, to the extent that spin-orbit coupling allows electric dipole optical transitions with  $\Delta S \neq 0$  in complex molecules, Förster energy transfer can occur by the dipole-dipole mechanism. Transfer is likely to be slower than for exchange processes where transitions for donor and acceptor are fully allowed. But since the actual radiative lifetimes of the triplet states ( ${}^3D^*$ ) are also long, the long-range energy transfer process may still be important relative to radiative process ( ${}^3D^* \rightarrow {}^1D$ ). This is the Förster triplet-singlet transition

$${}^{3}D^{*} + {}^{1}A \rightarrow {}^{1}D + {}^{1}A^{*}.$$
 (10.3)

Triplet –singlet exchange has in fact been detected by the emission of sensitized delayed fluorescence in rigid glasses of triphenylamine (donor) and chrysoidine (acceptor). This mechanism has also been used to achieve 100% internal quantum efficiency  $\eta_{int}$  for fluorescent dye using efficient phosphor to convert triplets to singlets by pumping the dye.<sup>23</sup>

In electron exchange Dexter transfer, only the total system spin must be conserved, thus the triplet-triplet energy transfer is allowed here:

$${}^{3}D^{*} + {}^{1}A \rightarrow {}^{1}D + {}^{3}A^{*}.$$
 (10.4)

Of course, singlet-singlet is also an allowed Dexter transition. However, since Forster singlet-singlet transfer is much faster and of longer range, Dexter type singlet-singlet transfer is normally negligible compared to Förster type.

Figure 1.7 shows Förster and Dexter type singlet – singlet transfer processes.

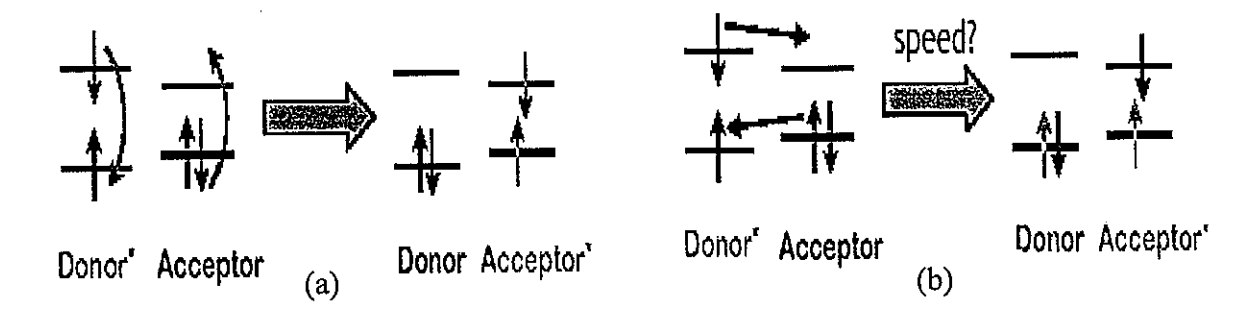


Figure 1.7. (a) Förster and (b) Dexter energy transfer for singlet – singlet energy transfer

## II. OLED Device Physics

In general, the physical processes underlying the operation of OLEDs are: charge injection from the metallic electrodes into the organic layers, charge transport across these layers, electron-hole recombination and exciton emission. Figure 1.8 shows these processes in a single-layer device. In this section, I will discuss these processes briefly.

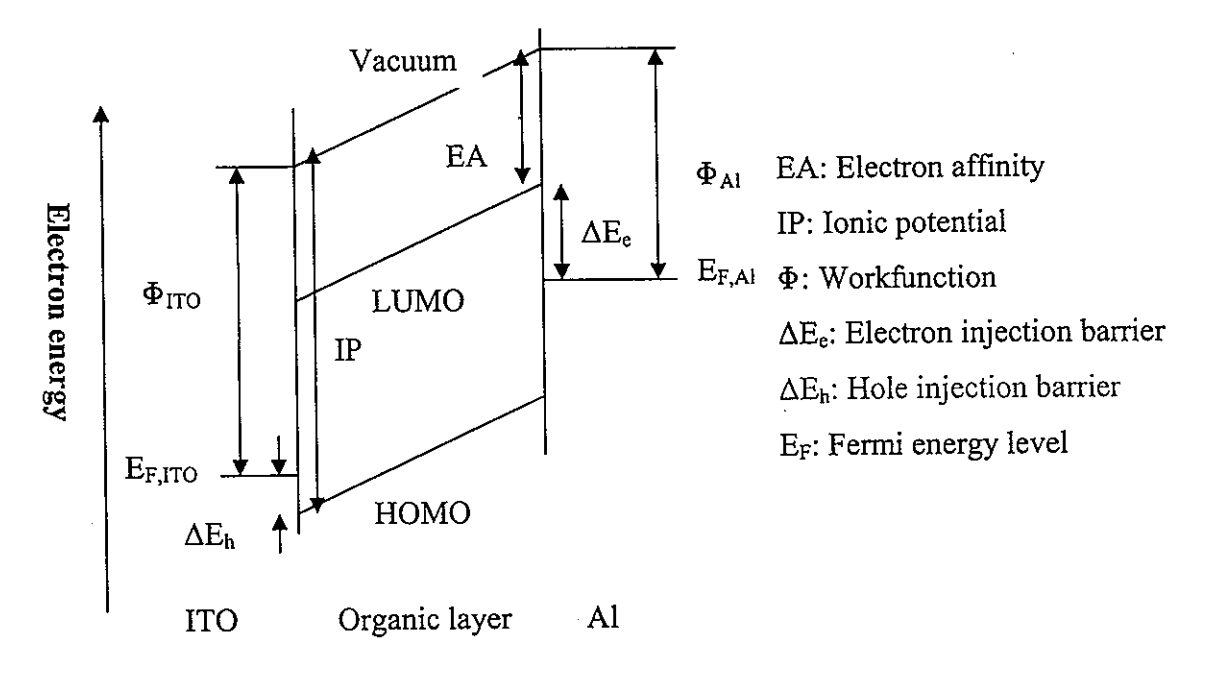


Figure 1.8. Principle of single layer OLED operation

#### 1. Carrier Injection

In organic materials, disorder, low bandwidth, electron-phonon interactions, and temperature all work together to localize charges carriers. Thus the primary injection event consists of a transition from an extended band-like state in the metal electrodes into a localized molecular polaronic state in the organic material. Microscopically, each individual transition can be described as a tunneling event from a thermally excited state in the metal to the HOMO or LUMO of the target molecule.

There are two principle mechanisms for injection of charge carriers in the presence of a barrier: thermionic emission and quantum mechanical tunneling.

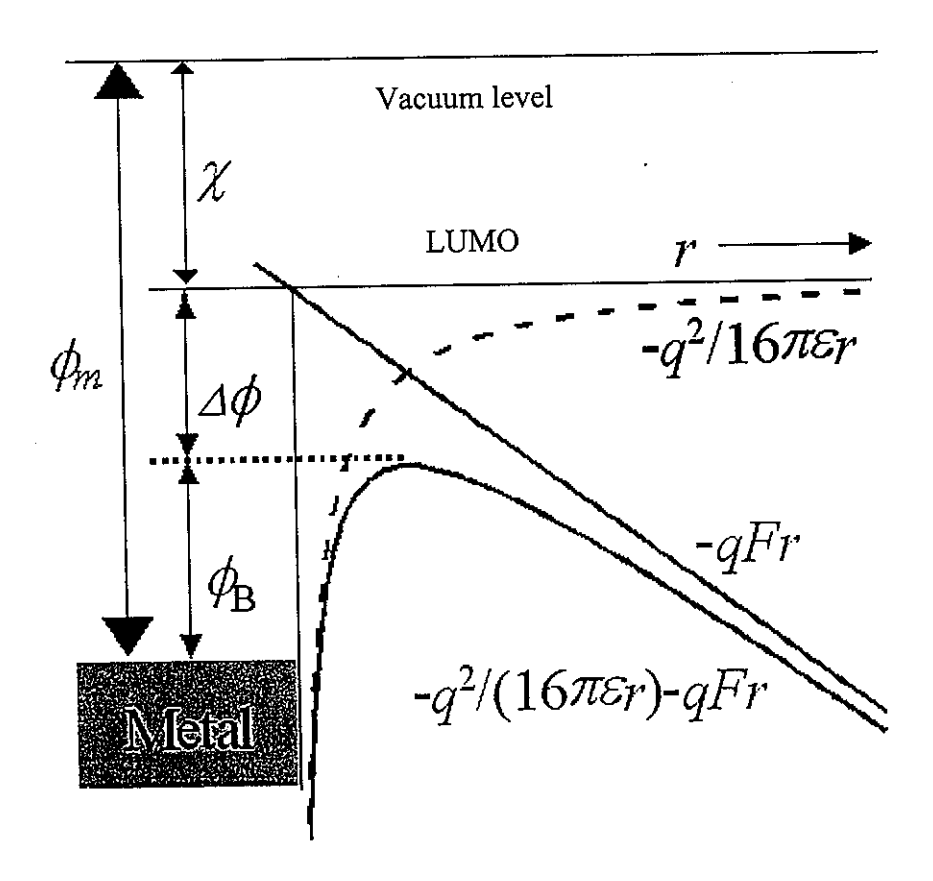


Figure 1.9. Image force barrier lowering at metal-organic interface

When discuss carrier injection over a barrier, image-force lowering of barrier height need to be considered (Figure 1.9). When an electron is placed at a distance x from a metal surface, a positive charge is induced on the surface of the metal. The effect of this charge is the same as that of an image charge placed at a distance x behind the surface.

$$\psi(r) = \phi_m - \chi - \frac{q^2}{16\pi\varepsilon r} - qFr = \phi_B - \frac{q^2}{16\pi\varepsilon r} - qFr$$

$$\varepsilon = \varepsilon_r \varepsilon_0$$
(11)

we get the effective potential barrier height as:

$$\phi_B = (\phi_m - \chi) - \sqrt{\frac{q^3 F}{4 \pi \varepsilon}}$$
 (12)

where  $\phi_m$  is metal work function,  $\chi$  is electron affinity (EA), F is electric field, and q is electron charge.

The barrier lowering is

$$\Delta \phi_B = \sqrt{\frac{q^3 F}{4\pi\varepsilon}} \tag{13}$$

The above treatment holds for neutral contact between metal and wide-gap intrinsic semiconductor, which is the case for organic semiconductors since they are "undoped".

#### 1). Thermionic Emission

The first studies by Richardson and Dushman <sup>24</sup> on thermionic emission were on electrons from a metal surface into the vacuum.

Emtage and O'Dwyer (EO)<sup>25</sup> solved drift-diffusion equation for the injection from metal into a wide-gap intrinsic semiconductor, in which the depletion width is infinite without injection. The results involves integral and EO derive that:

(a) in the low field limit,  $E \ll 4\pi \varepsilon k^2 T^2 / q^3$ 

$$J = N_0 q \mu E \exp(-q \phi_B / kT) \tag{14.1}$$

and

(b) in the high field limit

$$J = N_0 \mu \left(\frac{kT}{q}\right)^{1/2} \left(16\pi \epsilon q E^3\right)^{1/4} \exp(-q\phi_B/kT) \exp(f)^{1/2}$$
 (14.2)

Although not explicitly shown, the backflow current is present. The origin of the backflow in wide bandgap organic semiconductors is disorder.

The existence of disorder in organic semiconductors adds an obstacle to the injected carriers. Due to the disorder, a distribution of site energies is created, and carriers injected occupy the molecular sites in contact with electrodes and also at the low-energy end of the distribution. To move further into the organic materials, the carriers must overcome random energy barriers in addition to the image potential. For this reason, most injected carriers will backflow into the electrode at low applied field strength. When the electric field is increased, the efficiency of injection increment will be more significant than in the case when only image force is considered. This thermal injection process has been proved both by Monte Carlo simulation <sup>26</sup> and experiment <sup>27</sup>.

#### 2). Field Emission

At sufficiently low temperatures or for large barriers at high fields, emission due to quantum tunneling through the barrier-field emission-- can be important.

Fowler-Nordheim (FN) tunneling theory predicts that <sup>28</sup>

$$J \propto F^2 \exp(-bF) \tag{15.1}$$

where F is electric field. For tunneling through a triangular barrier,

$$b = \frac{8\pi\sqrt{2m^*\phi_B^{2/3}}}{3qh} \tag{15.2}$$

where h is Planck constant

At the current understanding of carrier injection, it is widely accepted that thermionic emission dominate at low bias, while FN tunneling becomes significant at high bias.

#### 2. Carrier transport in OLEDs

In single crystals the trap energy levels are generally discrete, while in amorphous and polycrystalline materials they are distributed in accordance with certain distribution functions. The latter has been attributed to the intrinsic disorder of the lattice, which is due to the variation of the nearest-neighbor distances.

## 1) Space-Charge Limited Current (SCLC)

With no traps, using Poisson's equation:

$$dF(x)/dx = \rho/\varepsilon, \qquad (16)$$

and 
$$J = q\mu F(x)$$
, with  $\rho = qp(x)$ 

we can get Mott and Curney equation for trap-free SCL current:

$$J = \frac{9}{8} \varepsilon \mu \frac{V^2}{d^3} \tag{17}$$

At low applied voltage, if the density of thermally generated free carriers (say  $p_0$ ) is

predominant, i.e.  $qp_0\mu\frac{V}{d}\rangle\rangle\frac{9}{8}\varepsilon\mu\frac{V^2}{d^3}$ , the J-V characteristics will be Ohmic. And the

transition voltage is

$$V_{\Omega} = \frac{8}{9} \frac{q p_0 d^2}{\varepsilon} \tag{18}$$

With traps confined in discrete energy levels, the SCL current becomes

$$J = \frac{9}{8} \varepsilon \mu \theta_a \frac{V^2}{d_{eff}^3}$$

$$\theta_a = \frac{p}{p + p_t}$$
(19)

where  $p_t$  is the trapped carrier density.

Starting from the Ohmic region, as the applied voltage is increased, the density of free carriers resulting from injection can increase to such a value that the quasi-Fermi level  $E_F$  moves down below the shallow hole trapping level  $E_t$ , and most traps are filled. The trapsfilled limit (TFL)  $V_{TFL}$  is the condition for the transition from the trapped J-V to the trap-free J-V characteristics.

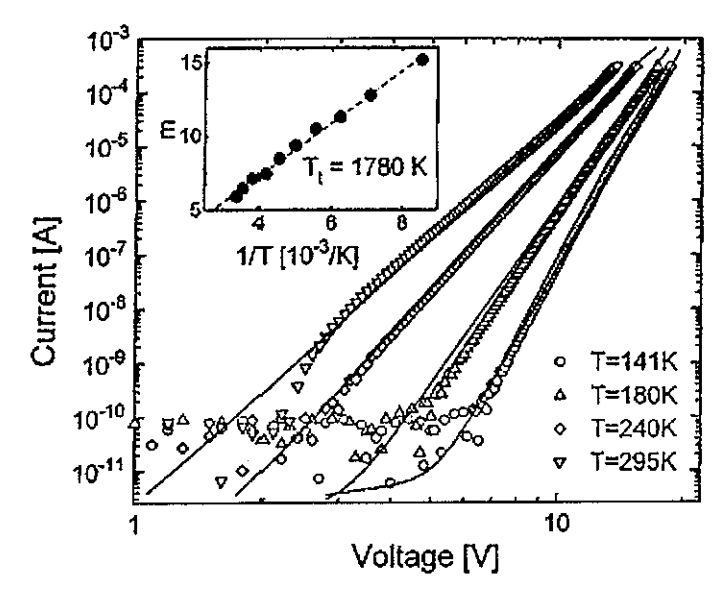


Figure 1.10. Current-voltage characteristics of TPD 27nm/Alq3 55 nm OLED at various temperature. Inset: Temperature dependence of the power law parameter implying  $T_c = 1780$  K.<sup>29</sup>

In organic semiconductors, the trap distribution is usually found to be exponential. The current density can be shown to have the form

$$J \propto \frac{V^{(T_C/T+1)}}{d_{eff}^{(2T_C/T+1)}} \tag{20}$$

Using this model, Burrows<sup>29</sup> derived the width of the exponential trap distribution of  $\sim 0.15 \, \text{eV}$  and  $T_c \sim 1780 \, \text{K}$  for tris(8-hydroxyquinoline) (Alq<sub>3</sub>). The results were shown in Figure 1.10.

#### 2) Field dependent mobility

Unlike inorganic semiconductors, in which the carrier mobility is generally independent of the applied field, in most organic materials, the carrier mobility is strongly dependent on the applied electric field. Over a reasonable range of fields by time-of-flight (TOF) measurements <sup>30,31,32,33</sup> confirmed the phenomenological result.

$$\mu = \mu_o \exp[-\Delta_o/k_B T] \exp[\beta F^{1/2}((1/k_B T) - (1/k_B T_o))]$$
Or simply  $\ln \mu \propto S * F^{1/2}$ , where S is a constant, and F is electric field.

The dependence of  $\ln \mu$  on  $F^{1/2}$  is of the Poole-Frenkel type. The Poole-Frenkel effect describes the electric-field-assisted detrapping phenomenon. When a field is applied, the trap-potential in which a carrier is trapped will be deformed into an asymmetric shape. The situation is very similar to Schottky barrier lowering due to image force with the difference being that one is in the bulk and the other is in the interface. Both cases result in the  $F^{1/2}$  dependence.

Although the Poole-Frenkel mechanism predicts a field-dependence in agreement with experiment, it is not possible to have a high concentration of charged traps in all organic

materials, as is necessary for the usual application of Poole-Frenkel theory. The temperature coefficient of the mobility was found to be independent of the chemical composition, which is clear evidence against the dominance of impurity effects. In addition, a deviation of both the magnitude of S and its temperature dependence from the prediction of Poole-Frenkel theory is observed.<sup>16</sup>

Gaussian disorder models  $^{16}$ , and most recently a theory based on the spatial correlation of energetic disorder  $^{34}$  have been suggested. The energy DOS is typically 0.1 eV. Spatial correlation can be caused by molecular density fluctuations. In the case of  $\pi$ -conjugated polymers, additional energetic disorder arises from the distribution of the conjugation lengths. The existence within the polymer of more crystalline and less crystalline regions also suggests spatial correlations.

# 3. Bimolecular charge Recombination (Langevin recombination)

After carrier injection and transport, carriers meet and recombine. The recombination of a hole and electron releases considerable energy and one must consider how this energy is dissipated. Recombination can lead to the creation of a charge-pair state that decays to the ground state by emission of a photon plus some phonons (radiative recombination), or exclusively by phonon emission (non-radiative recombination).

For organic semiconductors, the narrow bands lead to very low mobility ( $< 1 \text{ cm}^2\text{V}^{-1}\text{S}^{-1}$ ). In Langevin theory, the mean free path  $\lambda$  of the carriers must be less than the radius of capture of one carrier by the other. In organic semiconductor, the scattering length is of the order of the lattice parameter and the Coulombic capture radius  $r_c$  is  $\sim 10^{-6}$  cm. Hence the Langevin requirement is satisfied.

Longevin theory is applicable to the case where random diffusive motion of charges is dominant and drift can be viewed as a small bias in the time-averaged displacement, the average electron-hole pair that approach each other within a distance such that their Coulombic binding energy exceeds kT will ultimately recombine.

The radius of capture  $r_c$  is defined as the distance where coulombic energy equals the thermal energy.  $\frac{e^2}{4 \pi \epsilon r_c} = kT$ 

$$\frac{e^2}{4\pi\varepsilon r_c} = kT$$

$$r_c = \frac{e^2}{4\pi\varepsilon kT} \tag{22}$$

Since the carriers thermalize quickly, the recombination may be viewed as the drift of two charges together under the action of the Coulombic field F. From another stand point, we can regard one carrier as static while the other moves with (total) mobility

$$\mu_T = \mu_e + \mu_h \tag{23}$$

It can be shown that the recombination rate constant is then

$$\gamma_{eh} = e\mu_T / \varepsilon \tag{24}$$

Assuming that the e-h capture process is spin-independent (as implicit in the Langevin model), excitons in the triplet and singlet configuration would be formed in the ratio  $r_{SE/TE}=1/3.$ 

There is evidence that in polymers, the singlet and triple exciton formation cross sections are not equal. Consequently,  $r_{SE/TE} > 1/3$  and could be as large as 1. <sup>35 36 37 38</sup> This conclusion is still being debated intensively. 39,40

## III. Optimization of OLED performance

In this section, I briefly review the important steps in the optimization of OLED performance.

As a guideline, we first consider the external quantum efficiency  $\phi_{EL}$ , which is defined as photons extracted in the forward direction per electron injected.

$$\phi_{FL} = \chi \phi_{PL} \eta_r \eta_e \tag{25}$$

where

 $\chi$  is the fraction of charge carrier recombination in the material resulting in emittable excitons, which from spin statistics is presumed to be  $\frac{1}{4}$  in small molecular fluorescent OLEDs (but may be higher in polymer OLEDs). In phosphorecent OLEDs, it can be nearly 1.

 $\phi_{PL}$  is the photoluminescence quantum efficiency of the emitting material.

 $\eta_r$  is the fraction of injected charge carriers that form excitons (determined by charge balance)

 $\eta_e$  is the fraction of emitted photons that are emitted from the device in the forward direction.  $\eta_e$  is determined by the geometry of device; it typically is  $\sim 1/n^2$ , where n is the index of refraction of the organic material.

We now consider  $\eta_e$  briefly.

The typical OLED structure consists of a planar glass substrate ( $t_{sub} \sim 1$  mm,  $n_{sub} = 1.51$ ), an ITO anode ( $t_{ITO} \sim 100$  nm,  $n_{ITO} \sim 1.8$ ), organic layers ( $t_{org} \sim 100$  nm,  $n_{org} = 1.6-1.8$ ) and a reflecting metal cathode.

The output-coupling efficiency is defined as the light emitted out of the glass substrate over the total light generated internally. Since the organic layers and the glass have a higher

index of refraction than air, organic-air critical angle is the major limiting factor. From Snell's law, this critical angle is  $\theta_c = \sin^{-1}(n_{air}/n_{org})$ .

Assuming the cathode is a perfect reflector, and assuming isotropic emission in the organic layer, the fraction of generated light escaping from the substrate is <sup>41</sup>

$$\eta_{ext,cp} = \int_{0}^{\theta_c} \sin \theta d\theta = 1 - \cos \theta_c = 1 - \sqrt{\left(1 - \frac{1}{n_{org}^2}\right)} \approx \frac{1}{2n_{org}^2}$$
(for large  $n_{org}$ ) (26)

A more detailed half-space radiating dipole model <sup>42</sup> predicts the out-coupling efficiency can be  $0.75 n^{-2}$  for isotropic dipole case, and as large as  $1.2 n^{-2}$  for the in-plane dipole case.

Under the same assumption, the external luminous intensity distribution (with  $\theta_{\rm ff}$  be the view angle in the far field) is given by Gu, et al. <sup>43</sup>, to be

$$I_{ext}(\theta_{ff}) = \frac{F}{2\pi} \frac{n_{air}^2 \cos \theta_{ff}}{n_{org}^2 \sqrt{1 - \left(\frac{n_{air}}{n_{org}} \sin \theta_{ff}\right)^2}}$$
(27)

where  $\theta_{ff}$  is the viewing angle at far field. This result is similar to the cosine intensity profile of a Lambertian emitter.

To improve the out coupling efficiency, methods like introducing rough or textured surfaces, <sup>44</sup> mesa structures and lenses, <sup>45</sup> and the use of reflecting surface or distributed Bragg reflectors, <sup>46</sup> even ordered microlens arrays <sup>47</sup> were used. When use a substrate with an index matched or slightly higher than the organic and a large lens, the total emitted light could be improved as much as a factor of five. <sup>48</sup>

#### 1. Single layer to multilayer device

Tang and VanSlyke <sup>1</sup> introduced their classic double-layer structure in 1987. In single layer devices, the recombination zone is not well defined. Unless the energy levels of the

cathode and anode are extremely well matched to the molecular levels of the organic compound, and the carriers' mobilities are well matched (which is very rare), the electron and hole currents are not balanced. The dominant carrier will then cross the entire structure without finding a carrier of the opposite sign with which to recombine. In this case the recombination will occur at the appropriate organic/electrode interface, where severe quenching of emission will occur. This situation is wasteful of energy and leads to low efficiency in the conversion of electrical to optical power.

In the double layer device (Figure 1.11(a)), a hetero-structure is formed when the materials are chosen properly, so one mainly transports holes and the other is optimized for electron injection and transport. In Tang's structure, diamine is the hole transport material, and Alq<sub>3</sub> is electron transport and emitting material. This leads to two effects: (i) it blocks the transmission of the majority carrier, creating a space charge and balance carriers transport. (ii) Electrons and holes accumulate at the diamine/Alq<sub>3</sub> interface. The recombination zone is confined far from organic/electrodes interfaces, so it improves the efficiency significantly.

Adachi introduced another layer specifically chosen for its luminescent efficiency and formed a triple-layer structure <sup>49</sup> (Figure 1.11(b)). Each of the three organic layers can be separately optimized for electron transport, for hole transport, and for luminescence.

The majority of OLED structures in the literature are derived from the double layer structure. The reasons might be difficulty in finding proper material just for emission layer, and one layer (either hole or electron transporting layer) can act as emitting layer since the emission is at the heterojunction.

# 2. Organic/electrode interface engineering

The organic/electrode interface is very important not only for carrier injection, but also for device lifetime.

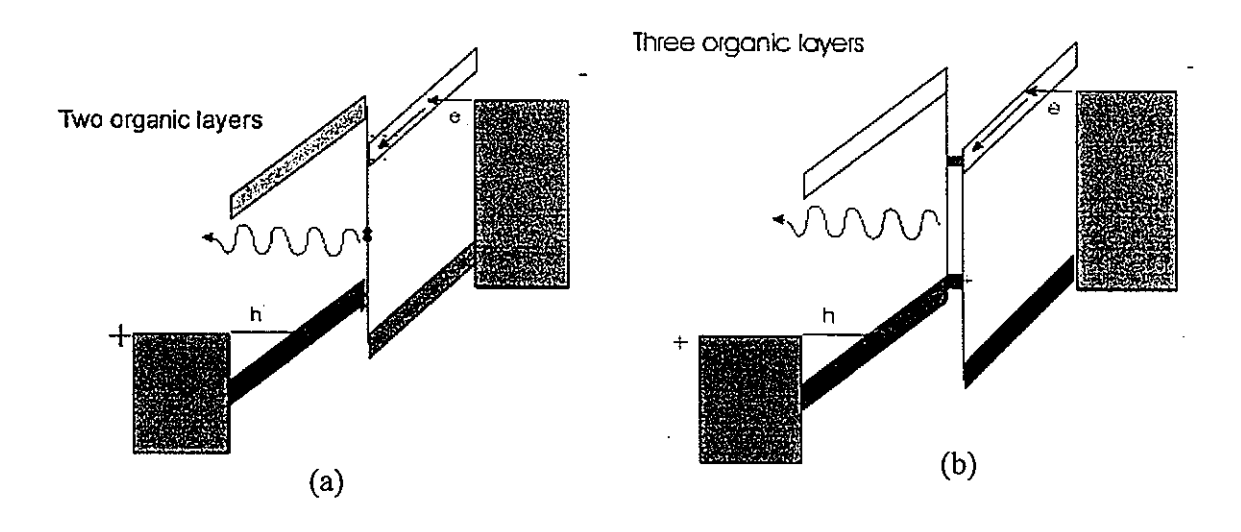


Figure 1.11. Double-layer (a) and Triple-layer (b) OLED device structures

There is a barrier for electron (hole) injection at the organic/cathode (anode) interface. To reduce the device operation voltage, the barrier should be minimized. On the cathode side, low work-function  $\Phi$  metals like Ca<sup>50</sup> ( $\Phi$ =2.9eV), Mg <sup>1</sup>( $\Phi$ =2.9 eV), and Li ( $\Phi$ =3.7eV) were used instead of Al ( $\Phi$ =4.3 eV). However, low work-function metals are generally reactive and unstable in air. Thus, compound cathodes have been developed, which deliver superior performance. The most widely used, with the best performance ones were LiF/Al <sup>51</sup> and CsF/Al <sup>52</sup>. Others like AlO<sub>x</sub> <sup>53</sup>, CuO, NaF, Cs acetate, were also reported to improve electron injection. The mechanisms behind the behavior of compound cathodes are believed to be either the dissociation of LiF or CsF, and/or the formation of a dipole layer across the thin buffer layer.

On the anode side, indium-tin-oxide (ITO) has been the only anode material to have a high work function ( $\Phi$ ~4.8 eV), low resistivity ( $\sim$ 2\*10<sup>-4</sup>  $\Omega$  cm) and excellent transparency (>90% at 550 nm)1. Zinc oxide (ZnO)54 and its variant with Al doping (AlZnO),55 and Zirconium-doped Indium dioxide <sup>56</sup> have also been studied. After a cleaning process, such as ultrasonic action in an organic solvent, acid treatment 57, UV-Ozone treatment 58, O2 plasma treatment 59, all to increase the ITO work function, the ITO's contact with the hole transport material (e.g. N,N'-diphenyl-N,N'-bis(3-methylphenyl)-1,1'-biphenyl-4,4'-diamine (TPD) or 4,4'-bis[N-(1-naphyl)-N-phenyl-amino]biphenyl (NPB)) is still not optimized. A buffer layer is used to further reduce the barrier to hole injection and also improve the ITO/organic contact. One such buffer material is copper phthalocynine (CuPc). 60 By inserting a CuPc layer, the initial driving voltage and the device stability are significantly improved. The CuPc thickness is <20 nm, so it is not enough to smooth the ITO surface. On the other hand, the conducting polymer polystyrenesulphonic acid (PSS)-doped poly(dioxyethylene thienylene) (PEDOT) 61 first used in polymer OLEDs, and now in small molecular OLEDs as well, smoothes the ITO and improves hole injection. The thickness of PEDOT:PSS can be very thick and the device characteristics becomes independent of the ITO properties such as surface roughness, inhomogenity, or work function. The thicker layer also reduces the probability of pinholes and short circuits.

# 3. High thermal stability organic materials

Basically, the heat stability of an OLED is governed by the glass transition temperature  $(T_g)$  of the organic materials in it. Low  $T_g$  material will easily gets crystallize and degrade the device. In a classic CuPc/TPD/Alq<sub>3</sub> device, the  $T_g$ s' of organic materials are

>200°C/63°C/175°C, respectively. Thus, TPD is the weak link in this structure. By replacing TPD with NPB ( $T_g = 96$ °C), the thermal stability of the device is largely improved <sup>62</sup>. Hole-transport materials with even higher  $T_g$  were also reported as starburst molecules. <sup>63</sup>. Another example is replacing 4,4'-bis(2,2'-diphenylvinyl)-1,1'-biphenyl (DPVBi) ( $T_g = 64$ °C) with Spiro-DPVBi ( $T_g = 130$ °C) in efficient blue emitting devices.

# 4. Doping with fluorescent or phosphorescent dyes

In reality, few organic material luminance with a high PL efficiency in the neat solid state. This leads to limitations for high efficiency OLEDs, as seen from the equation of external quantum efficiency. However, when some dyes are doped into proper host materials, the  $\eta_{PL}$  is very high and so is the EL efficiency. For example, rubrene in TPD or Alq<sub>3</sub> was shown to have  $\eta_{PL}=100\%$ . Doping is also a very important method to tune the color of OLEDs. In addition, it is also the key route to achieve highly bright white OLEDs. As mentioned in the previous section, crystallization is a major degradation mechanism for small molecule OLEDs; doping Alq<sub>3</sub> or TPD was shown to strongly inhibit the crystallization of these amorphous thin films and the lifetime of devices based on them was significantly improved.

Rubrene, perylene, coummin, are examples of fluorescence dyes, for which the energy transfer from the host to the dye occurs via the long range dipole-dipole Förster energy transfer mechanism. In this energy transfer, only SEs are involved. As mentioned in the former section, if the formation cross section of SEs and TEs are the same, then only 25% are SEs whose radiative decay gives fluorescence. The remaining 75% are triplets whose radiative transition to the ground singlet state is forbidden.

Although radiation from triplet states is "forbidden", some materials can emit efficiently from the TE state. In such materials, the SE & TE states are mixed, so the radiative decay of the triplet state is partly allowed. The most important interaction mixing singlet and triplet states is the spin-orbit coupling, which refers to the interaction between an electron's spin and the magnetic moment created by the electron oscillating in a closed orbit. To increase the spin-orbital coupling, organic materials with heavy metals like platinum (Pt) or iridium (Ir) are needed. The first two reported phosphorescence dyes are 2,3,7,8,12,13,17,18-octaethyl-21H,23H-porphine platinum (II) (PtOEP) <sup>64</sup>, and fac tris(2-phenylpyridine) iridium (Ir(ppy)<sub>3</sub>) <sup>65</sup>. The energy transfer from the fluorescent host to the phosphorescent guest is Dexter transfer, which is a contact-energy-transfer and thus requires a relatively high concentration (~6%) compared to Förster energy transfer (~1%).

The phosphorescent OLEDs (Ph-OLEDs) operates as follow: The host SE transfers its energy to the phosphorescent guest SE by Förster (mainly) or Dexter energy transfer; the host TE energy is transferred to the guest TE state by the Dexter mechanism; then the guest SE intersystem crosses to the guest TE; finally, the guest TE decays radiatively, resulting in the phosphorescence.

# 5. Alternating Current (AC) driving scheme

Early lifetime measurements used DC continuous operation. It was observed that this causes polarization of the device due to charge trapping, which reduces the stability of the devices. Using a constant current mode in the forward bias and reverse biasing in the constant voltage mode were observed to suppress the increase of driving voltage required to maintain a constant current.<sup>66</sup> It is believed that the reverse bias efficiently prevents a buildup

of trapped space charge in the organic layers, accumulated during the current flow in the forward cycle, by "de-trapping" them during the reverse bias. Also, the reverse bias may cause the burn out of any localized conducting filaments that might connect the two parallel electrodes in the thin film device.

Forrest and coworkers achieved a half-life  $\tau_{1/2} > 10^7$  h in phosphorescent OLEDs with AC excitation scheme.

# IV. Fabrication of OLEDs

Two types of OLEDs with different geometries were fabricated for different measurements.

For ODMR studies, the geometry was  $\sim$  4.5mm wide by 20 mm long to fit into the microwave cavity. The other geometry was for combinatorial studies of exciplex formation, for which a 2" x 2" ITO substrate was used and a sliding shutter technique was used to fabricate 5x5 = 25 OLEDs with a systematic variation in the thickness of two active layers.

Prior to device fabrication, the substrates were thoroughly cleaned by ITO detergent, electronic grade isoprpanol, and acetone. The substrate was then blown dry by pure Ar gas. For the 2"x2" substrate, partial etching of ITO by diluted aquaregia was also performed in order to reduce device driving voltage and improve the efficiency of the OLEDs.

All the fabrication processes were performed in an Ar-filled glovebox, in which the deposition chamber located. The deposition of the organic materials and metals was performed in the evaporation chamber by thermal evaporation, in which tungsten filaments were the heating source. A co-deposition technique was used when doping was needed. The

deposition rates were independently controlled by adjusting the currents of two independent power supplies.

#### References

- 1. C. W. Tang and S. A. VanSlyke, Appl. Phys. Lett. 51 (12), 913 (1987)
- 2. Burroughes, J. H., et al. Nature 347, 539 (1990)
- 3. C. Adachi, M. Baldo, M. E. Thompson, and S. R. Forrest, J. Appl. Phys. 90, 5048 (2001)
- 4. J. Kido, Y. Lizumi, Appl. Phys. Lett., 73, 2721 (1987)
- 5. N. Tessler, N. Harrison, and R. Friend, Adv. Mat. 10, 64 (1998)
- 6. K. Vaeth, Information Display, 19, 16 (2003)
- 7. http://www.pioneer.co.jp/press/release39.html (9/28/98)
- 8. S. Johnson, Archit. Lighting, Nov./Dec. 2000
- 9. Pope, M. Kallmann, H. & Magnante, P. J. Chem. Phys. 38, 2042 (1963)
- 10. W. Helfrich and W.G. Schneider, Phys. Rev. Lett. 14, 229 (1965)
- 11. Vinvett, P. S., Barlow, W. A., Hann, R. A. & Roberts, G. G. Thin Solid Films 94, 171 (1982)
- 12. J. Sheats, Science, 273, 884 (1996)
- 13. http://www. Kodak.com
- 14. http://www.universaldisplay.com
- 15. R.H.Young and J.J. Fitzgetald, J. Chem. Phys. 102, 2209 (1995)
- 16. H. Bässler, Phys. Stat. Sol (b), 175, 15 (1993)
- W.-P. Su, J.R. Schrieffer and A.J. Heeger, Phys. Rev. Lett. 42, 1698 (1979); Phys. Rev. B 22, 2099 (1980)

- S.A. Brazovskii and N.N. Kirova, JETP Lett. 33, 4 (1981); R.H. Friend, D.D.C. Bradley,
   and P.D. Townsend, J. Phys. D: Appl. Phys. 20, 1367 (1987)
- T. Holstein, Appl. Phys. (N.Y.) 8, 325 (1959); 8, 343 (1959); W. Warta and N. Karl,
   Phys. Rev. B 32, 1172 (1985)
- 20. Z. Shuai, J.L. Bredas, and W.P. Su, Chem. Phys. Lett. 228, 301 1994)
- 21. D. Beljonne, Z. Shuai, R.H. Friend and L.J.Bredas, J. Chem. Phys. 102, 2042 (1994)
- 22. T. Förster, Discuss. Faraday Soc. 27, 7 (1959); Förster, T. (1965) "Action of Light and Organic Molecules." In Modern Quantum Chemistry, part 2, O. Sinanoglu, ed. (Acdamic Press);
- 23. M. Baldo, M. E. Thompson and S.R. Forrest, Nature, 403, 750, (2000)
- O. W. Richardson, Philos. mag. 28, 633 (1914); DushmanS. Dushman, Phys. Rev. 21,
   623 (1923)
- 25. P.R. Emtage and J. J. O'Dwyer, Phys. Rev. Lett. 16, 356 (1966)
- 26. Y. Gartstein and E. M. Conwell Chem. Phys. Lett., 255, 93 (1996)
- 27. M. Abkowitz, H. Mize, and K. facci, Appl. Phys. Lett., 66, 1288 (1995)
- 28. R. H. Fowler and L. Nordheim, Proc. R. Soc. London Ser. A 119, 173 (1928)
- 29. P. E. Burrows, et al., J. Appl. Phys. 79, 7991 (1996)
- 30. S.J. Santos Lemus and J.Hirsch, Phil.Mag. B53,25 (1986)
- 31. L.B.Schein, A. Rosenberg, and S.L. Rice, J. Appl. Phys. 60, 4287 (1986)
- 32. A. Peled, L.B. Schein, and D. Glatz, Phys. Rev. B 41, 10835 (1990)
- 33. P. M. Borsenberger, Appl. Phys. 68, 6263 (1990)
- 34. Y. Garstein and E.M. Conwell, Chem. Phys. Lett, 245, 351 (1995)

- 35. M. Wohlgennant, K. Tandon, S. Mazumdar, S. Ramasesha, and Z. V. Vardeny, Nature (London) 409, 494 (2001)
- 36. Z. Shuai, et al., D. Beljonne, R. J. Silby and J. L Bredas, Phys. Rev. Lett. 84, 131 (2000)
- 37. Y. Cao, I. Parker, G. Yu, Z.C., and A. Heeger, Nature (Londn) 397, 414 (1999)
- 38. J. Wilson, et al., Nature, 413, 828 (2000)
- 39. M.A. Baldo, D.F. O'Brien, M.E. Thompson, and S.R. Forrest, Phys. Rev. B, 60, 14 422 (1999)
- 40. M. Segal, M.A. Balco, R.J. Holmes, S.R. Frrest and Z.G. Soos, Phys. Rev. B 68, 075211 (2003)
- 41. B. E. Saleh and M. C. Teich, Fundamentals of photonics (Weley New York, 1991)
- 42. J.-S. Kim, P. K. H. Ho, N. C. Greenham, and R. H. Friend, J. Appl. Phys. 88, 1073 (2000)
- 43. G. Gu, D. Z. Garbuzov, P. E. Burrows, S. Venkatesh, and S. R. Forrest, Opt. Lett. 22, 396 (1997)
- A. A. Bergh and R.H. Saul, US Patent No.3739217 (1973); I. Schmitzer, E.
   Yablonovitch, C. Caneau, T.J. Gmitter, and A. Scherer, Appl. Phys. Lett. 63, 2174 (1993)
- 45. R.H. Haitz, US Patent No. 5087949 (1992); R. Windisch, P. Heremans, A. Knobloch, P. Kiesel, G. H. Dohler, B. Dutta, and G. Borghs, Appl. Phys. Lett. 74, 2256 (1999)
- 46. F.A. Kish, Jr. and S.A. Stockman, US Patent No. 6015719 (2000)
- 47. S. Moller and S. R. Forrest, Appl. Phys. Lett.,
- 48. C. F. Madigan, M. H. Lu and J. C. Sturm, Appl. Phys. Lett. 76, 1650 (2000)
- 49. C. Adachi, K. Nagai, and N. Tamoto, Appl. Phy. Lett., 68, 2679 (1995)
- 50. D. Braun and A. J. Heeger, Appl. Phys. Lett. 58, 1982 (1991)

- 51. L. S. Hung, C. W. Tang, and M. G. Mason, Appl. Phys. Lett. 70, 152 (1997)
- G. E. Jabbour, B. Kippelen, N. R. Armstrong and N. Peyghambarian, Appl. Phys. Lett.
   1185 (1998)
- 53. F. Li, H. Tang, J. Anderegg and J. Shinar, Appl. Phys. Lett. 70, 1233 (1997)
- 54. J.Hu and R.G. Gordon, J. Appl. Phys. 71, 880 (1992)
- H.Kim, C.M. Gilmore, J.S. Horwitz, A.Pique, H.Murata, G.P.Kushto, R.Schlaf,
   Z.H.Kafafi and D.B. Chrisey, Appl. Phys.Lett 76, 259 (2000)
- 56. H.Kim, J.S. Horwitz, G.P.Kushto, S.B. Qadri, Z.H.Kafafi and D.B. Chrisey, Appl. Phys.Lett. 78, 1050 (2001)
- 57. F. Li, H. Tang, J. Shinar, O. Resto, and S. Z. Weisz, Appl. Phys. Lett. 70, 2741 (1997)
- 58. K. Sugiyama, H. Ishii, Y. Ouchi, and K. Seki, J. Appl. Phys. 87, 295 (2000)
- 59. M. Ishii, T. Mori, H. Fujikawa, S. Tokito, and Y. Taga, J. Lumin. 87-89, 1165 (2000)
- 60. C. W. Tang, S. A. VanSlyke, and C. H. Chen, J. Appl. Phys. 65, 3610 (1989)
- 61. Y. Gao, G. Yu, C. Zhang, R. Menon, and A. J. Heeger, Syn. Met. 87, 171 (1997)
- 62. Sato, Semiconductors and semimetals, 64, 209 (2000)
- 63. Y. Shirota, J. Mater. Chem. 10, 1 (2000)
- M. A. Baldo, D. F. O'Brien, Y. You, A. Shoustikov, S. Sibley, M. E. Thompson, and S.
   R. Forrest, Nature 395, 151 (1998)
- 65. T. Tsutsui, M.-J. Yang, M. Yahiro, K. Nakamura, T. Watanabe, T. Tsuji, Y. Fukuda, T. Wakimoto, and S. Miyaguchi, Jpn. J. Appl. Phys. 38, L1502 (1999)
- 66. Van Slyke, Appl. Phys. Lett., 69 2160, (1996)

# Chapter 2. Introduction to Optically Detected Magnetic Resonance (ODMR)

### I. Background

Magnetic resonance spectroscopy has been one of the most important experimental tools in physics and chemistry. Few other spectroscopic methods offer such direct and detailed insights into the structure and dynamics of atoms, molecules and condensed matter.

A magnetic resonance experiment involves the absorption of a rf or a microwave photon that changes the populations of magnetic substates of nuclei, atoms, or molecules with non-zero total angular momentum. Depending on the origin of the angular momentum, electron spin resonance (ESR, also known as electron paramagnetic resonance (EPR)) and nuclear magnetic resonance (NMR) are the two major types of magnetic resonance spectroscopies, other variants include both electronic and nuclear moments.

Magnetic resonance spectroscopy study originated from Van Vleck's theoretical work on magnetic relaxation <sup>1</sup> and Cleeton and Williams' primitive microwave spectrometer, which was used to detect the inversion of the ammonia molecule in 1934. <sup>2</sup> In 1936, Gorter introduced a technique to detect a magnetic resonance in solid. However, it was the great radar research during World War II that provided the necessary microwave and electronic technology for realizing ESR with sufficient sensitivity and resolution. Magnetrons, highly directional antennas, sensitive crystal detectors, narrow-band amplifiers, lock-in detectors and noise-reducing circuits, etc., are among the many critical components invented during this period. The first ESR experiment was performed by Zavoisky<sup>5</sup> in 1944, and the first NMR experiments followed quickly in 1946 by Purcell<sup>6</sup> and Bloch<sup>7</sup>.

A major handicap of magnetic resonance spectroscopy is low sensitivity. To get a detectable signal, large numbers of spins are needed (10<sup>16</sup>- 10<sup>18</sup> for NMR, 10<sup>10</sup> – 10<sup>12</sup> for ESR). Although ESR requires far fewer spins than NMR, it is often not sensitive for the monitoring thin films and thin film devices. For example, Due to a low concentration of paramagnetic defects, ESR is normally undetectable for polymer and small molecule thin films.<sup>8</sup>

A successful technique to enhance the sensitivity is to transfer the detection of microwave absorption by paramagnetic species to the optical domain, i.e., the detection of changes of an optical quantity under magnetic resonance conditions. This takes advantage of the concomitant increase in photon energy to enhance the sensitivity of the experiment. For semiconductors, the approach is based on the fact that recombination processes are often spin-dependent. Microwave transitions between Zeeman sublevels may result in a change in the absorbed and /or emitted light associated with the excitation. This method is generally called optically detected magnetic resonance (ODMR), and it has proven to be a highly sensitive method to detect paramagnetic excited states in a variety of organic and inorganic materials, usually semiconducting or insulating. Indeed, ODMR is usually  $10^3 - 10^5$  times more sensitive than conventional ESR. As a matter of fact, in 1993 a single molecular spin was detected by ODMR on single pentacene molecules embedded in a p-terphenyl host crystal, independently by Köhler et al. 9 and J. Wrachtrup et al.. 10

ODMR on organic molecules was first reported by M. Sharnoff in 1967-68 in the form of photoluminescence (PL)-detected magnetic resonance (PLDMR). The change in the PL of a sample in a microwave cavity was monitored as the magnetic field was varied slowly. Sharnoff detected the " $\Delta m_s = \pm 2$ " transition in the lowest triplet state of naphthalene through

a change in the phosphorescence intensity at the field for resonance. In 1973, van Dorp<sup>12</sup> showed that the change in fluorescence intensity upon a magnetic-resonance transition could also serve as a detection channel, which enables the study of non-phosphorescent triplet states. Absorption-detected magnetic resonance (ADMR) can be used to study non-radiative systems since the absorption or emission of a microwave photon may lead to a change in the optical absorption; Clarke et al.<sup>13</sup> reported the first ADMR experiment in 1972.

### II. Spin-dependent Decay Channels in $\pi$ -conjugated Materials

The radiative decay of singlet excitons (SEs) is the source of the PL and EL in fluorescent  $\pi$ -conjugated materials and OLEDs. Thus the competing decay channels of SEs are of at most importance in OLED research.

In chapter one, we discussed the excitations in  $\pi$ -conjugated materials, including polarons, excitons and bipolarons (or dianions and dications in small molecular materials). The interactions among them are important not only for ODMR, but also for all OLED development. If the decay process is spin dependent, then an ODMR may occur.

Former studies distinguished two types of polarons, free and trapped. If the recombination of the p<sup>+</sup> - p<sup>-</sup> trapped polaron pairs is nonradiative, i.e.,

$$p_t^+ + p_t^- \to S_0 + phonons \tag{1}$$

where  $S_0$  is the ground state. This is a spin-dependent process in which the antiparallel configuration is needed for decay. The trapped polarons are thus essentially charge-transfer states. They are also efficient non-radiative SE quenching centers, i.e.,

$$S_1^* + p_t^{\pm} \rightarrow S_0 + p_t^{\pm} + phonons \tag{2}$$

Free polarons, to which the injected electrons and holes immediately relax, are the origin of the excited singlet states:

$$p_f^+ + p_f^- \to S_1^* \to 1^1 B_u \to S_0 + h\nu + phonons \qquad \text{or}$$

$$p_f^+ + p_t^- \to S_1^* \to 1^1 B_u \to S_0 + h\nu + phonons \qquad \text{or}$$

$$p_t^+ + p_f^- \to S_1^* \to 1^1 B_u \to S_0 + h\nu + phonons \qquad (3)$$

where  $1^1B_u$  is the group theory notation of the lowest state in the singlet manifold of  $\pi$ conjugated materials. To form  $S_1^*$ , the two polarons must be in the singlet pair configuration.

If they are in the triplet pair configuration, they will form triplet excitons (TEs).

$$p_f^+ + p_f^- \rightarrow T_1$$
 or 
$$p_f^+ + p_i^- \rightarrow T_1$$
 or 
$$p_i^+ + p_f^- \rightarrow T_1$$
 (4)

These processes are clearly spin-dependent.

Due to trapping, the lifetime of trapped polarons is much longer than that of free polarons. Thus although both trapped and free polarons generate an electrical field, due to their long lifetime, the trapped polarons are much more efficient SE quenching centers than free polarons. In addition, the lower energy of a trapped polaron pair may also exclude them from forming singlet excitons.

Bipolarons (or dianions or diacations) are doubly charged spinless excitations formed by the fusion of like-charged polarons:

$$p^{\pm} + p^{\pm} \to bp^{\pm\pm} \tag{5}$$

Since polarons are spin-1/2 and bipolarons are spin-0, this process requires that the like-charged polarons be in the singlet pair configuration. Bipolaron formation is therefore a spin-dependent process.

The most likely decay process for bipolarons is by recombination with a free polaron:

$$bp^{\pm\pm} + p_f^{\mu} \to p_t^{\pm} \tag{6}$$

Thus bipolarons are probably longer lived and have a low mobility. These properties and their double charge enhance the role of bipolarons as efficient SE quenching centers, in addition to their "consumption" of free polarons, which otherwise can contribute to SE formation.

TEs can also interact with each other or with other excitations. TE-TE annihilation into SEs is a well-established phenomenon in some organic systems, e.g., anthracene:

$$T_1 + T_1 \rightarrow S_1^* \rightarrow S_0 + h\nu + phonons$$
 (7)

This process is spin-dependent and was proposed to explain some early ODMR results in  $\pi$ -conjugated polymers. However, this process is generally very weak in most luminescent  $\pi$ -conjugated materials, and the mechanism is ruled out by photoinduced absorption (PA)-detected magnetic resonance (PADMR) results.

TEs can also interact with SEs to quench the SEs:

$$T_1 + S_1^* \to T_1 + S_0 + phonons \tag{8}$$

i.e., TE acts as a SE quenching center.

The energy levels of the excitations are qualitatively given by the scheme in Figure 2.1.

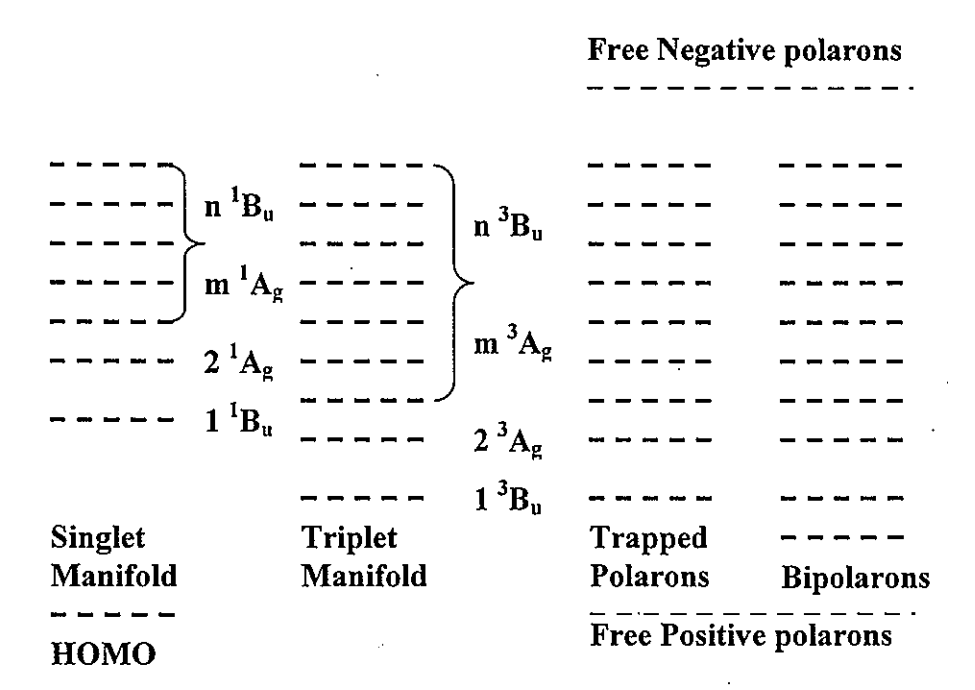


Figure 2.1. Schematic energy levels of SEs, TEs, trapped and free polarons, and the bipolaron manifold in luminescent  $\pi$ -conjugated materials.<sup>14</sup>

#### III. The Spin 1/2 Polaron Resonance

In organic semiconductors, electrons (or hole) interact with lattice, becoming "dressed" with a strain field. The resulting particle is called a polaron. The energy of a polaron is lower than that of an electron or hole, so it produces a state in the gap.

When a particle with non-zero spin is placed in a magnetic field, its magnetic energy can be expressed by the well-known spin Hamiltonian:

$$H = \vec{S} \bullet \vec{g} \beta \bullet \vec{H} \tag{9}$$

Where  $\vec{S}$  is the spin of the particle,  $\vec{g}$  is a tensor describing the interaction of the field particle with the field  $\vec{H}$ , and  $\beta$  is Bohr magneton.

As mentioned by Gordy, <sup>15</sup> organic molecules have nearly isotropic gyromagnetic ratios or Lande g-factor. This is because the electrons in  $\pi$  orbitals are locked in fixed directions, relative to the molecular frame, by the electric field of the chemical bonds, and are not free to precess or become oriented in an applied magnetic field. Thus the electronic orbital motion is decoupled from the spin in a so-called "quenching" process. The result is that the orbital angular momentum is effectively quenched and the organic molecules have nearly isotropic g factor close to that of the free electron, which is g = 2.0023. Under this condition, the Hamiltonian can be simplified to:

$$H = g\beta \vec{S} \bullet \vec{H} \tag{10}$$

For weakly bounded Wannier excitons or polaron pairs, the spin-spin coupling energy is negligibly small compared to the Zeeman splitting. The energy levels formed in these electron-hole systems can be expressed as

$$\varepsilon = 1/2(\pm g_e \pm g_h)\beta \bullet H_0 \tag{11}$$

where the subscripts e and h represent electron and hole respectively, and  $H_0$  is the magnitude of the applied magnetic field.

Figure 2.2 shows the energy levels for weakly bound e-h pairs (Wannier excitons) in a magnetic field.

A necessary condition for the observation of a resonance is that the populations of the spin sublevels be different off-resonance. When the ground state is the singlet state, only the singlet pair configuration of the e-h states can decay radiatively to the ground state. Hence the decay of parallel spin states 1 and 4 is slower than that of 2 and 3. Hence off-resonance,  $n_2$ ,  $n_3 < n_1$ ,  $n_4$ . At low enough temperature, the spin-lattice relaxation rates are slower than the

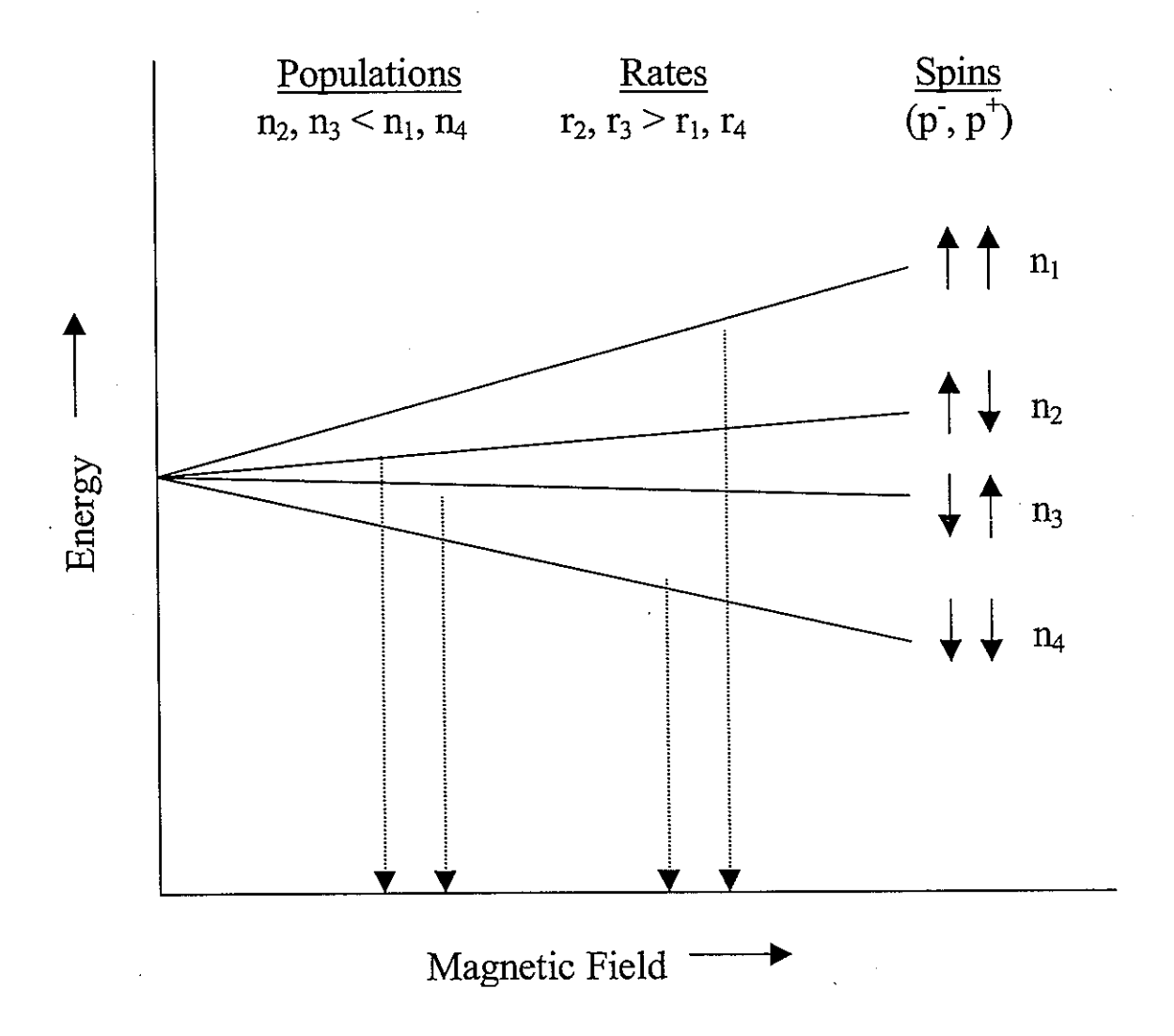


Figure 2.2. Energy levels for weakly bound e-h pairs in a magnetic field.

decay rate. Thus this condition is satisfied. When microwave photons with energy

$$hv = g_e \beta H_o \text{ or } hv = g_h \beta H_o$$
 (12)

was applied on the sample, they induce a net transfer of population of pairs from states 1 and 4 to states 2 and 3. The process is called spin mixing, as it tends to equalize the singlet and triplet polaron pair configuration populations.

# IV. Spin-1 Triplet Resonance

In  $\pi$ -conjugated materials, when a large number of electrons and holes couple to form an excited state, if the cross sections for formation of SEs and TEs are the same, only 1/4 will be SEs, while the other  $\frac{3}{4}$  will be TEs. Unlike the uncorrelated or weakly correlated electronhole system we discussed in spin  $\frac{1}{2}$  resonance, both SEs and TEs are tightly bounded, or Frenkel excitons. Thus the spin-spin interaction must be considered.

In a magnetic field, the Hamiltonian of a pair of interacting spin-1/2 particles is

$$H = H_{z} + H_{s-s} + H_{hfs} {13}$$

Where  $H_Z$  is Zeeman interaction of spins,  $H_{S-S}$  is the spin-spin dipole interaction and  $H_{h/s}$  is hyperfine interaction between electronic and nuclear dipoles. Note there is a much stronger exchange interaction which separates the singlet and triplet state. However, it is the magnetic dipole-dipole forces between two unpaired electrons that removes the degeneracy of triplet states. Here we assume that the molecule is exclusively in the triplet state.

The systems of interest in  $\pi$ -conjugated polymer and small-molecular materials are mostly disordered. As a result, fast exciton diffusion leads to fast sampling of all possible hyperfine environments. On the other hand, the triplet resonances detected ("powder pattern") are pretty wide (>200G), so the hyperfine interaction only leads to a slight broadening of the triplet resonance. Thus  $H_{hfs}$  term can be neglected.

The general dipole contribution to the Hamiltonian of two spins  $S_1$  and  $S_2$  is:

$$H_{S1-S2} = (g\beta)^2 \left[ \frac{\vec{S}_1 \cdot \vec{S}_2}{r^3} - 3 \frac{(\vec{r} \cdot \vec{S}_1)(\vec{r} \cdot \vec{S}_2)}{r^5} \right]$$
 (14)

In matrix form,

$$H = \vec{S} \bullet \vec{D} \bullet \vec{S} \quad , \tag{15}$$

where  $\vec{D}$  is spin-spin coupling tensor, with its component be  $^{17}$ 

$$D_{ij} = \frac{(g\beta)^2}{2} \left\langle \frac{r^2 \delta_{ij} - 3r_i r_j}{r^5} \right\rangle \tag{16}$$

where the bracket means the average over the spatial part of the wavefunction,  $\beta$  is Bohr magneton, i, j, = x, y, z are the coordinates of the relative positions of the two spins.

The D matrix can be diagonalized, and the new basis determines the principal axis of the triplet.

$$H_{S1-S2} = -\frac{(g\beta)^{2}}{2} \left[ \left\langle \frac{r^{2}-3x^{2}}{r^{5}} \right\rangle S_{X}^{2} + \left\langle \frac{r^{2}-3y^{2}}{r^{5}} \right\rangle S_{Y}^{2} + \left\langle \frac{r^{2}-3z^{2}}{r^{5}} \right\rangle S_{Z}^{2} \right]$$

$$= -\left( XS_{X}^{2} + YS_{Y}^{2} + ZS_{Z}^{2} \right)$$
(17)

Since X + Y + Z = 0, only two of the parameters are independent. Choose

$$D = -\frac{3Z}{2} = \frac{3}{4} (g\beta)^{2} \left\langle \frac{r^{2} - 3z^{2}}{r^{5}} \right\rangle$$

$$E = \frac{Y - X}{2} = -\frac{3}{4} (g\beta)^{2} \left\langle \frac{x^{2} - y^{2}}{r^{5}} \right\rangle$$
(18)

then the spin-spin interaction Hamiltonian can be written as

$$H_{S1-S2} = D[S_z^2 - \frac{1}{3}S(S+1)] + E(S_X^2 + S_Y^2)$$
 (19)

D and E are called zero-field splitting (ZFS) parameters and have units of energy. When the triplet state is axially symmetric, E = 0. When  $E \neq 0$ , the axial symmetry breaks. So E is a measurement of the departure from axial symmetry. The axes x, y and z are defined such that E is always smaller or equal to D/3, and the z axis is the one split the farthest from the other two. The splitting between the X and Y sublevels is 2E.

The splitting of the TE energy levels in the absence of an external field is shown below.

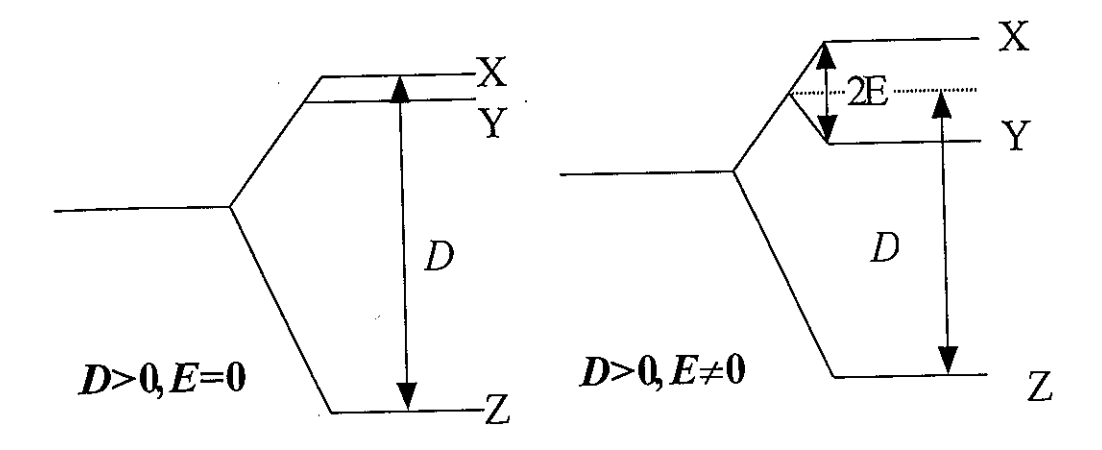


Figure 2.3. Splitting of triplet energy levels in the absence of an external magnetic field

Since

$$D \le \frac{3}{4} (g\beta)^2 \left\langle r^{-3} \right\rangle \tag{20}$$

it sets an upper limit for the extent of the triplet wavefunction.

$$r_{UB} = \left| \frac{3(g\beta)^2}{4D} \right|^{1/3} \tag{21}$$

The system's Hamiltonian The final form of this system's Hamiltonian now becomes:

$$H = g\beta \vec{S} \bullet \vec{H} + D[S_Z^2 - \frac{1}{3}S(S+1)] + E(S_X^2 - S_Y^2)$$
 (22)

In the cases that the magnetic field H being along the axis of the system, closed form solutions for the energy can be obtained.

The eigenvalues of the spin Hamiltonian depends on both the magnitude of external magnetic field  $H_0$  and its direction relative to the principal axes of the organic molecule. Thus the orientation of the molecule relative to  $H_0$  will determine the energies of the triplet sublevels.

Figure 2.4 shows the energies vs. magnetic field diagrams of the three triplet states when the field is along one of its three principle axes.

The |0> sublevel is the one whose axis is parallel to the applied field. The other two sublevels |+1> (and |-1>) are split upwards (downwards) in energy with applied field.

A and B represent the so-called full-field transition ( $|-1> \rightarrow |0> \text{ or } |0> \rightarrow |+1>$ ), while C represent half-field transition (|-1> to |+1>).

Depending on the orientation of the principal axes of the triplet state relative to the magnetic field, the triplet resonance signal will be detected at different fields. When a single crystal sample is used, by measuring the positions of the resonance transitions at different orientations of the crystal with respect to magnetic field, the ZFS parameters can be determined.

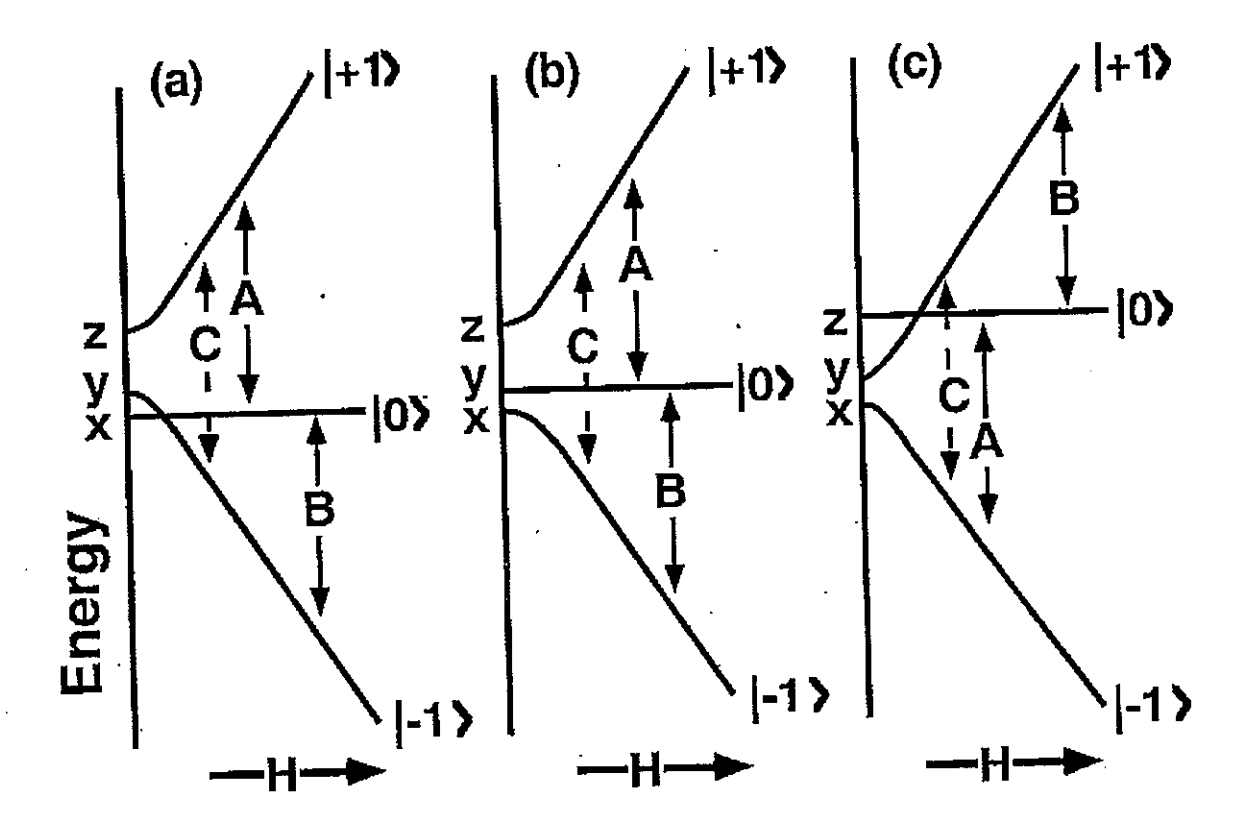


Figure 2.4. Energies of triplet levels for a magnetic field  $H_0$  aligned with each of the three principal axes.

#### Powder patterns

For triplets in polycrystalline or amorphous samples, a "powder pattern" is formed due to the random orientation of the principal axes of the TEs with respect to the applied field  $H_0$ . In OLEDs, all the organic material is in the amorphous state, thus a "powder pattern" is expected. While the analysis is somewhat more complex than for a single crystal, it is not difficult to extract the ZFS parameters D and E from a powder pattern.

Powder patterns are determined by first finding the resonant magnetic field H, at which the absorption of microwaves occur;  $H_0(n, \phi)$  is a function of the polar angle  $\theta$  ( $n = \cos \theta$ ) and the azimuthal angle  $\phi$ .

Detailed theoretical treatment of triplet powder patterns can be found in L.S. Swanson's thesis. The simplest case is when E=0, in which the resonance field is independent of  $\phi$ . The probability of finding  $H_0$  at angle  $\theta$  is proportional to  $\sin \theta$  d  $\theta$  = -dn. The intensity of absorption at  $H_0 = H$  is then:

$$dI = \sum_{n} A(H, n) \frac{dn}{dH} dH \tag{23}$$

where H = H(n) has been inverted to n = n(H) and A(H, n) is the transition probability.

In general, the full-field powder pattern due to the  $\Delta m_s = \pm 1$  transitions has the following critical points:

singularities at 
$$H = H_0 \pm (D-3E)/2g\beta$$
 (24)

shoulders at 
$$H = H_0 \pm (D + 3E)/2g\beta$$
 (25)

and steps at 
$$H = H_0 \pm D/g \beta$$
 (26)

where  $H_0 = h \nu / g \beta$ .

The half-field powder pattern due to the  $\Delta m_s = \pm 2$  transitions are much narrower since it is dependent on D and E in second order only. The half-field powder pattern has the following two critical points:

A singularity at

$$H = \sqrt{\frac{h\nu}{2g\beta}^2 + \frac{D^2 + 3E^2}{(g\beta)^2}} = \frac{1}{2}H_0\sqrt{1 - [4(D^2 + 3E^2)/(g\beta H_0)^2]}$$
(27)

and a shoulder at

$$H = \frac{h \nu}{g \beta} \sqrt{1 - \frac{1}{2} \left(\frac{D - E}{h \nu}\right)^2} = H_0 \sqrt{1 - \left[(D - E)/2H_0\right]^2}$$
 (28)

The following are two typical simulations of full field (g  $\sim$  2, Figure 2.5) and half field (g  $\sim$  4, Figure 2.6) PLDMR triplet powder patterns by Swanson. In Figure 2.5, D=520 G, E=0, and Figure 2.6, D=602 G, E=0.

# V. Frequency resolved ODMR (FR-ODMR)

In the CW mode ODMR, frequency resolved technique can be used to get useful information about the lifetimes of the species responsible for the ODMR. The method is simple as setting the magnetic field on resonance and simply varying the microwave chopping frequency  $\nu_c$ . The dependence of ODMR on  $\nu_c$  then yields the lifetime(s).

FR-ODMR has been applied to study the kinetics of radiative recombination.<sup>18</sup> It is a phase shift spectroscopy technique in which the phase shift between the microwave pulse and the resonant change of the luminescence (PL or EL) is measured to deduce the time constants of processes contributing to the recombination. Under resonance conditions, by varying the modulation frequency of the microwave power, the in-phase and out-of-phase (quadrature) output signals of the lock-in detector are measured.

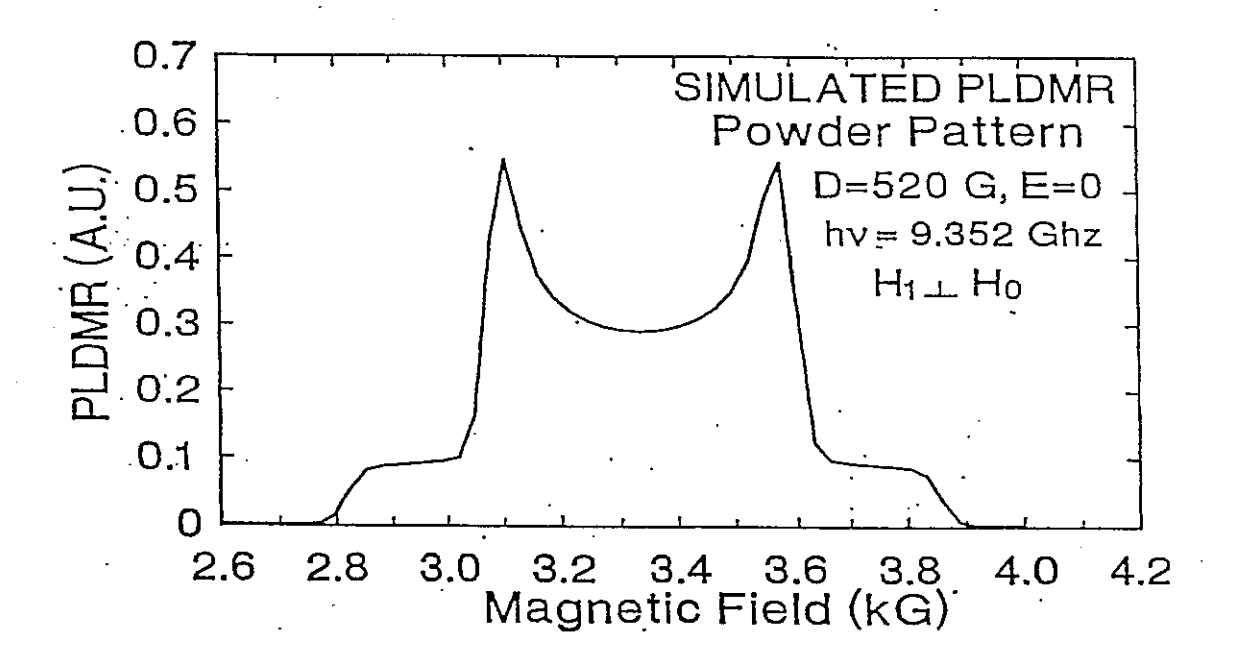


Figure 2.5. PLDMR full field  $(g \sim 2, \Delta m_s = \pm 1)$  powder pattern simulation for D = 520 G, E = 0. Microwave frequency is at 9.352 G Hz.

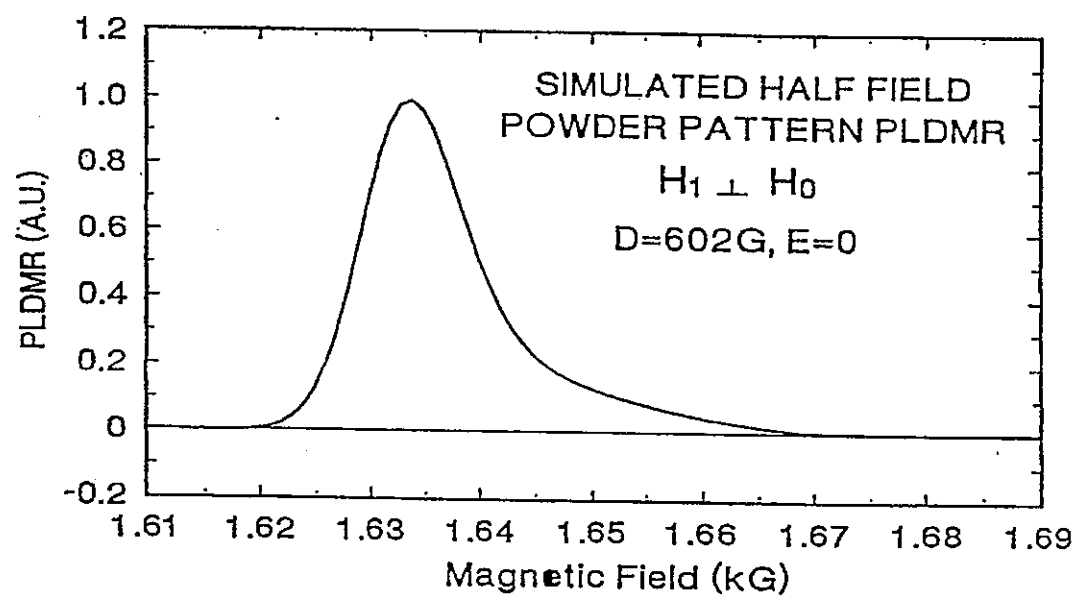


Figure 2.6. PLDMR half field  $(g \sim 4, \Delta m_s = \pm 2)$  powder pattern simulation for D = 602 G and E = 0.

Following Depinna et al., for a sine-shaped modulation of the excitation, the lock-in inphase output signal is:

$$X(\omega,\tau) = V_0 \frac{1}{1 + (\omega \pi)^2} \tag{29}$$

The lock-in quadrature output signal is:

$$Y(\omega,\tau) = V_0 \frac{\omega\tau}{1 + (\omega\tau)^2}$$
(30)

The total output signal then has a form

$$S(\omega,\tau) = V_0 \frac{1}{\sqrt{1 + (\omega\tau)^2}}$$
(31)

In all these expressions,  $\tau$  is the lifetime and  $\omega$  is the chopping frequency of the microwaves. As can be seen, the quadrature signal reaches its maximum when  $\omega \tau = 1$ , which can be used to derive the lifetime of the process. This is the simplest form of FR-ODMR. However, it is problematic if the resonance involves two or more processes with different lifetimes. On the other hand, fitting the resonance magnitude  $S(\omega \tau)$  vs.  $\omega$  curve to Eq. (31) also commonly used. If the process involves is more than one lifetime, the observed behavior is fitted to the sum of two Lorenzians, each given by Eq. (31).

# VI. Description of ODMR Experimental Apparatus

All ODMR spectra shown in this thesis were obtained using an ODMR spectrometer modified from an ESR system. The system detects the microwave-induced change in an optical transition vs. the applied magnetic field.

In this scheme, when using single crystal samples, the zero-field splitting (ZFS) parameters can be precisely determined. When polycrystalline or amorphous samples (as in all materials in OLEDs), the analysis of triplet powder patterns can also provide the ZFS parameters.

#### Zero-field ODMR

Zero-field ODMR does not require external magnetic field. In this technique, the microwave frequency is swept through a resonance condition, which occurs at the frequency equal to the zero-field splitting between the magnetic sublevels. Since the field is zero, it does not yield a powder pattern for random orientation of triplets. However, it cannot be used to study paramagnetic species with no zero-field splitting.

In electroluminescence (EL)-detected magnetic resonance (ELDMR) spectroscopy of OLEDs, the EL of the OLEDs is focused by lenses to an appropriate photodiode (with gain up to ~10<sup>6</sup>). The change of the EL is monitored by a lock-in detector, which allows one to detect signals with very low signal/noise ratio (SNR). When a specific wavelength range is of particular interest, optical filters or a monochrometer can be used to detect signals within that band. In this thesis, the ELDMR of a phosphorescent dye (PtOEP) lightly doped into Alq<sub>3</sub>, which yields both PtOEP and Alq<sub>3</sub> emission, was obtained by using a red and a green filter, respectively.

ODMR signals are normally very small, requiring lock-in detection. The output of the silicon photodiode which monitors the EL is therefore fed into the input of a lock-in amplifier and the signal is referenced to the amplitude modulation frequency. To detect an ODMR, the period of the modulation frequency should be long compared with the spin-lattice relaxation time (T<sub>1</sub>). By increasing the modulation frequency, the spin polarization is artificially limited, and this phenomena can be used to detect the lifetime of the species of interest (FR-ODMR).

Figure 7 is a schematic of the ODMR spectrometer used in this study. Most of the measurements were ELDMR. In PLDMR, visible excitaiton is provided by an argon ion laser (Ar+). A proper filter is used to block the laser light from entering the detector.

The system is mainly made of two sub-systems.

- 1. Microwave system: X-band microwaves were generated at ~9.45 GHz by a Gunn diode oscillator. The microwave amplitude is controlled by a calibrated attenuator and modulated by a pin-switch diode. The microwaves are amplified by a solid state linear amplifier, to up to 1400 mW. The coupling of the high-Q microwave cavity was done by adjustment of both the microwave frequency and a coupling screw at the cavity inlet.
- 2. Cryostat system: OLED samples were inserted into an Oxford Instruments continuous helium gas flow cryostat. The cryostat was made of quartz to avoid absorption of microwaves and centered in a high-Q TE mode microwave cavity. The temperature control was achieved by adjusting the helium flow rate and then using a temperature controller, in which a built-in heater is used to stablize the temperature to with in ~0.1K. The achievable temperature range is between ~5K to 300K.

In the ODMR measurement of OLEDs, the OLED is mounted on a sample holder rod made of Teflon. The sample holder is sealed onto a quartz tube. Two thin copper wires were connected to the electrodes of the OLED pass through the quartz tube and are connected the Kepco power supply. The current through the OLED is read from a Keithley 2000 multimeter.

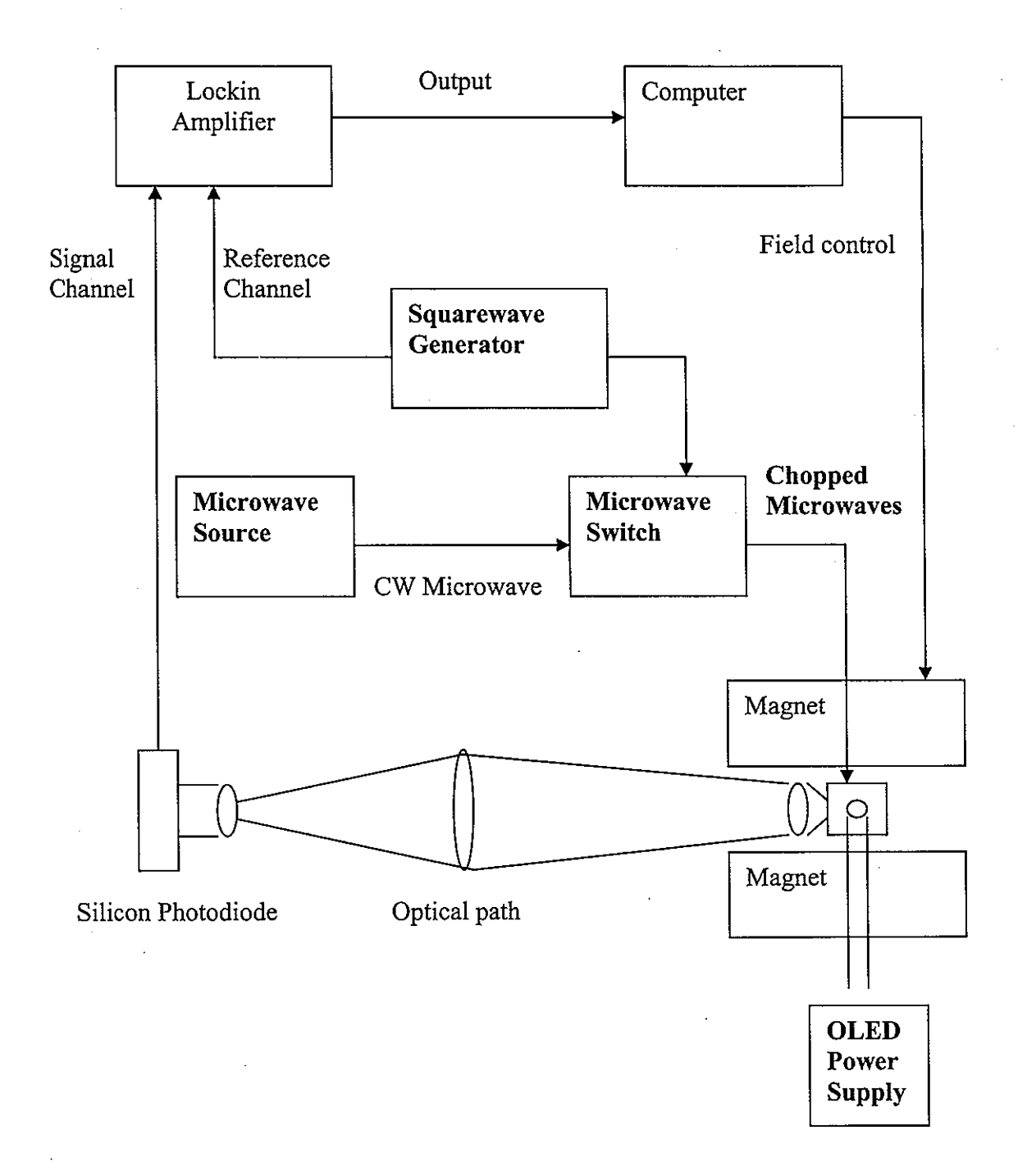


Figure 2.7. Schematic diagram of ODMR spectrometer used in this study, Set for ELDMR measurements.

# VII. Description of Dissertation organization

This dissertation consists of six chapters. The first two chapters are introduction of OLEDs and ODMR, respectively. In Chapter 3, the first magnetic resonance studies of tris-(8-hydroxyquinoline) Aluminum (Alq<sub>3</sub>)-based fluorescent OLEDs are described. EL-, PL-and EDMR techniques were used to study Alq<sub>3</sub> film and devices with different buffer layer between Alq<sub>3</sub> and Al cathode. Chapter 4 describes the ELDMR studies of Plantium octaethyl porphyrin (PtOEP) doped Alq<sub>3</sub> -based phosphorescent OLEDs. Devices with 4 different concentrations (1, 3, 6, and 20 wt-%) and one no dopping devices were studied. A general conclusion chapter summarizes the content in this dissertation.

#### References

- 1. J.H. van Vleck, The Theory of Elelctric and magnetic Susceptibilities, Oxford University Press, Oxford, (1932)
- 2. C. E. Cleeton and N. H. Williams, Phys. Rev. 45, 234 (1934)
- 3. C. J. Gorter, Physica 3, 995, (1936)
- C. P. Poole, Jr., Electron Spin Resonance: A Comprehensive Threaties on Experimental Techniques, 2<sup>nd</sup> Ed. (Dover Publications, Inc., Minneola, New York, 1996)
- 5. E. Zavoisky, J. Phys. USSR 9, 211 (1945)
- 6. E. M. Purcell, H. C. Torrey, and R. V. Pound, Phys. Rev. 69, 37 (1946)
- 7. F. Bloch, W. W. Hansen, and M. Packard, Phys. Rev., 69, 127 (1946)
- 8. J. Gmeiner, Acta Polym. 44, 201 (1993)
- 9. J. Köhler, J.A. J.M. Disselhorst, M. C. J. M. Donckers, E. J.J. Groenen, J. Schmidt, and W. E. Moerner, Nature, 363, 242 (1993)

- 10. J. Wrachtrup, C. von Borczyskowski, J. Bernard, M. Orrit, R. Brown, Nature 363, 244 (1993)
- 11. M. Sharnoff, J. Chem. Phys. 46, 3263 (1967)
- W. G. van Dorp. T. J. Schaafsma, M. Soma, and J. H. van de Waals, Chem. Phys. Lett.
   21, 221 (1973)
- 13. R. H. Clarke, and J. M. Hayes, J. Chem. Phys., 57, 569 (1972)
- 14. J. Shinar in handbookof Organic Conductive Molecules and Polymers Vol. 3 edited by H.S. Nalwa, (John Wiley & Sons, NY 1997) Chapter 7.
- 15. W. Gordy, Theory and Application of Electron Spin Resonance, Vol. 15 of Techniques of Chemistry (John Wiley & Sons, Inc., Minnelo, New York, 1996)
- 16. J.E. Wertz and J.R. Bolton, Electron Spin Resonance, Elementary Theory and Practical Applications, (McGraw-Hill, Inc., 1972)
- 17. N.M. Atherton, Elelctron Spin Resonance Theory and Applications (Halsted, NweYork, 1973)
- 18. S. P. Depinna and D. J. Dunstan, Philos. Mag. B 50, 579 1984

# Chapter 3. Magnetic Resonance Studies of Tris-(8-hydroxyquinoline) Aluminum-Based Organic Light-Emitting Devices

(Submitted to Physics Review B)

G. Li, <sup>1</sup> C. H. Kim, <sup>1</sup> P. A. Lane, <sup>2</sup> and J. Shinar <sup>1</sup>

<sup>1</sup>Ames Laboratory - USDOE and Department of Physics and Astronomy

Iowa State University, Ames, IA 50011

<sup>2</sup>C. S. Draper Laboratory, 555 Technology Square, Cambridge, MA 02139

#### **Abstract**

Electroluminescence (EL)-, electrically, and photoluminescence (PL)-detected magnetic resonance studies of tris-(8-hydroxyquinoline) aluminum (Alq<sub>3</sub>)-based organic light-emitting devices (OLEDs) and films are described. At low temperatures, a spin-1/2 resonance enhances the current density J, the EL intensity  $I_{EL}$ , and the PL intensity  $I_{PL}$  ( $\Delta J/J$ ,  $\Delta I_{EL}/I_{EL}$ , and  $\Delta I_{PL}/I_{PL} > 0$ ).  $\Delta J/J$  and  $\Delta I_{EL}/I_{EL}$  are insensitive to the nature of the Alq<sub>3</sub>/cathode interface. They weaken with increasing T and become unobservable above 60 K.  $\Delta I_{PL}/I_{PL}$  also decreases with T, but more slowly, and it is still observable at 250 K. The resonance is attributed to either of two mechanisms: (i) The reduction of singlet exciton (SE) quenching by a reduced population of polarons in the bulk of the Alq<sub>3</sub> layer, and/or (ii) the enhanced formation of SEs at the expense of triplet excitons (TEs). These assignments are discussed in relation to the yield of SEs and TEs in OLEDs in general and in Alq<sub>3</sub>-based devices in particular.

At  $T \approx 60$  K, another spin-1/2 resonance, which reduces both J and  $I_{EL}$  (but is unobservable in the PL), emerges and grows with increasing T. This negative J and EL-

detected resonance is sensitive to the buffer layer between Alq<sub>3</sub> and the cathode, and is attributed to magnetic resonance enhancement of the spin-dependent formation of negative spinless bipolarons from spin-1/2 negative polarons at the organic/cathode interface. Its behavior provides insight into the nature of this interface and the interface's strong impact on the device properties. In particular, the increase in the negative charge density at this interface, and the resulting increase in the field throughout the organic layers by this negative sheet of charge, which increases the field-induced SE dissociation rate, are in quantitative agreement with the behavior of this negative resonance.

PACS Nos. 85.65.+h, 85.60.-q, 85.30.-z, 76.90.+d

### I. Introduction

Organic light-emitting devices (OLEDs) have drawn extensive attention since electroluminescence (EL) was observed from devices based on tris-(8-hydroxy quinoline) Al  $(Alq_3)^1$  and poly(para-phenylene vinylene) (PPV)<sup>2</sup>. The brightness, efficiency, and lifetime of OLEDs have increased dramatically over the past decade. However, with the exception of OLEDs using phosphorescent dopants<sup>3</sup>, the external EL quantum efficiency  $\eta_{ext}$  remains stubbornly capped at ~5%. This cap has been attributed to the product of the maximum formation efficiency of singlet excitons (SEs) from nongeminate polaron recombination  $\eta_{SE} = 25\%^4$  and the outcoupling efficiency of the emission to the front face of the device  $\gamma = 1/(2n^2) \sim 1/6$ , where  $n \sim 1.7$  is the refractive index of the substrate<sup>4</sup>. Recent theoretical<sup>5,6</sup> and experimental<sup>7,8</sup> studies imply that  $\eta_{SE}$  could be as high as 60% and  $\gamma = 1/n^2 \sim 1/3$ , so the maximal  $\eta_{ext}$  could be as high as ~20%. However, the experimental evidence for the high values of  $\eta_{SE}$  is either model-dependent<sup>7</sup> or restricted to polymers containing Pt in their backbone <sup>8</sup>.

Nonradiative SE quenching processes such as electric-field induced SE dissociation<sup>9</sup>, energy transfer to the electrodes<sup>10</sup>, and quenching by polarons <sup>11</sup> and triplet excitons (TEs) <sup>12</sup>, could contribute significantly to the large gap between the observed and theoretical  $\eta_{ext}$ . Since the dynamics of polarons and TEs are spin-dependent, it is not surprising that magnetic resonance spectroscopy has proven to be a powerful tool in studying the physics of these materials and devices<sup>7,11-18</sup>. These studies have provided direct evidence for the presence of long-lived polarons and triplet excitons in both photoexcited films and biased OLEDs, and they have been used to explore the interactions of these excitations with SEs.

This paper describes EL- and electrically (i.e, current density J)-detected magnetic resonance (ELDMR and EDMR, respectively) studies of N,N'-diphenyl-N,N'-bis(3methylphenyl)-(1,1'-biphenyl)-4,4'-diamine  $(TPD)/Alq_3$ OLEDs, well the photoluminescence (PL)-detected magnetic resonance (PLDMR) of Alg<sub>3</sub> films. The measurements yield a positive (i.e., EL-, J-, and PL-enhancing) spin-1/2 resonance at low temperatures, which is due either to reduced quenching of SEs by a reduced population of polarons<sup>19</sup> or to enhanced formation of SEs at the expense of TEs<sup>7,18</sup>. However, the latter assignment implies that the SE yield in Alq<sub>3</sub> OLEDs is greater than 25%, which is contrary to previous conclusions 7,8,20,21. Besides this low-temperature positive spin-1/2 resonance, a high-temperature negative spin-1/2 ELDMR and EDMR (but no negative PLDMR) is also observed. It is concluded to result from the spin-dependent formation of negative spinless bipolarons from spin-1/2 polarons<sup>19</sup> at the Alq<sub>3</sub>/cathode interface, as it is highly sensitive to the presence and nature of the buffer layer between the Alq3 and the cathode. Formation of bipolarons at the organic/cathode interface increases the areal density of charge at that interface. Since the active area of the devices is ~20 mm<sup>2</sup> but the total thickness of the

organic layers is only ~100 nm, an increase in the areal charge density at the organic/cathode interface increases the electric field by a uniform amount everywhere in the device. In particular, it also increases the electric field in the recombination zone, which is adjacent to the TPD/Alq<sub>3</sub> interface. This increase in the electric field increases the field-induced dissociation of SEs and results in reduced EL. Indeed, several theoretical studies have predicted that a high density of negative bipolarons forms at the organic/cathode interface<sup>22-24</sup>, and UV and X-ray photoelectron spectroscopy measurements have confirmed their presence <sup>25,26</sup>.

# II. Experimental Methods

The OLEDs consisted of an indium tin oxide (ITO) anode, a 15 nm-thick copper phthalocyanine (CuPc) hole-injection layer, a 25 nm-thick TPD hole-transport layer, and a 40 nm-thick emissive Alq<sub>3</sub> layer. A ~1 nm-thick CsF<sup>27-29</sup> or ~3 nm-thick AlO<sub>x</sub> buffer layer<sup>30</sup> was evaporated on top of the Alq<sub>3</sub> layer, followed by evaporation of the Al cathode. The chemical structures of CuPc, TPD, and Alq<sub>3</sub> are shown in Fig. 1 and the device structure is shown in the inset of Fig. 2(a).

The OLEDs were fabricated by thermal vacuum evaporation in a  $\sim 10^{-6}$  torr vacuum chamber installed in an argon-filled glove box, typically containing  $\sim 0.5$  ppm oxygen and water. Prior to deposition of the organic layers, the ITO coated glass was thoroughly cleaned as described elsewhere  $^{30,31}$ . The deposition rates were monitored by a Maxtek TM-100 thickness monitor. The organic layers were deposited at  $\sim 2$  Å/sec. The CsF was deposited similarly at  $\sim 0.1$  Å/s. The AlO<sub>x</sub> layer was fabricated by depositing a  $\sim 15$  Å layer of Al, followed by 5 min exposure to air. The OLEDs had an active area of  $\sim 0.2$  cm<sup>2</sup>.

The magnetic resonance spectra were measured by placing an OLED or an Alq<sub>3</sub> film in an optically accessible microwave cavity between the pole pieces of a DC electromagnet, as described previously <sup>11-15,17</sup>. Changes in the EL intensity (ELDMR), current density *J* (EDMR), or PL (PLDMR) were measured by lock-in detection of the changes in the EL, *J*, or PL induced by the microwaves, which were chopped at 500 Hz. For the changes in the EL and *J*, the microwave power was 360 mW at 9.45 GHz; for the changes in the PL, it was 811 mW at 9.34 GHz. Magnetic resonance conditions occur when the Zeeman splitting between two spin sublevels equals the microwave photon energy

$$h v = g \beta H, \tag{1}$$

where  $h\nu$  is the microwave photon energy, g is the gyromagnetic ratio,  $\beta$  is the Bohr magneton, and H is the magnetic field strength <sup>32</sup>. Magnetic resonance conditions equalize the populations of the spin sublevels, which in turn affects the populations of the excited states<sup>32</sup>.

#### III. Results

Fig. 2(a) shows the room-temperature current density-voltage J(V) characteristics of CsF-and AlO<sub>x</sub>-buffered OLEDs. Both devices show rectifying behavior; the behavior of the EL-voltage curve  $I_{EL}(V)$  was similar. Note that the buffer layer has a dramatic effect on J(V). The AlO<sub>x</sub>-buffered device requires roughly 2 V higher bias than the CsF-buffered device to achieve the same current density. The buffer layer also affects the EL efficiency, as shown in Fig. 2(b). The peak efficiency of the CsF-buffered OLED is more than double that of the AlO<sub>x</sub>-buffered devices. The efficiency of both devices decreases at higher bias, owing to

increasing quenching by the electric field and, possibly, quenching of SEs by polarons, either free or trapped.

Fig. 3 shows the spin-1/2 ELDMR spectra of (a) AlO<sub>x</sub>- and (b) CsF-buffered OLEDs at temperatures from 15 to 295 K. Both devices have a positive (EL-enhancing) resonance below 60 K that decreases in amplitude with increasing temperature and a negative (EL-quenching) resonance that becomes evident at T = 60 K and increases in amplitude with increasing temperature. The enhancing and quenching resonances have similar g values, though the linewidths are different. This can be seen in the 60 K ELDMR of the AlO<sub>x</sub> device, which contains both positive and negative resonances. While the amplitude  $|\Delta I_{EL}/I_{EL}|$  of the positive resonance is similar in the two types of devices, the negative resonance is much weaker in the CsF-buffered devices.

Fig. 4 shows the dependence of the ELDMR amplitude  $|\Delta I_{EL}/I_{EL}|$  on J. The behavior of the amplitude of the quenching resonance differs qualitatively from that of the enhancing resonance and between the two devices. In the CsF-buffered OLEDs, it decreases with increasing J as  $J^{0.4}$ , whereas in the AlO<sub>x</sub>-buffered devices it increases from  $2.2 \times 10^{-4}$  at 0.5 mA/cm<sup>2</sup> to  $2.9 \times 10^{-4}$  at 7 mA/cm<sup>2</sup>. In contrast to the positive resonance, the negative resonance increases with increasing temperature.

Fig. 5 shows the spin-1/2 PLDMR spectrum of an Alq<sub>3</sub> film at several temperatures. The resonance is positive ( $\Delta I_{PL}/I_{PL} > 0$ ) and its amplitude decreases from  $9.1 \times 10^{-5}$  at T = 10 K to  $2.4 \times 10^{-5}$  at T = 250 K. This decrease with increasing T is much more moderate than that of the positive ELDMR  $\Delta I_{EL}/I_{EL}$ . It is suspected that the positive ELDMR decreases much more rapidly due to overlap with the negative resonance. The similarity between the behavior of

the positive ELDMR and PLDMR leads us to assign the positive resonance to enhanced polaron recombination under magnetic resonance conditions. This mechanism requires the presence of both positive and negative polarons, which occurs only in the bulk of an OLED under operation.

Fig. 6 shows the laser power-dependence of the spin-1/2 PLDMR of the Alq<sub>3</sub> film. As clearly seen, at low power  $\Delta I_{PL}/I_{PL}$  depends linearly on the power, but it saturates to a sublinear behavior at high power. This behavior is qualitatively similar to that of the positive spin-1/2 PLDMR of various oligomers and polymers studied to date 11,13,17,18.

Fig. 7 shows the spin-1/2 EDMR spectra of both CsF- and AlO<sub>x</sub>-buffered OLEDs from 15 to 295 K. Similar to the ELDMR, the EDMR is positive (*J*-enhancing) below 60 K and negative (*J*-quenching) above 60 K.

The distinct behavior of the positive and negative resonances suggests different origins. In turning to the discussion of these resonances, we consequently treat each resonance separately.

#### IV. Discussion

#### IV(a). The Positive Spin-1/2 Resonance.

In both devices, the amplitude of the positive spin-1/2 ELDMR decreases rapidly with temperature and increases sublinearly with current density. This behavior is similar to the temperature- and laser power-dependence of the positive spin-1/2 PLDMR amplitude of various  $\pi$ -conjugated polymers [11,13,17,18]. In all previous studies, this resonance was attributed to magnetic resonance enhancement of the overall polaron recombination rate. This enhancement of the overall polaron recombination rate is confirmed by several photoinduced

absorption (PA)-detected magnetic resonance (PADMR) measurements, which demonstrated that the overall polaron population decreases at resonance <sup>7,11,16,18,21</sup>.

One scenario that has been proposed for the origin of the positive spin-1/2 resonance is based on the assumption that the enhanced polaron recombination is due to the difference between the cross section for SE formation from singlet polaron pairs  $\sigma_{SE}$  and TE formation from triplet polaron pairs  $\sigma_{TE}$  <sup>7,8,18.21</sup>. In that scenario,  $\sigma_{SE} > \sigma_{TE}$ . Hence, off-resonance, the population of nongeminate singlet polaron pairs  $n_{SPP}$  is depleted relative to the population of nongeminate triplet polaron pairs  $n_{TPP}$ . On resonance,  $n_{SPP}$  increases at the expense of  $n_{TPP}$ , and the PL increases. Wohlgenannt et al. have shown that in several polymers the excitation power-dependence of this resonance is in good agreement with a model based on this scenario <sup>18</sup>. Yet if this scenario is the origin of the resonance in Alq<sub>3</sub>, it implies that in this material  $\sigma_{SE} > \sigma_{TE}$  and the yield of SEs in Alq<sub>3</sub>-based OLEDs is greater than 25%. This conclusion is contrary to that of several previous studies <sup>7,8,18,21</sup>.

Another scenario that has been proposed for the origin of the positive spin-1/2 resonance is based on the well-known evidence that polarons quench SEs <sup>11,17,33,34</sup>. At resonance a reduced polaron population reduces the SE quenching rate, thereby increasing the emission. List et al. have shown that in oligophenylenes and methyl-bridged ladder-type poly(*p*-phenylenes) the excitation power dependence of the resonance is in good agreement with a rate equation model based on this scenario <sup>11</sup>.

## IV(b). The Negative Spin-1/2 Resonance.

As mentioned above, the *J*-dependence of the amplitude of the quenching resonance (Fig. 4) differs qualitatively from that of the enhancing resonance and between the two devices. In

the CsF-buffered OLEDs, it decreases with increasing current as  $J^{0.4}$ , whereas in the AlO<sub>x</sub>-buffered devices it increases moderately with J, from  $2.2 \times 10^{-4}$  at  $0.5 \text{ mA/cm}^2$  to  $2.9 \times 10^{-4}$  at  $7 \text{ mA/cm}^2$ . In contrast to the positive resonance, the amplitude of the quenching resonance increases with temperature.

There are two nonradiative species that can be generated from polaron recombination: Spin-1 TEs and spinless bipolarons. Resonant enhancement of TE formation at the expense of SEs would reduce the EL intensity. However, it has been shown that the TE population decreases at the spin 1/2 resonance field <sup>7,11,16,18,21</sup>. Furthermore, this process would not affect the current density in the device and hence the EDMR spectrum should contain only a positive resonance. However, as mentioned above, Fig. 8 shows that similar to the ELDMR, the EDMR is positive (*J*-enhancing) below 60 K and a negative (*J*-quenching) above 60 K. Hence, enhanced triplet formation cannot account for the negative spin-1/2 resonance.

The observation of negative EL- and *J*-detected spin-1/2 resonances is, however, entirely consistent with bipolaron formation. Several theoretical studies have suggested that a high density of negative bipolarons -- indeed a bipolaron lattice -- may be generated to form a dipole layer at the organic/metal cathode interface of OLEDs <sup>22-24</sup>. UV and X-ray photoelectron spectroscopy (UPS and XPS, respectively) studies have confirmed the presence of bipolarons at the interface <sup>25,26</sup>. Furthermore, there is direct experimental evidence for enhanced bipolaron formation under magnetic resonance conditions in both small molecules and polymers <sup>35,36</sup>.

The mobility of bipolarons should be much lower than that of polarons in. Hence, the negative ELDMR and EDMR signals are correlated with one another. We therefore conclude that the EL- and J-quenching resonances are due to the spin-dependent formation of spinless

bipolarons; their strong dependence on the buffer layer demonstrates that these bipolarons are located at the organic/cathode interface. Since the positive charge density is very low near the cathode, the resonance is assigned to the enhanced formation of negative bipolarons at this interface.

The negative ELDMR cannot be due to direct quenching of SEs by bipolarons since the recombination zone lies on the Alq<sub>3</sub> side of the TPD/Alq<sub>3</sub> interface while the bipolarons must be located at the Alq<sub>3</sub>/cathode interface. Likewise, relatively few positive polarons will reach the counter electrode and be quenched. We propose that the quenching ELDMR is due to the enhanced electric field generated throughout the organic layers by the enhanced charge layer at the Alq<sub>3</sub>/cathode interface. Kalinowski et al. have previously shown that the EL external quantum yield of the EL  $\eta_{ext}$  in TPD/Alq<sub>3</sub> OLEDs decreases above an electric field of 0.75 MV/cm<sup>37</sup>.

The effect of bipolaron formation and consequent enhanced negative charge density at the Alq<sub>3</sub>/cathode interface on the EL (which results in the negative ELDMR) can be estimated from the magnitude of the EDMR signal. The generation rate of bipolarons is  $G = \eta_{BP}J/et$ , where  $\eta_{BP}$  is the fraction of current that is trapped to form biplarons, e is the electron charge, and t is the thickness of the charge layer. The current density in the AlO<sub>x</sub>-buffered devices is 40 mA/cm<sup>2</sup>, the EDMR signal gives the fractional change in trapped charge  $\Delta J/J = 5 \times 10^{-4}$ , and we assume  $t \sim 2.5$  nm. Hence  $G = 5 \times 10^{20}$  cm<sup>-3</sup>sec<sup>-1</sup>. The steady state density of trapped charge is  $n = G\tau$ , where  $\tau$  is the bipolaron lifetime. Bipolaron lifetimes in molecular semiconductors are typically  $10^{-5} - 10^{-4}$  sec<sup>-38</sup>. The trapped charge density is therefore of order  $5 \times 10^{15} \le n \le 5 \times 10^{16}$  cm<sup>-3</sup> and the associated electric field  $10^3 \le F = \sigma/e_0 = net/e_0 \le 10^4$ 

V/cm. Assuming a built-in potential of 2.5 V, the electric field in the active layer of the  $AlO_x$ -buffered OLED should be ~1 MV/cm, sufficient for field quenching of the EL. The magnetic resonance-induced electric field modulation of  $10^3$  -  $10^4$  V/cm will reduce  $\eta_{ext}$  by 0.25% - 2.5%, in excellent agreement with the behavior of the room temperature ELDMR (Figs. 3 and 4). The behavior of the CsF-buffered OLEDs shows a similar correlation between the ELDMR and EDMR spectra.

The bipolaron model also explains the J-dependence of the Lorentzian linewidth  $\Delta H_{1/2}$ and  $|\Delta I_{EL}/I_{EL}|$ . Fig. 8 shows that in the CsF-buffered devices,  $\Delta H_{1/2} \approx 22$  G, almost independent of J. In contrast, in the AlO<sub>x</sub>-buffered OLEDs, it increases from ~23 G at low Jto  $\sim$ 34 G at J = 7.5 mA/cm<sup>2</sup>. The dipolar broadening contribution to  $\Delta H_{1/2}$  can provide an estimate of the average distance d between polarons<sup>32</sup>. A residual linewidth of ~15 G was estimated from measurements on similar OLEDs with no intentional buffer layer and is attributed to mechanisms other than dipolar broadening (e.g., hyperfine interaction between the polarons and protons in Alq<sub>3</sub>) <sup>32</sup>. Taking into account the residual linewidth,  $d \approx 1.1$  nm in the CsF-buffered devices. In the AlO<sub>x</sub>-buffered OLEDs, it decreases from ~1.0 nm to ~0.8 nm as J increases to 7.5 mA/cm<sup>2</sup>. Since bipolarons require a counterion for stabilization  $^{39,40}$ , the model implies that the density of counterions is much higher in AlO<sub>x</sub>-buffered devices. Previous SEM and XPS measurements on the AlOx-buffered devices revealed pinholes and a very high carbon content in the buffer region<sup>41</sup>. Other UPS and XPS studies have demonstrated a strong reaction between Al metal and Alq342. This issue clearly deserves additional attention.

The decrease of  $|\Delta I_{EL}/I_{EL}|$  with increasing J in CsF-buffered devices implies that the density of bipolarons reaches its maximal value at low J. As J increases, the formation of bipolarons becomes less spin-dependent and  $|\Delta I_{EL}/I_{EL}|$  consequently decreases. This behavior and scenario are consistent with previous studies of poly(p-phenylene vinylene) OLEDs <sup>15</sup>.

The bipolaron model also explains the temperature dependence of the quenching ELDMR. Since there is a Coulomb barrier to form bipolarons from polaron pairs, increasing T enhances their formation, so  $|\Delta I_{EL}/I_{EL}|$  increases. Fig. 9 shows  $\log(|\Delta I_{EL}/I_{EL}|)$  vs. 1000/T for the AlO<sub>x</sub>-buffered devices. The behavior above T = 100 K yields an activation energy of 11.6 meV. The results deviate from the straight line below for T = 100 K due to overlap of the positive and negative resonance.

The foregoing results and analysis demonstrate the importance of the buffer layer in determining the behavior of the OLEDs. The observation of the negative resonance in OLEDs with a CsF buffer layer demonstrates that further improvement in buffer layers is possible and desirable.

#### V. Summary and Concluding Remarks

In conclusion, the spin-1/2 ELDMR and EDMR of Alq<sub>3</sub>-based OLEDs with thin CsF or AlO<sub>x</sub> buffer layers between the Alq<sub>3</sub> and the Al cathode is positive (EL- and current-enhancing) below 60 K and negative (EL-quenching) above 60 K. The positive resonance is attributed to enhanced recombination of polarons in the recombination zone. The negative resonance was shown to result from magnetic resonance enhancement of formation of negative spinless bipolarons at the organic/cathode interface. The increased charge density at the injecting electrode increases the internal electric field within the device, reducing the

radiative yield. This increased charge density also reduces current injection, reducing device efficiency and increasing the operating bias. Thus, the superior performance of the CsF-buffered OLEDs relative to the AlO<sub>x</sub>-buffered devices may be due to a reduced negative charge density at the organic/cathode interface, which should result in a smaller barrier for electron injection from the cathode.

## Acknowledgements

Ames Laboratory is operated by Iowa State University for the US Department of Energy under Contract W-7405-Eng-82. This work was supported by the Director for Energy Research, Office of Basic Energy Sciences.

#### References

- 1. C. W. Tang and S. A. Van Slyke, Appl. Phys. Lett. 51, 913 (1987).
- 2. J. H. Burroughes, D. D. C. Bradley, A. R. Brown, R. N. Marks, K. MacKay, R. H. Friend, P. L. Burn, and A. B. Holmes, Nature 347, 539 (1990).
- M. A. Baldo, D. F. O'Brien, Y. You, A. Shoustikov, S. Sibley, M. E. Thompson, and S. R. Forrest, Nature 395, 151 (1998).
- R. H. Friend, R. W. Gymer, A. B. Holmes, J. H. Burroughes, R. N. Marks, C. Taliani, D. D. C. Bradley, D. A. Dos Santos, J. L. Brédas, M. Lögdlund, and W. R. Salaneck, Nature 397, 121 (1999).
- Ji-Seon Kim, Peter K. H. Ho, Neil C. Greenham, and Richard H. Friend, J. Appl. Phys. 88, 1073 (2000).
- 6. Z. Shuai, D. Beljonne, R. J. Silbey, and J. L. Bredas, Phys. Rev. Lett. 84, 131 (2000).

- 7. M. Wohlgenannt, Kunj Tandon, S. Mazumdar, S. Ramasesha, and Z. V. Vardeny, Nature 409, 494 (2001).
- J. S. Wilson, A. S. Dhoot, A. J. A. B. Seeley, M. S. Khan, A. Köhler, and R. H. Friend,
   Nature 413, 828 (2001).
- 9. R. Kersting, U. Lemmer, M. Deussen, H. J. Bakker, R. F. Mahrt, H. Kurz, V. I. Arkhipov, H. Bässler, and E. O. Göbel, Phys. Rev. Lett. 73, 1440 (1994).
- 10. H. Becker, S. E. Burns, and R. H. Friend, Phys. Rev. B 56, 1893 (1997).
- 11. E. J. W. List, C.-H. Kim, A. K. Naik, U. Scherf, G. Leising, W. Graupner, and J. Shinar, Phys. Rev. B 64, 155204 (2001).
- 12. E. J. W. List, U. Scherf, K. Müllen, W. Graupner, C.-H. Kim, and J. Shinar, Phys. Rev. B 66, 235203 (2002).
- 13. L. S. Swanson, J. Shinar, and K. Yoshino, Phys. Rev. Lett. 65, 1140 (1990).
- 14. L. S. Swanson, P. A. Lane, J. Shinar, and F. Wudl, Phys. Rev. B 44, 10617 (1991).
- L. S. Swanson, J. Shinar, A. R. Brown, D. D. C. Bradley, R. H. Friend, P. L. Burn, A. Kraft, and A. B. Holmes, Phys. Rev. B 46, 15072 (1992).
- 16. X. Wei, B. C. Hess, Z. V. Vardeny, and F. Wudl, Phys. Rev. Lett. 68, 666 (1992).
- 17. N. C. Greenham, J. Shinar, J. Partee, P. A. Lane, O. Amir, F. Lu, and R. H. Friend, Phys. Rev. B 53, 13528 (1996).
- 18. M. Wohlgenannt, C. Yang, and Z. V. Vardeny, Phys. Rev. B 66, 241201(R) (2002).
- 19. In this paper, we neglect the distinction between electrons and negative polarons and between holes and positive polarons. Similarly, we neglect the distinction between negative bipolarons and dianions.

- 20. M. A. Baldo, D. F. O'Brien, M. E. Thompson, and S. R. Forrest, Phys. Rev. B 60, 14422 (1999).
- M. Wohlgenannt, X. M. Jiang, Z. V. Vardeny, and R. A. J. Janssen, Phys. Rev. Lett. 88, 197401 (2002).
- 22. N. Kirova and S. Brazovskii, Syn. Met. 76, 229 (1996).
- 23. P. S. Davids, A. Saxena, and D. L. Smith, Phys. Rev. B 53, 4823 (1996).
- 24. M. N. Bussac, D. Michoud, and L. Zuppiroli, Phys. Rev. Lett. 81, 1678 (1998).
- 25. L. S. Liao, L. F. Cheng, M. K. Fung, C. S. Lee, S. T. Lee, M. Inbasekaran, E. P. Woo, and W. W. Wu, Chem. Phys. Lett. 325, 405 (2000); Phys. Rev. B 62, 10004 (2000).
- 26. G. Greczynski, M. Fahlman, and W. R. Salaneck, J. Chem. Phys. 113, 2407 (2000).
- 27. L. S. Hung, C. W. Tang, and M. G. Mason, Appl. Phys. Lett. 70, 152 (1997)
- 28. G. E. Jabbour, B. Kippelen, N. R. Armstrong, and N. Peyghambarian, Appl. Phys. Lett. 73, 1185 (1998).
- G. E. Jabbour, B. Kippelen, N. R. Armstrong, and N. Peyghambarian, Appl. Phys. Lett.
   73, 2218 (1998).
- 30. F. Li, H. Tang, J. Anderegg, and J. Shinar, Appl. Phys. Lett. 70, 1233 (1997).
- 31. F. Li, H. Tang, J. Shinar, O. Resto, and S. Z. Weisz, Appl. Phys. Lett. 70, 2741 (1997).
- 32. C. P. Poole, Electron Spin Resonance: A Comprehensive Treatise on Experimental Techniques (Dover Publications, Mineola, NY, 1983).
- 33. S. Hayashi, K. Kaneto, and K. Yoshino, Sol. St. Comm. 61, 249 (1987)
- 34. D. D. C. Bradley and R. H. Friend, J. Phys. Condensed Matter 1, 3671 (1989).
- 35. P. A. Lane, X. Wei, and Z. V. Vardeny, Physical Review Letters 77, 1544 (1996).

- 36. P. A. Lane, M. Liess, J. Partee, J. Shinar, A. J. Frank, and Z. V. Vardeny, Chem. Phys. 227, 57 (1998).
- J. Kalinowski, L. C. Picciolo, H. Murata, and Z. H. Kafafi, J. Appl. Phys. 89, 1866
   (2001).
- P. A. Lane, M. Liess, J. Partee, J. Shinar, A. J. Frank, and Z. V. Vardeny, Chem. Phys.
   227, 57 (1998).
- 39. E. Conwell, in *Primary Photoexcitations in Conjugated Polymers*, edited by N. S. Sariciftci, p. 489 (World Scientific Publications, Singapore, 1998)
- 40. W. R. Salaneck, R. H. Friend, and J. L. Bredas, Phys. Repts. 319, 231 (1999).
- 41. K. E. Junge, J. Shinar, M. J. Kramer, T.E. Bloomer, and J. Anderegg, unpublished results.
- 42. Q. T. Le, L. Yan, Y. Gao, M. G. Mason, D. J. Giesen, and C. W. Tang, J. Appl. Phys. 87, 375 (2000).

# Figures

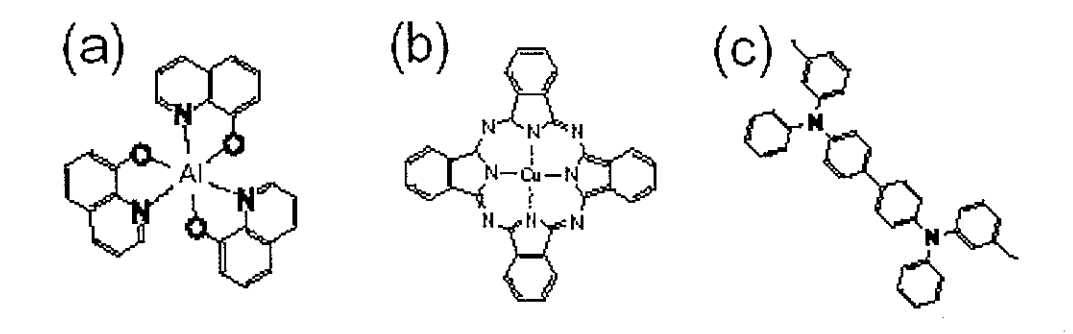


Fig. 1. Molecular structures of (a) tris-(8-hydroxy quinoline) Al (Alq<sub>3</sub>), (b) copper phthalocya-nine (CuPc), and (c) N,N'-diphenyl-N,N'-bis(3-methylphenyl)-(1,1'-biphenyl)-4,4'-diamine (TPD).

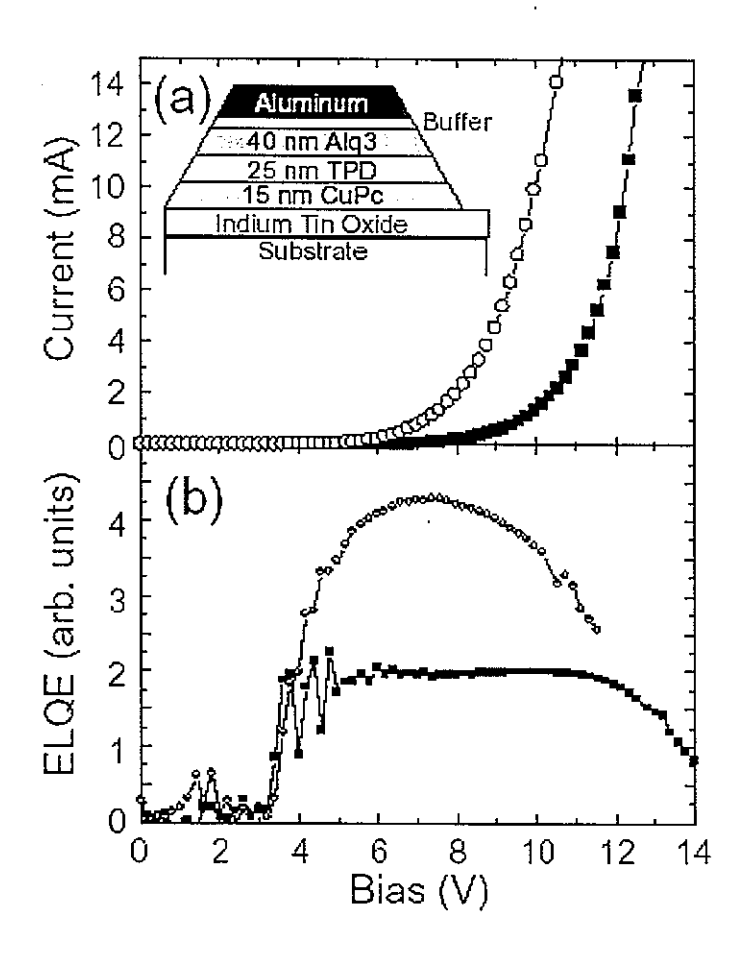


Fig. 2. The room-temperature (a) current density-voltage and (b) EL quantum efficiency (ELQE) of OLEDs with CsF buffer layers (open circles) and  $AlO_x$  buffer layers (solid squares) vs. the bias voltage V. Inset: The structure of the OLEDs.

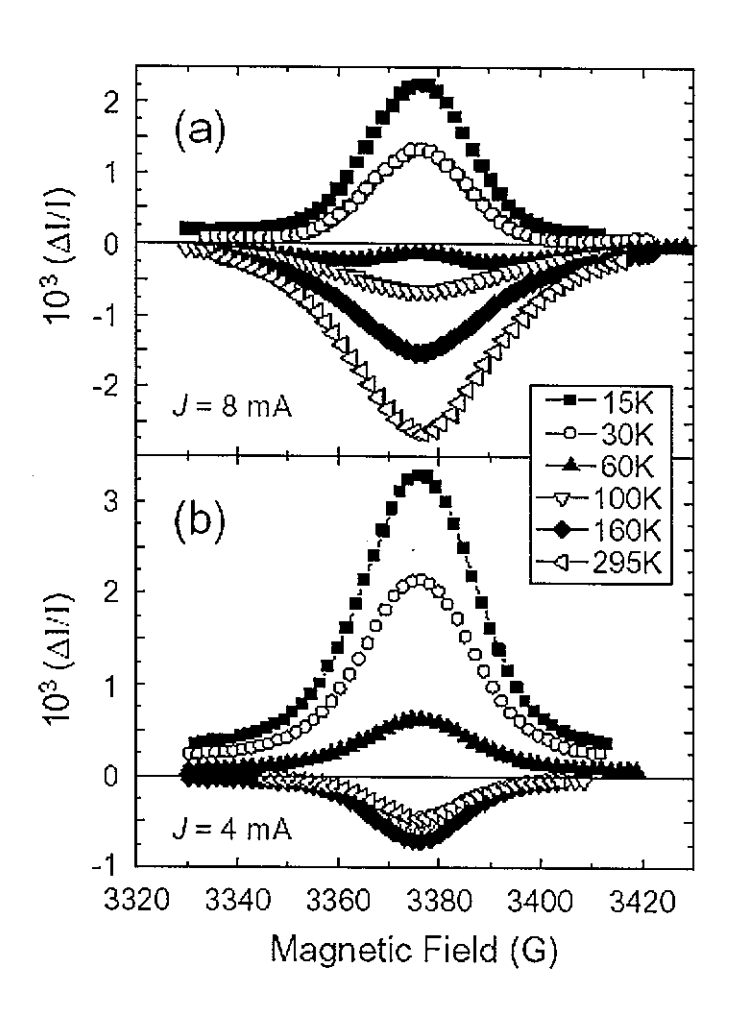


Fig. 3. The spin-1/2 ELDMR spectra of OLEDs with (a) AlO<sub>x</sub> and (b) CsF buffer layers, at  $15 \le T \le 295$  K.

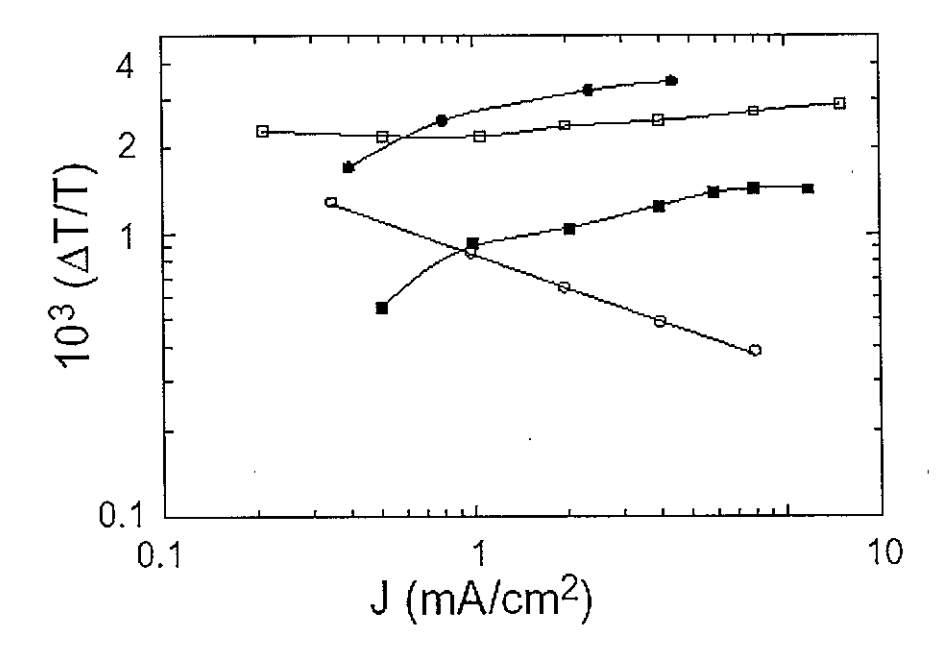


Fig. 4. The current density *J*-dependence of the amplitude of the spin-1/2 ELDMR  $|\Delta I_{EL}/I_{EL}|$ . The enhancing (quenching) resonance of CsF-buffered devices is shown as filled (open) circles. The enhancing (quenching) resonance of AlO<sub>x</sub>-buffered devices is shown as filled (open) squares.

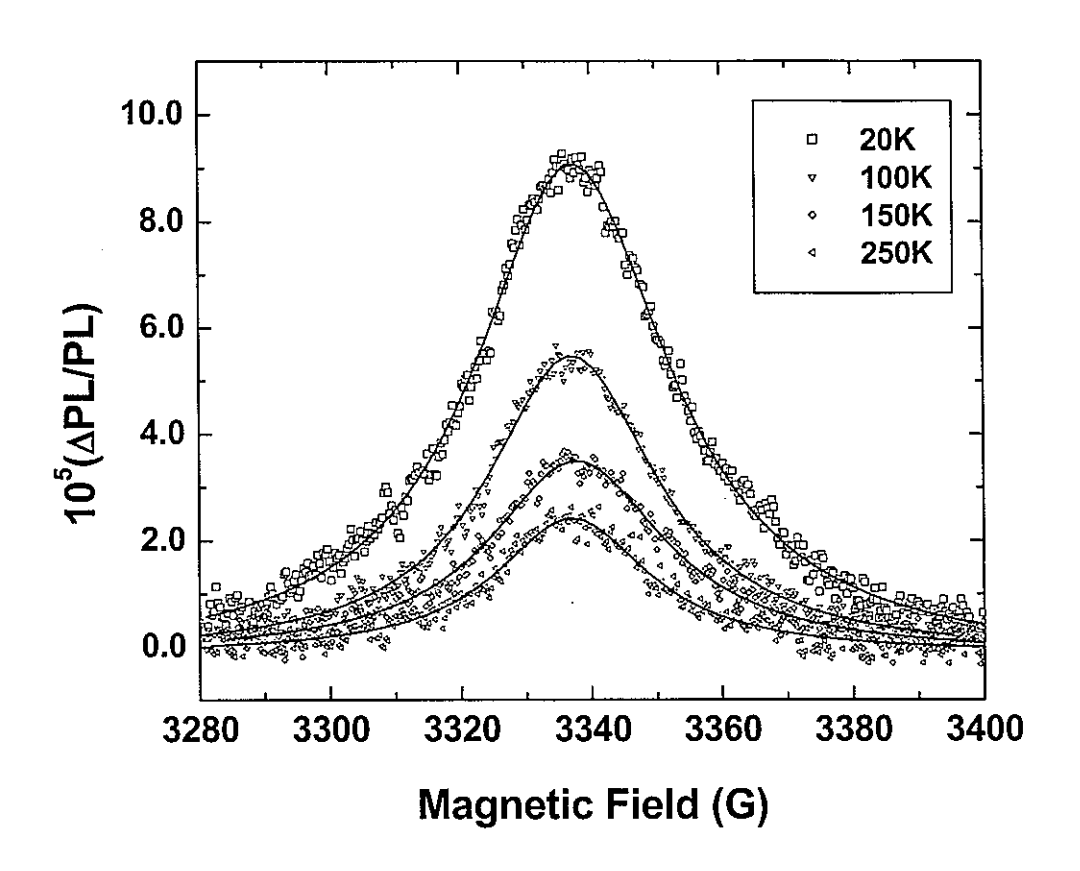


Fig. 5. The PLDMR of a 330 nm thick Alq<sub>3</sub> film vacuum evaporated on a quartz substrate, at T = 20, 100, 150, and 250 K (the amplitude decreases monotonically with increasing T). The PL was excited by the 65 mW UV multiline output of an Ar<sup>+</sup> laser at 351 – 363 nm.

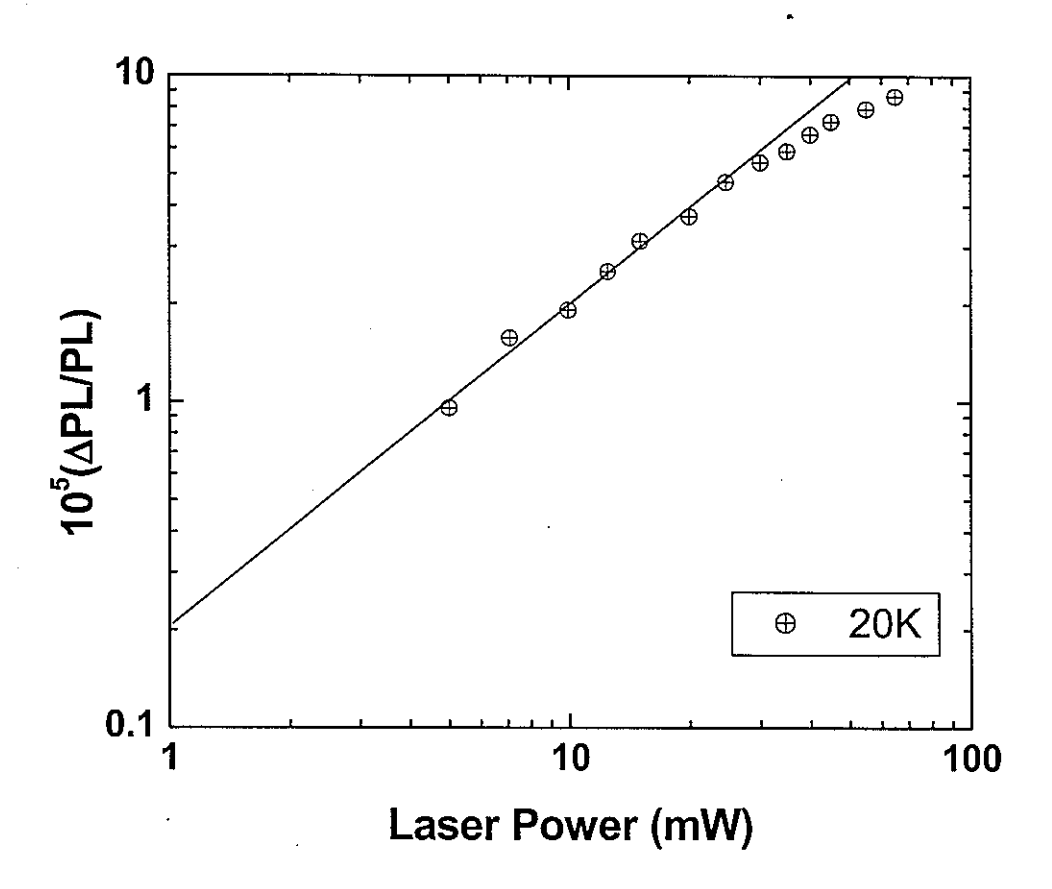


Fig. 6. Laser power-dependence of the PLDMR of an Alq<sub>3</sub> film at 20 K. The slope of the straight line is 1.

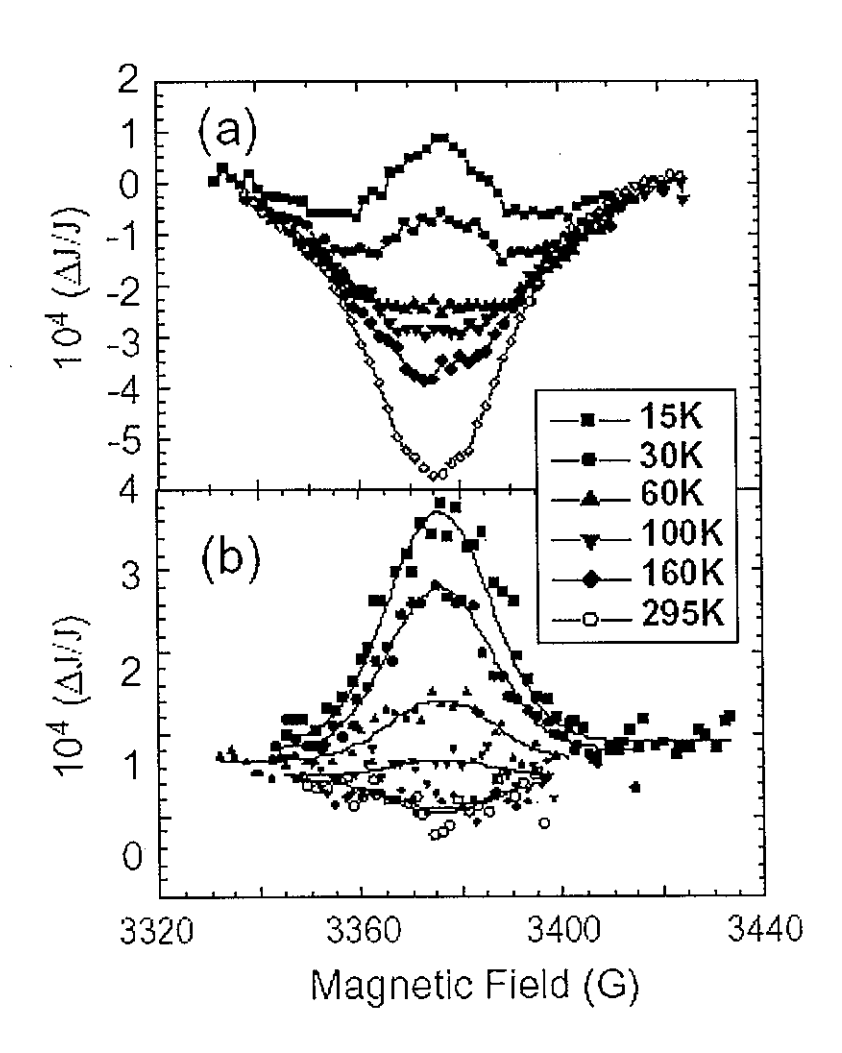


Fig. 7. The spin-1/2 EDMR spectra of OLEDs with (a) AlO<sub>x</sub> and (b) CsF buffer layers, at 15  $\leq T \leq$  295 K.

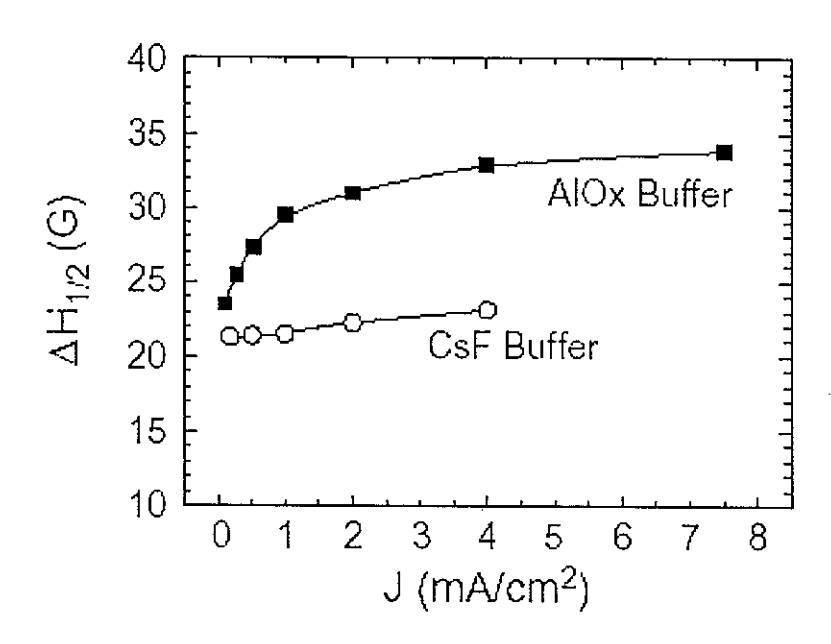


Fig. 8. The full-width-at-half-maximum linewidth  $\Delta H_{1/2}$  of the negative ELDMR at 295K vs. injected current density J in AlO<sub>x</sub>-buffered OLEDs (solid squares) and CsF-buffered OLEDs (open circles).

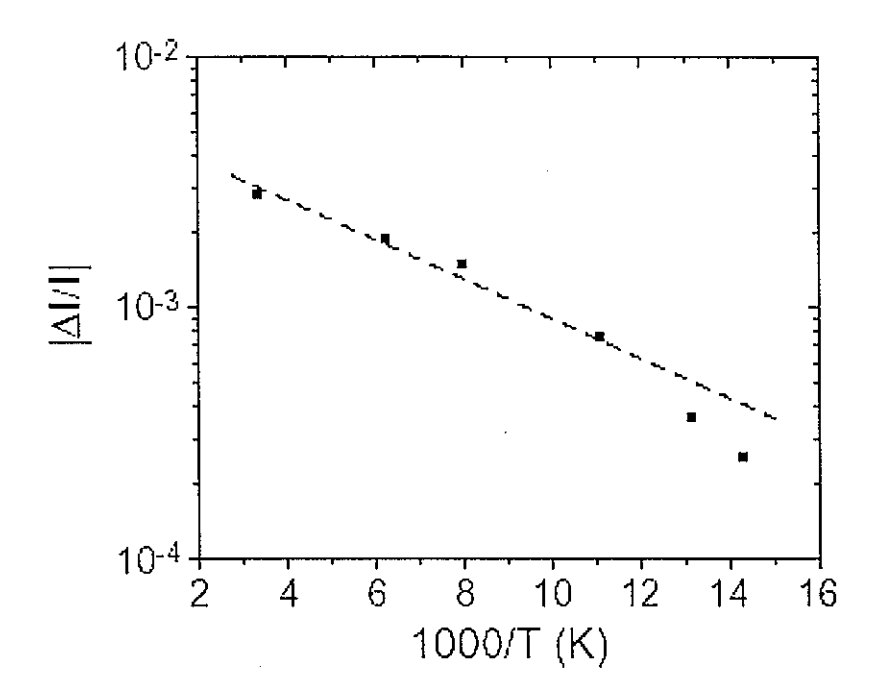


Fig. 9. The amplitude  $|\Delta I_{EL}/I_{EL}|$  of the negative ELDMR vs 1000/T in the AlO<sub>x</sub>-buffered OLEDs. The slope of the dashed line yields an activation energy of 11.6 meV.

# Chapter 4. Electroluminescence (EL)-Detected Magnetic Resonance Studies of Pt octaethyl porphyrin (PtOEP)-based Phosphorescent Organic Light-Emitting Devices

(Submitted to Physics Review B) G. Li, <sup>1</sup> J. Shinar, <sup>1</sup> and G. Jabbour<sup>2</sup>

<sup>1</sup>Ames Laboratory - USDOE and Department of Physics and Astronomy,

Iowa State University, Ames, IA 50011

<sup>2</sup>Optical Sciences Center & Department of Materials Science and Engineering,

University of Arizona, Tucson, AZ 85721

#### **Abstract**

The electroluminescence (EL)-detected magnetic resonance (ELDMR) of 0, 1, 3, 6, and 20 wt.% Pt octaethyl porphyrin (PtOEP)-doped tris(Al-8-hydroxyquinolinate) (Alq<sub>3</sub>) based phosphorescent multilayer organic light-emitting devices (OLEDs) is described. In 1 wt.% PtOEP-doped devices, the ELDMR from the PtOEP and Alq<sub>3</sub> emission are both very similar to that of undoped devices: They exhibit a positive (EL-enhancing) spin-1/2 polaron resonance at  $10 \le T \le 50$  K, whose magnitude  $\Delta I_{EL}/I_{EL}$  increases with current and weakens with increasing T, and a negative (EL-quenching) resonance at 50 K  $\le T$ , which grows with T. At 295K,  $|\Delta I_{EL}/I_{EL}|$  decreases with current. The enhancing resonance is attributed to the magnetic-resonance reduction of singlet exciton (SE) quenching by a reduced population of polarons. The quenching resonance is attributed to magnetic resonance enhancement formation of dianions at the organic/cathode interface. Both the enhancing and quenching resonances weaken as the PtOEP concentration increases; at 6 wt.%, the enhancing resonance is undetectable and the quenching resonance is very weak ( $|\Delta I_{EL}/I_{EL}| \sim 2 \times 10^{-5}$ ). The results

can be explained by assuming that the ELDMR of the guest emission is due to the effect of magnetic resonance conditions on the host SEs. A rate equation model is established to explain the evolution of the ELDMR with dye concentration. In the 20 wt.%-doped devices, the spin-1/2 polaron resonance is quenching at all T and  $|\Delta I_{EL}/I_{EL}|$ , and the resonance linewidth, decrease with increasing T;  $|\Delta I_{EL}/I_{EL}|$  is weakly current-dependent at both 20 K and 295 K. This behavior is consistent with the diamon model, if the diamon density decreases with increasing T.

PACS Nos. 85.65.+h, 85.60.-q, 85.30.-z, 76.90.+d

#### I. Introduction

The report on bright green electroluminescence (EL) from a bilayer device based on tris-(8-hydroxy quinoline) Al (Alq<sub>3</sub>)<sup>1</sup> spawned extensive studies on organic light emitting devices (OLEDs), both small molecule-<sup>1,2</sup> and polymer-based.<sup>3,4</sup> Extensive efforts have resulted in dramatic improvements in the brightness, efficiency, and lifetime of these devices. Doping the emitting layer with a guest molecule is one of the most effective approaches to improve device efficiency (as quantified by the external quantum efficienty  $\eta_{ext}$ ) and lifetime. While doping with fluorescent dye restricts the internal quantum efficiency  $\eta_{int}$  to 25%,<sup>2</sup> doping with a phosphorescent dye removes that restriction.<sup>5,9</sup> The phosphorescent dyes incorporate a heavy metal atom, usually Pt or Ir, to enhance the spin-orbital interaction. Indeed, devices doped with Pt octaethyl porphyrin (PtOEP) and fac tris(2-phenylpyridine) iridium [Ir(ppy)<sub>3</sub>] have achieved  $\eta_{ext} = 9\%^{10}$  and 19.2%,<sup>11</sup> respectively. In principle, both fluorescence- and phorsphorescence-based EL are due to the radiative decay of excitons generated by

recombination of electrons and holes injected from the electrodes in the emitting layer. This recombination and other processes involving the spin 1/2 negative and positive polarons ( $p^-$  and  $p^+$ , respectively), into which the holes and electrons convert upon injection, are spin-dependent. Hence, various optically-detected magnetic resonance (ODMR) measurements such as photoluminescence (PL)-, EL- and electrically- (i.e., current-) detected magnetic resonance (PLDMR, ELDMR, and EDMR, respectively) have proven to be powerful tools in elucidating the photophysics of luminescent  $\pi$ -conjugated materials and OLEDs. <sup>12-33</sup> This paper describes an ELDMR study of PtOEP-doped Alq<sub>3</sub>-based phosphorescent OLEDs.

In poly(p-phenylene vinylene) (PPV)- and poly(p-phenylene ethynylene) (PPE)-based OLEDs, the ELDMR and EDMR included narrow negative (i.e., current- and EL-quenching) and positive (i.e., current-enhancing and EL-enhancing) spin-1/2 polaron resonances, and half-field positive and negative triplet resonances. <sup>13,16-18,21,23-27</sup> The positive spin-1/2 ELDMR was attributed to the reduction in the population of polarons at the field-for-resonance, and consequent reduced quenching of singlet excitons (SEs) by polarons (see Sec. III below). <sup>23</sup> The negative spin-1/2 resonance was attributed to the enhanced spin-dependent formation of positive or negative spinless bipolarons ( $bp^{++}$  and  $bp^-$ , respectively). <sup>13,16,17,23</sup>

In Alq<sub>3</sub>-based small molecular OLEDs, a positive spin-1/2 ELDMR is observable at  $T \le$  60 K and a negative spin-1/2 ELDMR, whose magnitude  $|\Delta I_{EL}/I_{EL}|$  increases with T, is observed at  $T \ge 60$  K.  $|\Delta I_{EL}/I_{EL}|$  and the current (J)-dependence of the room temperature quenching ELDMR are found to be strongly dependent on the organic/cathode buffer layer. A positive half-field triplet exciton (TE) resonance is also observed. These results suggest that diamions formed at the organic/cathode interface and identified by several other studies,  $^{36-38}$  are responsible for the negative spin-1/2 EDMR and ELDMR.

The current ELDMR study of PtOEP-doped Alq<sub>3</sub>-based OLEDs provides evidence that the quenching of guest TEs by polarons and the sheet of charge at the organic-metal interface is negligible compared to the quenching of host SEs by these charges: The negative (ELquenching) ELDMR of the phosphorescence is shown to be due to the quenching of source host SEs, which would otherwise transfer their energy to the guest TEs. A rate equation model, which provides a quantitative assessment of this process, is described.

As the PtOEP concentration is increased, the polaron resonance becomes quenching at both 20 K and 295 K. Both the magnitude and the linewidth of the quenching resonance decreased as temperature increases. This agrees well with dianion model if the dianion density at low temperature is higher than room temperature. Higher dianion concentration will lead to linewidth broadening.

## II. Experimental Procedure

The structure of the devices used in this study was [indium tin oxide (ITO)]/[5 nm copper phthalocyanine (CuPc)]/[50 nm 4,4'-Bis((1-naphthyl)-phenylamino)-1,1'-biphenyl ( $\alpha$ -NPD)]/[40 nm x% PtOEP:Alq<sub>3</sub>]/[10 nm Alq<sub>3</sub>]/[1 nm CsF]/Al, x = 0, 1, 3, 6 and 20 wt.% (see Fig. 1). The CsF buffer layer improves electron injection and device efficiency dramatically.<sup>39</sup>

The devices were fabricated in a ~10<sup>-6</sup> torr vacuum chamber, which is installed in a pure Ar-filled glove box, typically containing <1 ppm oxygen. Prior to deposition of the organic layers, the ITO-coated glass was thoroughly cleaned by detergent, distilled water, isoproponol, and acetone, and blown-dry with Ar. The deposition rates were monitored by a Maxtek TM-100 thickness monitor. The organic materials were deposited at ~1.0 Å/s by

thermal vacuum evaporation. PtOEP and Alq<sub>3</sub> were codeposited and the deposition rates were carefully monitored to obtain the desired PtOEP concentration. The CsF and Al cathode were deposited at ~0.1 and ~4.5 Å/s, respectively. The active area of the OLED, defined by the overlap of the ITO and Al electrodes, was ~20 mm<sup>2</sup>.

The ODMR system used in this study was described previously. <sup>13,16,21,23,25,26</sup> The OLED was inserted into the quartz dewar of an Oxford Instruments Helium gas flow cryostat; the quartz dewar is inserted into an optically accessible X-band cavity. Bias is applied to the OLED and the EL is collected by a Si photodiode. The ELDMR was measured by lock-in detection of the changes in the EL induced by the ~9.45 GHz microwaves chopped at 100 Hz and amplified to ~360 mW.

#### III. Results and Discussion

Figure 1 shows the device structure and emission spectra of the 1 wt.%-doped device. In this lightly doped device, both the host and guest emission bands are clear seen.

## III.1. The Negative and Positive Spin 1/2 ELDMRs

Figure 2 shows the spin 1/2 ELDMR at various levels of the injected current J at (a) T=15 K and (b) 295 K of the PtOEP red emission in a 1 wt.%-doped device. At 15K, as J increases, the magnitude of the positive resonance  $|\Delta I_{EL}/I_{EL}|$  increases, approximately as  $J^{0.5}$ , indicating a bimolecular process.<sup>32</sup> At 295K, the resonance is quenching and  $|\Delta I_{EL}/I_{EL}|$  decreases as J increases. Both the low- and high-temperature resonances behave similar to that of Alq<sub>3</sub>-based fluorescent OLEDs with a CsF buffer layer.<sup>33,34</sup>

The behavior of the high-temperature negative ELDMR is similar to its behavior in undoped Alq<sub>3</sub> OLEDs and it is consequently attributed to the same mechanism, namely magnetic resonance enhanced formation of dianions at the organic/cathode interface.<sup>33,34</sup>

The g-value, linewidth, temperature dependence, and current dependence of the low-temperature positive ELDMR are similar to the g-value, linewidth, temperature dependence, and laser power-dependence of the positive PLDMR of  $\pi$ -conjugated polymers. <sup>12-14,22,32</sup> The positive ELDMR is therefore attributed to the same mechanism. This mechanism, however, has been controversial. It was initially suggested to be magnetic resonance enhancement of radiative polaron pair recombination. <sup>41,42,14</sup> This mechanism, however, is inconsistent with the voluminous evidence that polaron pairs do not decay directly to the ground state, but rather form SEs and triplet excitons (TEs). <sup>43</sup> A second mechanism was suggested to be magnetic resonance enhancement of the formation of TEs followed by TE-TE annihilation to SEs, resulting an enhanced PL due to enhanced delayed fluorescence. <sup>44</sup> This mechanism clearly requires that the population of TEs increase at the field-for-spin-1/2-resonance. Yet photoinduced absorption (PA)-detected magnetic resonance (PADMR) measurements showed clearly that at that field-for-resonance both the polaron and TE populations decrease. <sup>16,45</sup>

A third mechanism developed to account for the resonance invoked magnetic resonance enhancement of delayed PL due to nongeminate polaron pair recombination ("the delayed PL model"). This mechanism, however, requires that the cross-section for SE formation by polaron pairs in the singlet configuration  $\sigma_{SE}$  be greater than the cross-section for TE formation by polaron pairs in the triplet configuration  $\sigma_{TE}$ . This relation between  $\sigma_{SE}$  and  $\sigma_{TE}$  and the delayed PL model are inconsistent with various experimental results: (i) The

relation between  $\sigma_{SE}$  and  $\sigma_{TE}$  is inconsistent with the various results that indicate that the yield of SEs in Alq<sub>3</sub> OLEDs is no greater than 25%.<sup>48</sup> (ii) the delayed PL model is inconsistent with double modulation PLDMR measurements, which show that the contribution of the prompt PL to the PLDMR is similar to that of the delayed PL.<sup>49</sup> (iii) Combined thermally stimulated luminescence (TSL), which is due to delayed PL from (effectively) nongeminate polaron recombination, and PLDMR measurements, show that the TSL increases ~30 fold but the PLDMR decreases ~6 fold when the excitation photon energy is increased from 2.7 to 3.4 eV.<sup>50</sup>

The fact that the polaron population decreases at resonance invoked the "quenching model." This model, which is the only model consistent with all of the ODMR results reported to date, is based on quenching of SEs by polarons. The reduction of polaron population at resonance reduces the quenching of SEs and thus results in a positive PLDMR and ELDMR. The quantitative quenching model developed by List et al. was found to be in excellent agreement with experimental results. We therefore attribute the enhancing spin-1/2 ELDMR to this quenching mechanism.

It is important to note that the ELDMR shown in Figure 2 is due to the phosphorescent red emission from TEs in PtOEP. This raises the question whether polarons act as effective TEs quenching centers. It is well known that the binding energy of TEs is much larger than that of SEs, and the diffusion of guest TEs is negligible. Hence quenching of guest TEs by polarons is not likely to be as effective as that of host SEs. To clarify this, we compared the contributions of the red PtOEP phosphorescence and green Alq<sub>3</sub> fluorescence to the negative and positive spin 1/2 ELDMR.

Figure 3 shows the current J-dependence of the positive (at 15 or 20 K) and negative (at 295 K) ELDMR of the 0, 1, 3, and 6 wt.% PtOEP:Alq<sub>3</sub> devices. In the 1 wt.% device, the behavior of the ELDMR due to the red and green emission bands is identical, indicating either (a) direct quenching of the guest TEs by polarons, as effective as the quenching of host SEs, or (b) an indirect quenching process, in which quenching of PtOEP TE emission is due to quenching of the Alq<sub>3</sub> SEs which otherwise transfer their energy to PtOEP.

If the first scenario is correct, then the ELDMR should be largely independent of the PtOEP doping concentration. However, as seen in Figure 3, both the positive and negative ELDMRs decrease rapidly as the PtOEP concentration increases. Indeed, in the 6 wt.% PtOEP-doped device, the positive spin-1/2 ELDMR is unobservable, and the negative resonance at 295 K is very weak ( $|\Delta I_{EL}/I_{EL}| \sim 2 \times 10^{-5}$ ) over the whole range of J. We therefore conclude that quenching of guest TEs by either polarons or dianions is far less significant than quenching of host SEs, and that the PtOEP phosphorescence ELDMR is due to quenching of the host SEs, which are the source of the PtOEP TEs.

Figure 4 shows the temperature dependence of the spin-1/2 polaron ELDMR of the 3 wt.% PtOEP:Alq<sub>3</sub> OLED. Not only is the magnitude of the resonances small compared to the 1 wt.%-doped devices, but the resonance has a negative component even at 15 K. Figure 4 suggests that the "transition temperature" from the low-T positive to the high-T negative resonance is ~30 K; in undoped Alq<sub>3</sub> OLEDs this transition occurs at ~60 K<sup>33,34</sup> rather than ~30K.

#### III.2. The Half-Field TE ELDMR

The ODMR of luminescent  $\pi$ -conjugated materials and OLEDs usually includes not only positive and/or negative spin-1/2 polaron resonances at  $g \sim 2.002$ , but (generally positive) full- and half-field TE resonances as well. As for the positive spin 1/2 polaron resonance, different mechanisms were proposed to explain the half-field resonance, including (i) enhanced TE-TE annihilation to SEs, (ii) enhanced ground-state recovery from TEs, and (iii) reduced quenching of SEs by a reduced population of TEs at resonance. By monitoring the separate guest and host contributions to the distinct guest and host half-field TE resonances, List et al.<sup>47</sup> provided strong evidence that excluded mechanisms (i) and (ii). They also provided a model of long-range SE-TE annihilation due to a dipole-dipole transfer mechanism which established the quenching model (iii) as the origin of the half-field resonance.

Figure 5 shows the half-field ELDMR of the 0, 1, and 3 wt.% PtOEP:Alq<sub>3</sub>. The current-dependence of the half field resonance is relatively weak. The magnitude of the resonance decreases from  $1.7 \times 10^{-3}$  in the undoped device to  $< 1.5 \times 10^{-4}$  in the 3 wt.% device. In the 6 wt.% device, the half-field resonance is undetectable. In the 1 wt.% device, the magnitude of the green band half-field ELDMR is larger than that of red band. This can be explained by considering that the PtOEP TEs population is also reduced at resonance.

Recapping, we have attributed the (a) low-T positive spin-1/2, (b) high-T negative spin-1/2, and (c) low-T half-field triplet resonances to (a) reduced quenching of SEs by polarons, (b) enhanced quenching of SEs by dianions at the Alq<sub>3</sub>/cathode interface, and (c) reduced quenching of SEs by TEs, respectively. Hence, the red PtOEP phosphorescence ELDMR is due to an indirect process, i.e., quenching of source host SEs, which otherwise transfer their

energy to the PtOEP molecules. All three resonances weaken rapidly with increasing PtOEP concentration. We now provide a rate equation model to account for this behavior.

## III.3. Rate Equation Analysis of the ELDMR

Figure 6 shows the photophysical processes in PtOEP-doped Alq<sub>3</sub> OLEDs. Reverse energy transfer from PtOEP TEs to Alq<sub>3</sub> is ignored due to the high efficiency of the devices.<sup>52</sup> The terms used are:

 $[^{1}S_{1}], [^{3}T_{1}] [^{1}S_{0}]$ : Population of lowest excited SE state, lowest triplet state, and ground state, respectively. A PtOEP subscript refers to populations of states in PtOEP. The other states are states in Alq<sub>3</sub>.

 $k_{ISCi}$ : Intersystem crossing (ISC) rates.

 $k_{F\"{o}rster}$ ,  $k_{Dexter}$ : Förster<sup>53</sup> and Dexter<sup>54</sup> energy transfer rates.

 $k_r = A = \text{Einstein coefficient of spontaneous emission rate from }^1 S_1$ .

 $[M_i]$ : Population of quenching species (polarons, TEs, dianions, etc.).

 $\sum k_{ai}[M_i]$ : total quenching rate of SEs.

 $k_{nr}$ : Non-radiative decay rate excluding quenching channels.

 $I_{SE}$ ,  $I_{TE}$ : SE, TE generation rates due to charge injection

The rate equations are as follows.

In Alq<sub>3</sub>:

$$\frac{d[{}^{1}S_{1}]}{dt} = I_{SE1} - (k_{nr} + \sum k_{qi}[M_{i}] + k_{r} + k_{ISC1} + k_{Förster})[{}^{1}S_{1}] + k_{ISC2}[{}^{3}T_{1}]$$
(1)

$$\frac{d[^{3}T_{1}]}{dt} = I_{TE} + k_{ISC1}[^{1}S_{1}] - (k_{ISC2} + k_{ISC3})[^{3}T_{1}]$$
(2)

In PtOEP:

$$\frac{d\begin{bmatrix} {}^{1}S_{1}\end{bmatrix}_{PtOEP}}{dt} = k_{Förster}\begin{bmatrix} {}^{1}S_{1}\end{bmatrix} - k_{ISC,PtOEP}\begin{bmatrix} {}^{1}S_{1}\end{bmatrix}_{PtOEP} + O_{1}$$
(3)

$$\frac{d\begin{bmatrix}3T_1\end{bmatrix}_{PlOEP}}{dt} = k_{ISC,PlOEP}\begin{bmatrix}1S_1\end{bmatrix}_{PlOEP} + k_{Dexter}\begin{bmatrix}3T_1\end{bmatrix} - k_{ph}\begin{bmatrix}3T_1\end{bmatrix}_{PlOEP} + O_2$$
(4)

Where

$$k_{F6rster} \propto r^{-6}$$
 (5)

$$k_{Dartor} \propto \rho^{-\alpha r}$$
 (6)

and  $O_1$  and  $O_2$  are higher-order terms. In steady state, the Alq<sub>3</sub> emission will be governed by

$$d[^1S_1]/dt = 0 (7)$$

$$I_{SE1} = (k_{nr} + \sum_{i} k_{qi} [M_i] + k_r + k_{ISC1} + k_{Forster}) [^1S_1] - k_{ISC2} [^3T_1]$$
 (8)

$$I_{EL} = k_r \begin{bmatrix} {}^{1}S_1 \end{bmatrix} = \frac{k_r (I_{SE1} + k_{ISC2} \begin{bmatrix} {}^{3}T_1 \end{bmatrix})}{k_{nr} + \sum_{i} k_{qi} [M_i] + k_r + k_{ISC1} + k_{Forster}}$$
(9)

Similarly,

$$\frac{d\begin{bmatrix} {}^{3}T_{1} \end{bmatrix}}{dt} = 0 \Rightarrow \begin{bmatrix} {}^{3}T_{1} \end{bmatrix} = \frac{I_{TE} + k_{ISC1} \begin{bmatrix} {}^{1}S_{1} \end{bmatrix}}{k_{ISC2} + k_{ISC3}}$$

$$(10)$$

Thus

$$I_{EL} = \frac{k_r (I_{SE1} + \frac{k_{ISC2}}{k_{ISC2} + k_{ISC3}} I_{TE})}{k_{nr} + \sum_{i} k_{qi} [M_i] + k_r + k_{ISC1} \left(1 - \frac{k_{ISC2}}{k_{ISC2} + k_{ISC3}}\right) + k_{Forster}}$$
(11)

At resonance, if the population of SE quenching species  $[M_i]$  changes to  $[M_i] + \Delta [M_i]$ , the normalized EL change will be

$$\frac{\Delta I_{EL}}{I_{EL}} = \frac{-\sum k_{qi} \Delta [M_i]}{k_{nr} + \sum k_{qi} ([M_i] + \Delta [M_i]) + k_r + k_{ISC1} \left(1 - \frac{k_{ISC2}}{k_{ISC2} + k_{ISC3}}\right) + k_{Förster}}$$
(12)

As mentioned above, PADMR measurements demonstrate that the population of polarons and TEs decreases at the field-for-spin-1/2-resonance. If polarons and TEs are quenching centers of emissive SEs (thus they are M's), a negative  $\Delta[M_i]$  will yield a positive ELDMR.

In OLEDs, mobile polarons are on the one hand the source of SEs, and on the other hand quenchers of SEs. Their lifetime, however, is short (typically  $\sim 100$  ns, as determined by OLEDs' response to pulsed bias<sup>55</sup>. In contrast, the lifetime of trapped polarons is much longer (typically  $10 \, \mu s - 10 \, ms$ , as determined by measurements of the PLDMR vs the microwave chopping frequency<sup>56</sup>). Hence the quenching of SEs due to mobile polarons can be neglected relative to quenching by trapped polarons.

In PtOEP, under steady state condition, we set Eqs. (3) and (4) to 0, and ignore the  $O_l$  and  $O_2$  terms, since the internal quantum efficiency of the PtOEP emission is almost 100%.<sup>5</sup> We get two equations:

$$\begin{bmatrix} {}^{1}S_{1} \end{bmatrix}_{PiOEP} = \frac{k_{Forster}}{k_{ISC,PiOEP}}$$
 (13)

$$I_{EL,PlOEP} = k_{ph} \begin{bmatrix} {}^{3}T_{1} \end{bmatrix}_{PlOEP} = k_{ISC,PlOEP} \begin{bmatrix} {}^{1}S_{1} \end{bmatrix}_{PlOEP} + k_{Dexter} \begin{bmatrix} {}^{3}T_{1} \end{bmatrix}$$
 (14)

Combining these two, we get

$$I_{ELPlOEP} = k_{Forster} \begin{bmatrix} {}^{1}S_{1} \end{bmatrix} + k_{Dexter} \begin{bmatrix} {}^{3}T_{1} \end{bmatrix}$$
 (15)

Note that although Dexter energy transfer can also occur from a host SE to a guest SE, it is negligible compared to Förster SE-SE energy transfer.<sup>57</sup>

When the PtOEP concentration is low, only long-range Förster energy transfer occurs:

$$I_{ELP_tOEP} = k_{Forster} \begin{bmatrix} {}^{1}S_{1} \end{bmatrix} \tag{16}$$

Note the intensity of the PtOEP phosphorescence differs from the host Alq<sub>3</sub> fluorescence only by the constant  $(k_r/k_{F\"{o}rster})$ . Hence the normalized change in the phosphorescence intensity will also be given by an expression analogous to Eq. (12).

Thus this model accounts for the observed identical dependence of the host and guest ELDMR on the current, at both low and high T.

When the PtOEP concentration increases, the intermolecular distance r decreases, and both  $k_{F\"{o}rster}$  and  $k_{Dexter}$  increase. Consequently, as expected and predicted by Eq. (9), the host EL decreases. Eq. (12) of the model predicts that the magnitude of the normalized EL change will decrease as well, which agrees well with the experimental results (see Figure 3).

When the PtOEP concentration increases, Dexter energy transfer becomes significant.

Then the simplified relation

$$\Delta I_{EL} / I_{EL} = \Delta \begin{bmatrix} {}^{1}S_{1} \end{bmatrix} / \begin{bmatrix} {}^{1}S_{1} \end{bmatrix}$$
 (17)

derived from Eq. (15) when Dexter energy transfer is negligible, must be replaced by the relation

$$\frac{\Delta I_{EL}}{I_{EL}} = \frac{k_{Forster} \Delta \begin{bmatrix} {}^{1}S_{1} \end{bmatrix}}{k_{Forster} \begin{bmatrix} {}^{1}S_{1} \end{bmatrix} + k_{Dexter} \begin{bmatrix} {}^{3}T_{1} \end{bmatrix}}$$
(18)

The additional Dexter term in the denominator results in  $|\Delta I_{EL}/I_{EL}|$  decreasing even faster in the PtOEP phosphorescence than in the Alq<sub>3</sub> fluorescence ELDMR. When the Dexter term dominates, the phosphorescence ELDMR will be very small. This is in excellent agreement with the observation that the ELDMR in the 6 wt.% PtOEP-doped OLED is very weak and undetectable at low T. The observed weak negative ELDMR at 295 K may indicate that the dianions quench TEs slightly.

In the heaviest 20 wt.% PtOEP-doped device, the spin-1/2 ELDMR is quenching at all T. Figure 7 shows the temperature dependence of that resonance at  $J \sim 2$  mA/cm<sup>2</sup>.  $|\Delta I_{EL}/I_{EL}|$  and the linewidth both decrease when T increases;  $|\Delta I_{EL}/I_{EL}|$  is largely independent of the injected current at both 20 K and room temperature. This behavior is significantly different from that of the negative resonance in the undoped devices. In that case,  $|\Delta I_{EL}/I_{EL}|$  increases as T

increases, and decreases as J increases. The very different behavior in the 20 wt.% PtOEP-doped device suggests a new mechanism.

In attempting to identify the new mechanism, we note that the lifetime of PtOEP triplets was observed to decrease as the PtOEP concentration increases. <sup>52</sup>This is believed to be due enhanced nonradiative decay paths for TEs in PtOEP aggregates. At the same time, the TE-TE annihilation rate also increases with PtOEP concentration. <sup>52</sup>It is therefore plausible that the new quenching ELDMR is related to these two processes. However, the ELDMR of Ir(ppy)-doped 4,4'-bis(9-carbazolyl)biphenyl (CBP) OLEDs exhibits a similar quenching resonance from 20 K to 295K, even at 2 wt.% doping. <sup>58</sup> Since the Ir(ppy)<sub>3</sub> TEs exhibit a phosphorescence lifetime of ~1 μs<sup>6</sup> (compared to ~100 μs in PtOEP<sup>5</sup>), the TE-TE annihilation rate must be much lower in Ir(ppy)-based devices. In addition, aggregation should be negligible in 2 wt.% Ir(ppy)<sub>3</sub>-doped devices. Hence it is improbable that the new mechanism is related to aggregation effects.

In light of the foregoing considerations, the origin of the negative resonance in 20 wt.% PtOEP: Alq<sub>3</sub> OLEDs is tentatively assigned to the magnetic resonance enhanced formation of dianions in the bulk of the doped layer. As T decreases, the mobility of the TEs decreases, and the stability of the dianions increases. Thus, the density of dianions will increase with decreasing T. Hence, the magnitude and linewidth of the negative resonance will increase with decreasing T, in qualitative agreement with the observed behavior.

It is interesting to consider the correlation between the magnitude of the room temperature negative ELDMR and the efficiency of the PtOEP-doped devices: The 6 wt.% PtOEP-doped device is the highest efficiency device, and it has the weakest room temperature negative resonance.

In our previous ELDMR and EDMR study of Alq<sub>3</sub> OLEDs, we suggested that the quenching of SEs by the sheet of charge at the organic/cathode interface is an important quenching mechanism in OLEDs. The current results support this suggestion. Thus, the improved efficiency of optimized phosphorescent OLEDs is probably due to two effects: (i) The contribution of both Forster and Dexter energy transfer, which exploits 100% of the host excitons, resulting in virtually 100% internal quantum efficiency. (ii) The relative immunity of TEs to quenching due to the charge sheet at the organic/cathode interface, as compared to SEs, which are susceptible to this quenching process.

## IV. Summary and Conclusions

In conclusion, an ELDMR study of 0, 1, 3, 6, and 20 wt.% PtOEP-doped Alq<sub>3</sub> phosphorescent OLEDs was described. In 1 wt.% PtOEP-doped devices, the ELDMR is very similar to that of undoped Alq<sub>3</sub> OLEDs, i.e., it includes a positive spin 1/2 ELDMR at  $T \le 60$  K, and a negative spin 1/2 ELDMR which emerges at 60 K and increases with increasing T. The ELDMR of the red guest phosphorescence and green host fluorescence are almost the same.

The low T positive ELDMR decreases as the PtOEP concentration increases and disappears when the PtOEP concentration exceeds  $\sim 6$  wt.%. The room temperature negative ELDMR decreases from  $\sim 8\times 10^{-4}$  in 1 wt.% PtOEP device to  $\sim 2\times 10^{-5}$  in the 6 wt.%-doped device. In the 20 wt.%-doped device, the negative ELDMR is observed from 20 K to 295 K. The amplitude and linewidth of the resonance both decrease as T increases. The resonance is much less dependent on the current than in the other devices, indicating their different origin.

Due to its similarity to the positive spin ½ PLDMR, the enhancing ELDMR is attributed to resonance enhancement of polaron recombination, which reduces quenching of SEs by polarons. The quenching ELDMR for devices with < 6 wt.% PtOEP is believed to result from magnetic resonance enhanced formation of dianions at the organic/cathode interface. A rate equation model was developed to account for the behavior of the devices containing up to 6 wt.% PtOEP.

The abnormal negative spin 1/2 ELDMR in 20 wt.%-dope devices is not clear and may be due to magnetic resonance enhanced formation of dianions in the bulk of the doped layer.

#### Acknowledgements

Ames Laboratory is operated by Iowa State University for the US Department of Energy under Contract W-7405-ENG-82. This work was supported by the Director for Energy Research, Office of Basic Energy Science.

#### References

- 1. C. W. Tang and S. A. VanSlyke, Appl. Phys. Lett. 51, 913 (1987).
- 2. C.W. Tang, S.A. Vanslyke, and C.H. Chen, J. Appl. Phys. 65, 3610 (1989).
- 3. J. H. Burroughes, D. D. C. Bradley, A. R. Brown, R. N. Marks, K. MacKay, R. H. Friend, P. L. Burn, and A. B. Holmes, Nature 347, 539 (1990).
- R. H. Friend, R. W. Gymer, A. B. Holmes, J. H. Burroughes, R. N. Marks, C. Taliani, D. D. C. Bradley, D. A. Dos Santos, J. L. Brédas, M. Lögdlund, and W. R. Salaneck, Nature 397, 121 (1999).

- M.A. Baldo, D.F. O'Brien, Y. You, A. Shoustikov, S. Silby, M.E. Thompson, and S. R. Forrest, Nature 395, 151 (1998).
- 6. M.A. Baldo, S. Lamansky, P.E. Burrows, M.E. Thompson, and S.R. Forrest, Appl. Phys. Lett. 75, 4 (1999).
- 7. C. Adachi, M.A. Baldo, and S.R. Forrest, Appl. Phys. Lett. 77, 904 (2000).
- 8. D.F. O'Brien, M.A. Baldo, M.E. Thompson, and S.R. Forrest, Appl. Phys. Lett. 74. 442 (1999).
- 9. V. Cleave, G. Yahioglu, P. Le Barny, R. Fiend, and N. Tessler, Adv. Mater. 11, 285 (1999).
- 10. G. E. Jabbour, J. F. Wang, and N. Peyghambarian, Appl. Phys. Lett. 80, 13 (2002).
- 11. M. Ikai, S. tokito, Y. Sakamoto, T. Suzuki, and Y. Taga, Appl. Phys. Lett. 79, 156 (2001).
- 12. L. S. Swanson, J. Shinar, and K. Yoshino, Phys. Rev. Lett. 65, 1140 (1990).
- 13. L. S. Swanson, P. A. Lane, J. Shinar, and F. Wudl, Phys. Rev. B 44, 10617 (1991).
- 14. L. S. Swanson, J. Shinar, A. R. Brown, D. D. C. Bradley, R. H. Friend, P. L. Burn, A. Kraft, and A. B. Holmes, Phys. Rev. B 46, 15072 (1992).
- Q.-X. Ni, L. S. Swanson, P. A. Lane, J. Shinar, Y. W. Ding, S. Ijadi-Maghsoodi, and T. J. Barton, Syn. Met. 49-50, 447 (1992).
- 16. X. Wei, B. C. Hess, Z. V. Vardeny, and F. Wudl, Phys. Rev. Lett. 68, 666 (1992).
- 17. J. Shinar and L. S. Swanson, in *Electroluminescent Materials, Devices, and Large-Screen Displays*, edited by E. M. Conwell, M. Stolka, and M. R. Miller, *SPIE Conf. Proc.* 1910, 147 (1993).
- 18. L. S. Swanson, J. Shinar, Y. W. Ding, and T. J. Barton, Syn. Met. 55-57, 1 (1993).

- 19. V. Dyakonov, N. Gauss, G. Rösler, S. Karg, W. Rieß, and M. Schwoerer, Chem. Phys. 189, 687 (1994).
- J. Shinar, A. V. Smith, P. A. Lane, K. Yoshino, Y. W. Ding, and T. J. Barton, Mol. Cryst.
   Liq. Cryst. 256, 691 696 (1994).
- 21. Z. V. Vardeny and X. Wei, Mol. Cryst. Liq. Cryst. 256, 465 (1994).
- 22. J. Shinar, N. C. Greenham, and R. H. Friend, in Optical and Photonic Applications of Electroactive and Conducting Polymers, edited by S. C. Yang and P. Chandrasekhar, SPIE Conf. Proc. 2528, 32 (SPIE, Bellingham, WA, 1995).
- 23. W. Graupner, J. Partee, J. Shinar, G. Leising, and U. Scherf, Phys. Rev. Lett. 77, 2033 (1996).
- 24. N. C. Greenham, J. Shinar, J. Partee, P. A. Lane, O. Amir, F. Lu, and R. H. Friend, Phys. Rev. B 53, 13528 (1996).
- 25. J. Shinar, Syn. Met. 78, 277 (1996).
- 26. J. Shinar, in *Organic Electroluminescent Materials and Devices*, edited by S. Miyata and H. S. Nalwa, Chapter 4 (Gordon & Breach, NY, 1997).
- 27. J. Shinar, in Handbook of Organic Conductive Molecules and Polymers: Vol. 3.
  Conductive Polymer: Spectroscopy and Physical Properties, edited by H. S. Nalwa, Chap.
  7 (J. Wiley, NY, 1997).
- 28. V. Dyakonov, G. Rössler, M. Schwoerer, S. Blumstengel, and K. Lüders, J. Appl. Phys. 79, 1556 (1996).
- 29. V. Dyakonov, G. Rösler, M. Schwoerer, and E. L. Frankevich, Phys. Rev. B 56, 3852 (1997).

- 30. E. J. W. List, C. H. Kim, J. Shinar, A. Pogantsch, G. Leising, and W. Graupner, Appl. Phys. Lett. 76, 2083 (2000).
- 31. E. J. W. List, J. Partee, J. Shinar, U. Scherf, K. Müllen, E. Zojer, K. Petritsch, G. Leising, and W. Graupner, Phys. Rev. B 61, 10807 (2000).
- 32. E. J. W. List, C.-H. Kim, A. K. Naik, J. Shinar, G. Leising, and W. Graupner, Phys. Rev. B, 64, 155204 (2001).
- 33. K. Pichler, D. A. Halliday, D. D. C. Bradley, P. L. Burn, R. H. Friend, and A. B. Holmes, J. Phys.: Cond. Matt. 5, 7155 (1993).
- 34. G. Li and J. Shinar, in *Organic Light Emitting Materials and Devices V*, edited by Z. H. Kafafi, SPIE Conf. Proc. 4464, 113 (2002).
- 35. G. Li, J. Shinar, submitted to Phys. Rev. B.
- 36. N. Kirova and S. Brazovskii, Synth. Met. 76, 229 (1996).
- 37. P. S. Davids, A. Saxena, and D. L. Smith, Phys. Rev. B 53, 4823 (1996).
- 38. M. N. Bussac, D. Michoud, and L. Zuppiroli, Phys. Rev. Lett. 81, 1678 (1998).
- S. E. Shaheen, G.E. Jabbour, M. M. Morell, Y. Kawabe, B. Kippelen, N. Peyghambarian,
   M.-F. Nabor, R. Schlaf, E. A. Mash, and N. R. Armstrong, J. Appl. Phys. 84, 2324 (1998).
- 40. F. Li, H. Tang, J. Anderegg, and J. Shinar, Appl. Phys. Lett. 70, 1233 (1997).
- 41. R. A. Street, Phys. Rev. B 26, 3588 (1982)
- 42. F. Boulitrop, Phys. Rev. B 28, 6192 (1983)
- 43. M. Pope and C. E. Swenberg, Electronic Processes in Organic Crystals and Polymers, 2<sup>nd</sup> Edition (Oxford University Press, Inc., 1999)
- V. Dyakonov and E.L. Frankevich, Chem. Phys. 227, 203 (1998); V. Dyanokonov, G.
   Rosler, M. Schwoerer, and E. L. Frankevich, Phys. Rev. B 56, 3852 (1997)

- 45. M. Wohlgenannt, W. Graupner, G. Leising, and Z. Vardeny, Phys. Rev. B. 60, 5321 (1999)
- 46. M. Wohlgenannt, , C. Yang and Z. V. Vardeny, Phys. Rev. B, 66, 241201 (2002)
- 47. Z. Shuai, D. Beljonne, R. J. Silby and J. L Bredas, Phys. Rev. Lett. 84, 131 (2000); M. Wohlgennant, K. Tandon, S. Mazumdar, S. Ramasesha, and Z. V. Vardeny, Nature 409, 494 (2001); M. Wohlgennant, X. M. Jiang, Z. V. Vardeny, and R. A. Janssen, Phys. Rev. Lett., 88, 197401 (2002)
- 48. M. A. Baldo, D. F. O'Brien, M. E. Thompson, and S. R. Forrest, Phys. Rev. B 60, 14422-14428 (1999); M. Segal, M. A. Baldo, R. J. Holmes, S. R. Forrest, and Z. G. Soos, Phys. Rev. B 68, 075211 (2003)
- 49. M, -K Lee, M. Segal, J. Shinar, M. Baldo, and Z. Soo, (unpublished)
- 50. C, -H Kim, J. Shinar, (unpublished)
- 51. E. J. List, U. Scherf, K. Mullen, W. Graupner, C. -H. Kim, and J. Shinar, Phys. Rev. B 66, 235203-1, (2002)
- 52. M. A. Baldo, C. Adachi, and S. R. Forrest, Phys. Rev. B 62, 10967 (2000)
- 53. T. Förster. Discuss. Faraday Soc., 27, 7 (1959).
- 54. D. L. Dexter, J. Chem. Phys., 21, 836 (1953).
- 55. M. Yan, L. J. Rothberg, F. Papadimitrakopoulos, M. E. Galvin, and T. M. Miller, Phys. Rev. Lett. 73, 744 (1994)
- 56. W. Graupner, J. Partee, J. Shinar, G. Leising, and U. Scherf, Phys. Rev. Lett., 77, 2033 (1996)
- 57. M. A. Baldo, M. E. Thompson and S. R. Forrest, Pure Appl. Chem., 71, 2095(1999)
- 58. G. Li and J. Shinar, (unpublished)

# **Figures**

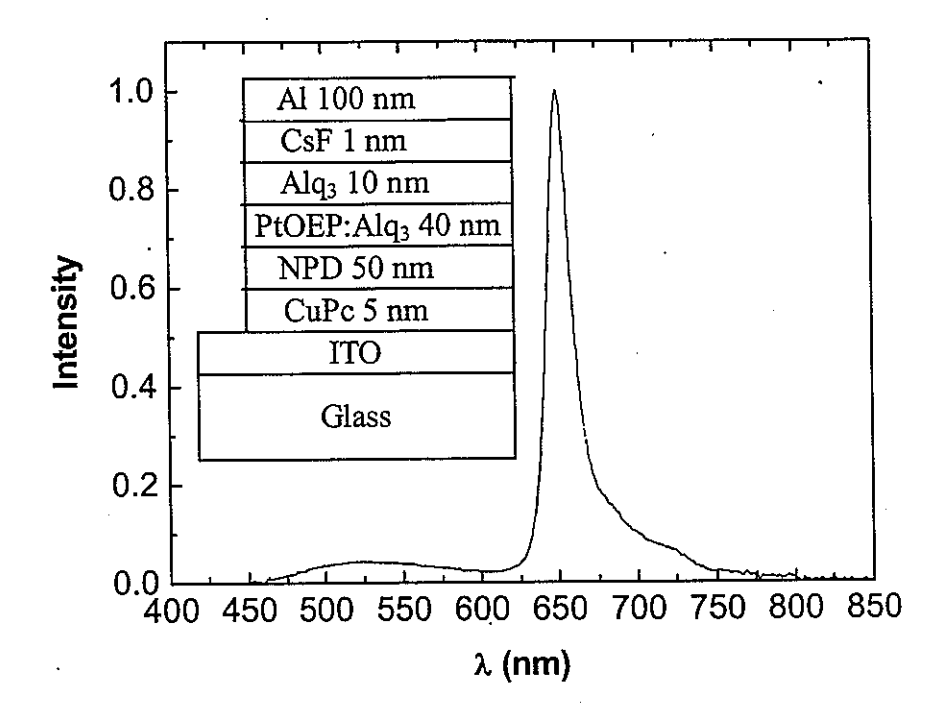


Figure 1. The device structure and emission spectra of 1 wt.% PtOEP doped Alq<sub>3</sub> OLED.

The PtOEP emission band around 650 nm dominates the EL, but the host Alq<sub>3</sub> emission band around 520 nm is still clearly visible.

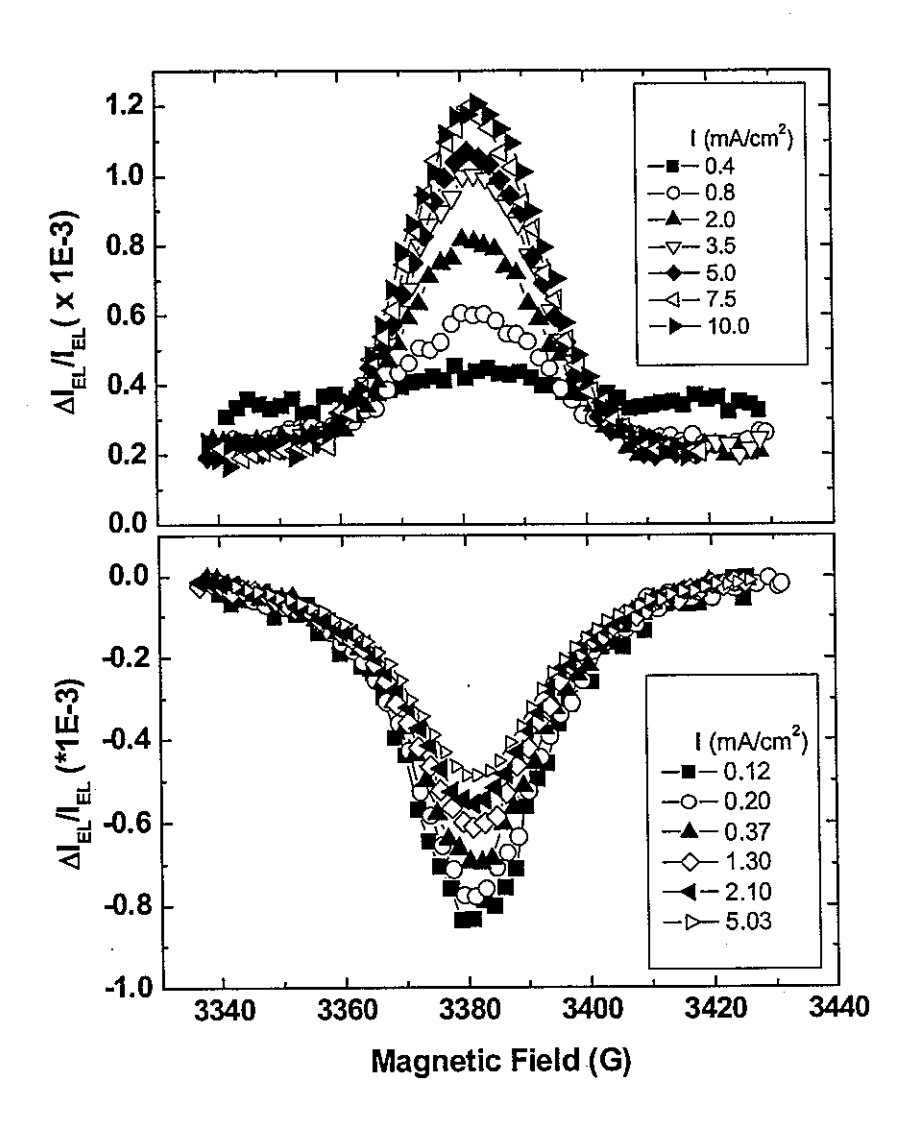


Figure 2. The spin 1/2 ELDMR of the red PtOEP phosphorescence in 1 wt.% PtOEP-doped Alq<sub>3</sub> OLEDs at different currents at (a) T = 15 - 20 K and (b) 295 K.

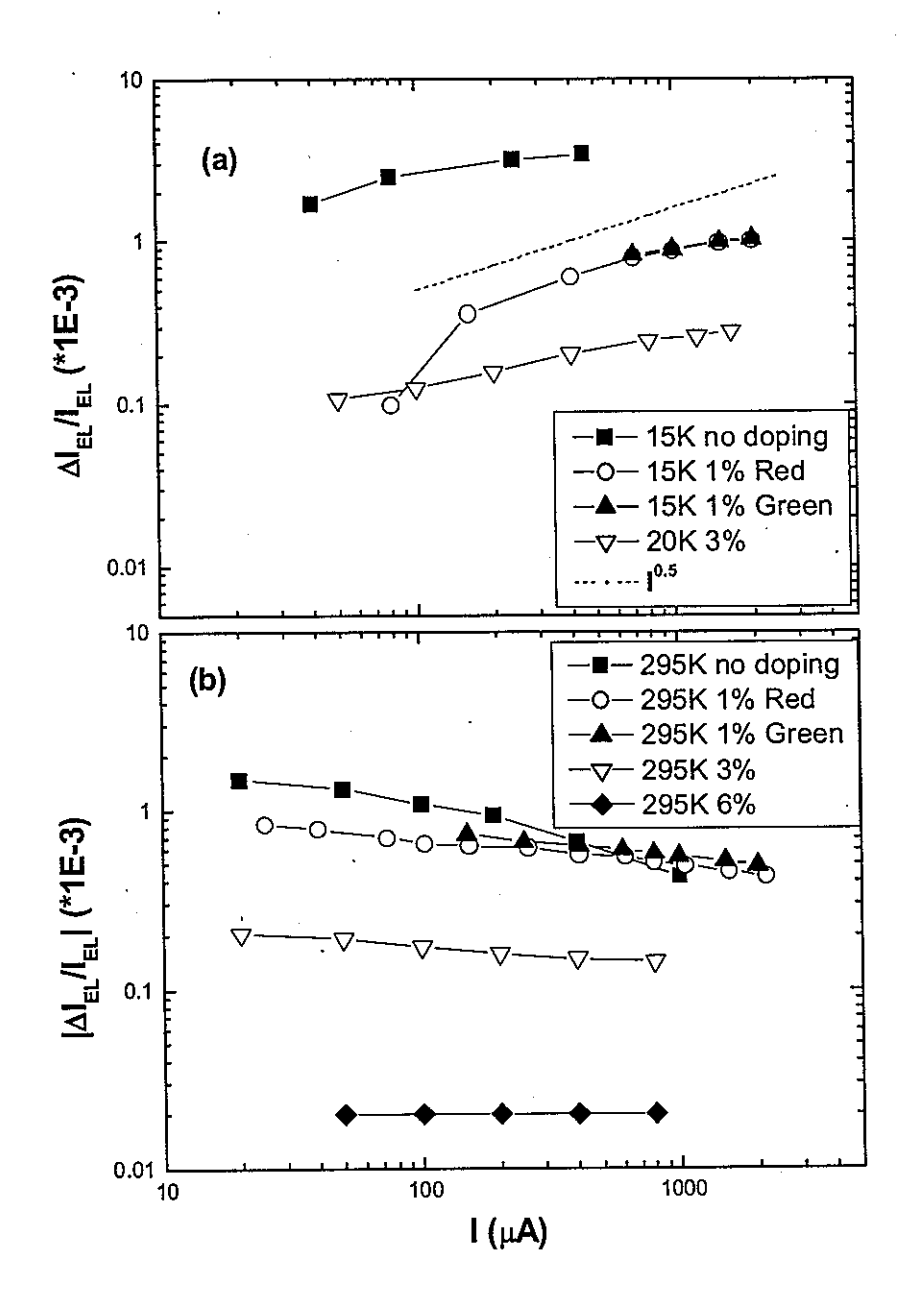


Figure 3. The current J-dependence of (a) the positive spin 1/2 ELDMR at 15-20 K and (b) the negative spin 1/2 ELDMR at 295 K of 0, 1, 3, and 6 wt.% PtOEP-doped Alq<sub>3</sub> OLEDs.

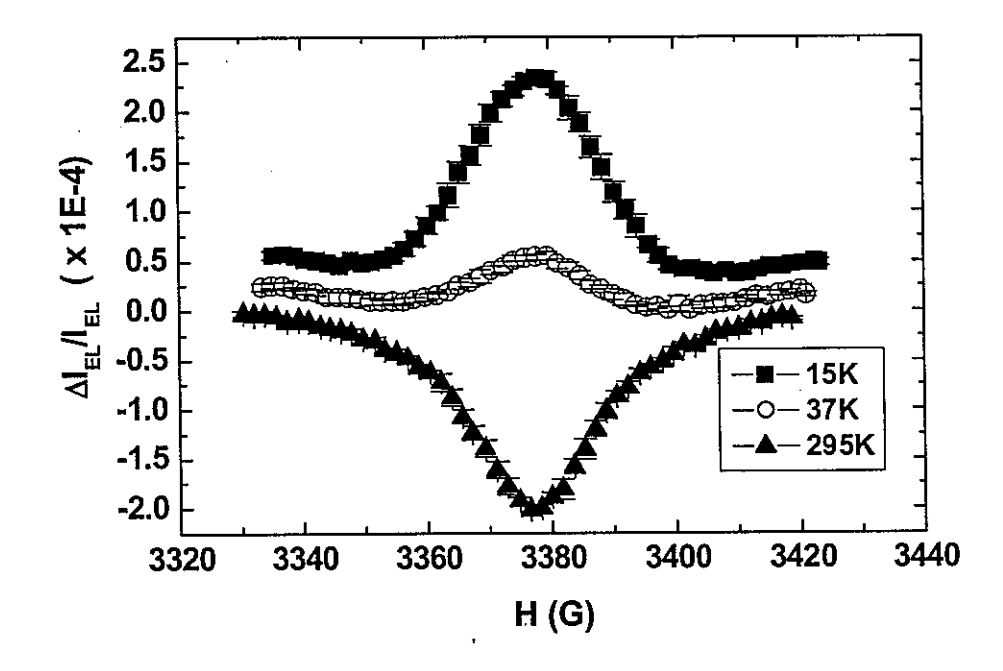


Figure 4. The spin-1/2 ELDMR of 3 wt.% PtOEP:Alq<sub>3</sub> OLED at 15, 37, and 295 K.

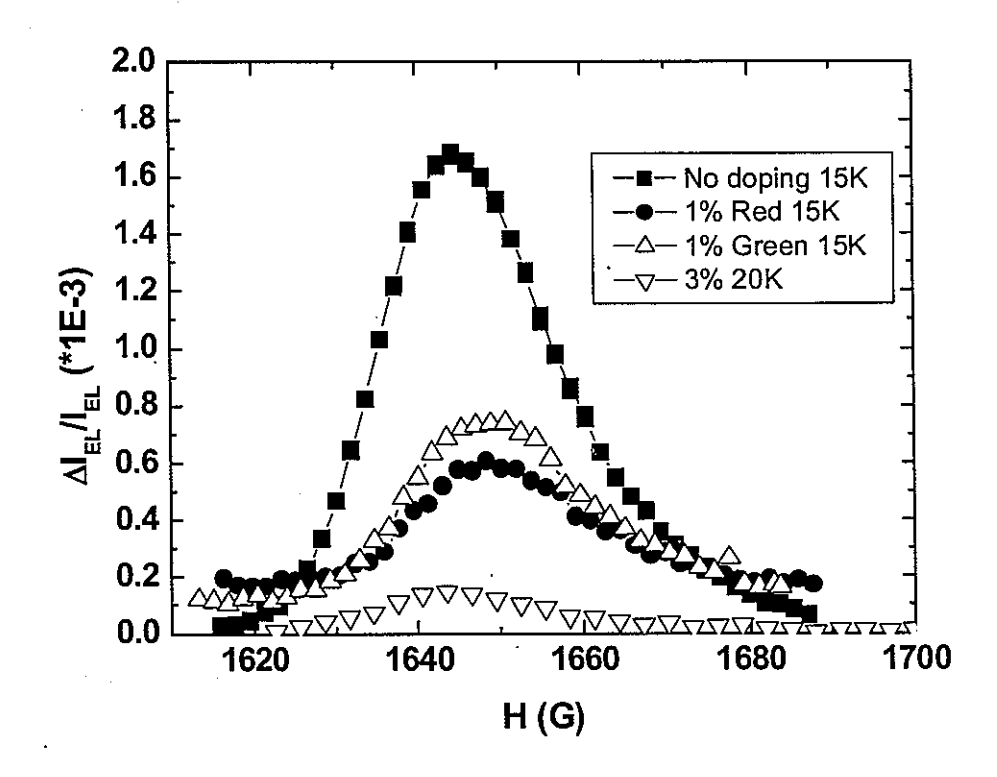


Figure 5. The half-field TE ELDMR of 0, 1, and 3% PtOEP:Alq<sub>3</sub> at low temperature.

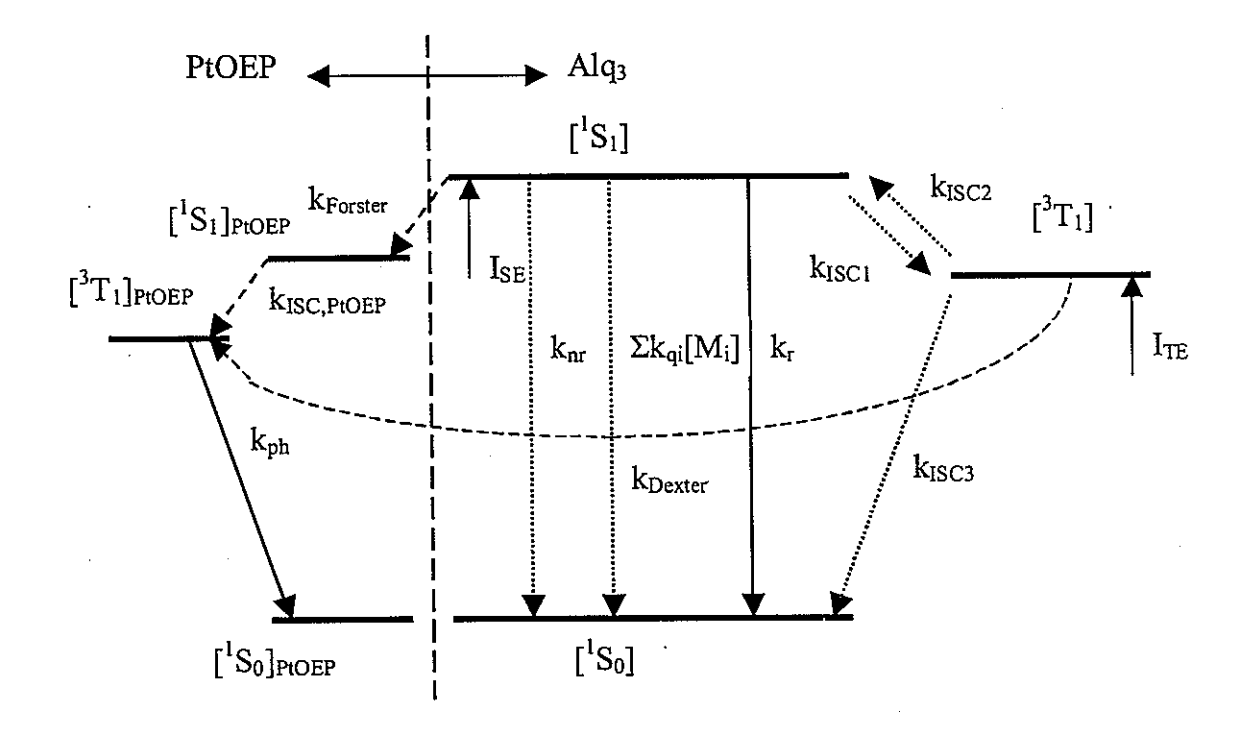


Figure 6. The photophysical processes in PtOEP-doped Alq<sub>3</sub> OLEDs.

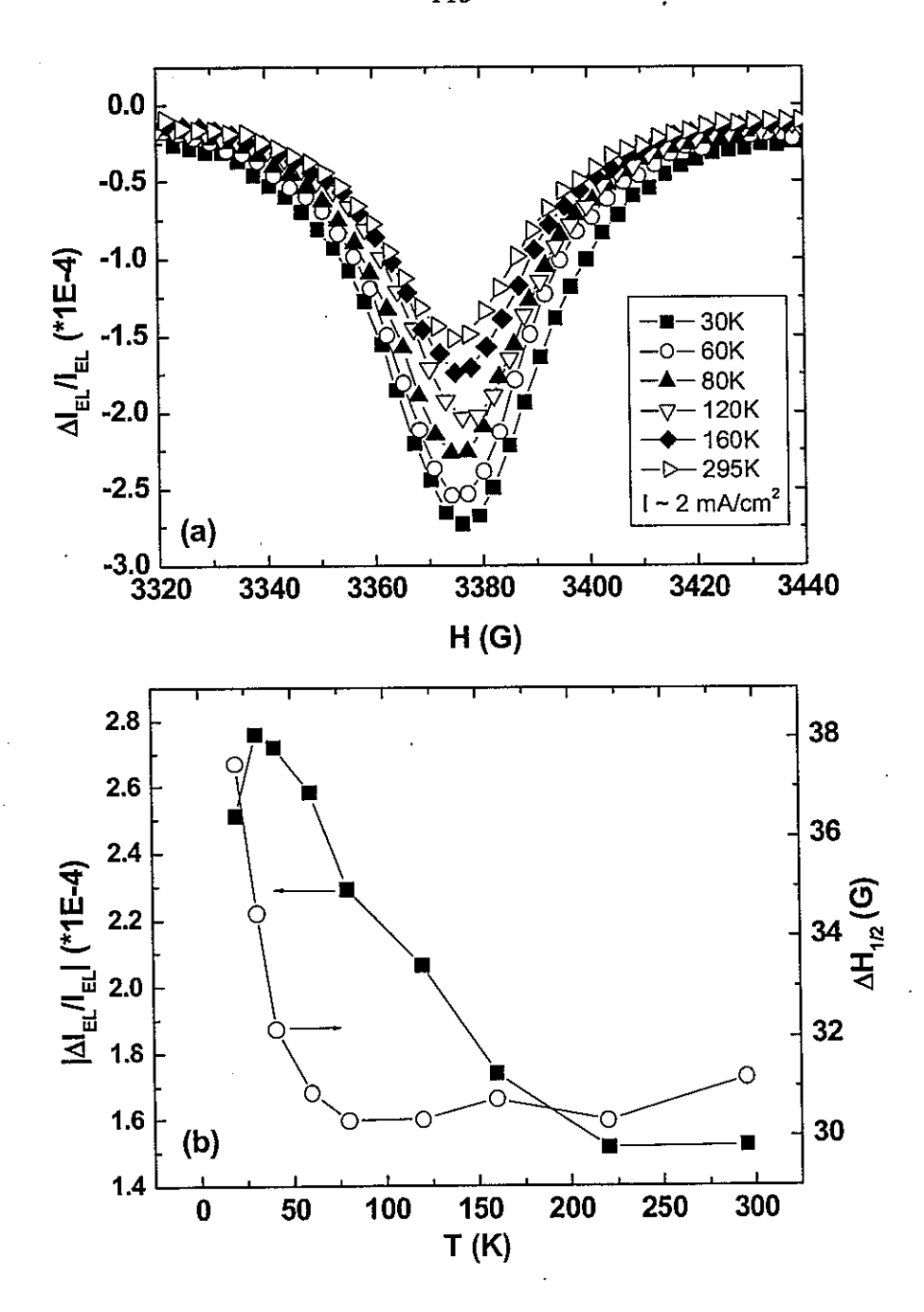


Figure 7. (a) The temperature dependence of the spin-1/2 ELDMR signal of 20 wt.% PtOEP OLEDs;  $J \sim 2 \text{ mA/cm}^2$ . Note that the magnitude of the negative resonance decreases when T increases. (b) The temperature dependence of the resonance linewidth  $\Delta H_{1/2}$  (open circles) and resonance amplitude  $|\Delta I_{EL}/I_{EL}|$  (solid squares).  $|\Delta I_{EL}/I_{EL}|$  is largely independent of the injected current at both 20 K and room temperature (not shown).

# Chapter 5. A Combinatorial Study of Exciplex Formation at Organic/Organic Interfaces in Organic Light-Emitting Devices

G. Li, L. Zou, C-H. Kim, and J. Shinara)

(Prepared for Applied Physics Letters)

Ames Laboratory-USDOE and Department of Physics and Astronomy

Iowa State University, Ames, Iowa 50011-3020

#### Y. Shirota

Department of Applied Chemistry, Faculty of Engineering, Osaka University, Yamadaoka,
Suita, Osaka 565, Japan

#### Abstract

The combinatorial matrix array technique was used to study exciplex formation in blends of the high glass-transition-temperature hole-transport-material 4,4',4"-tris[2-naphthyl (phenyl)-amino]triphenylamine (2-TNATA), and the electron-transport and blue-emitting material 2,2',7,7'-tetrakis(2,2'-diphenylvinyl)spiro-9,9'-bifluorene (Spiro-DPVBi). The blend layer was incorporated in ITO/2-TNATA/[(1:1) 2-TNATA:Spiro-DPVBi]/[N,N'-diphenyl-N,N'-bis(1-naphthylphenyl) -1,1'- biphenyl -4,4'-diamine (NPB) ]/ Spiro-DPVBi/ [tris(8-hydroxy quinoline) Al (Alq<sub>3</sub>)]/CsF/Al organic light-emitting devices (OLEDs), and the thicknesses of the blend and NPB layers were varied systematically. The low efficiency exciplex emission was avoided when the thickness of the NPB layer exceeded 8 nm.

PACS Nos.

a) Author to whom correspondence should be addressed; electronic mail: shinar@ameslab.gov

#### I. Introduction

Organic light-emitting devices (OLEDs) have been studied extensively since Tang and VanSlyke<sup>1</sup> demonstrated that vacuum-evaporation of multilayer thin film structures can yield efficient devices by improving carrier injection, balancing electron and hole injection, and confining the recombination zone to a region far from the metal contacts. These key steps were crucial for the development of OLEDs as serious candidates for next-generation displays and solid-state lighting. One of the significant results of the multilayer structure was the appearance of exciplexes at the organic/organic interfaces. The exciplex is formed from two distinct chromophores, a donor D and an acceptor A, with one in the excited state and the other in the ground state:

$${}^{1}D + {}^{1}A^{*} \rightarrow {}^{1}(D^{+}A^{-}) \quad \text{or} \quad {}^{1}D^{*} + {}^{1}A \rightarrow {}^{1}(D^{+}A^{-})$$
 (1)

The exciplex is metastable as a result of resonant contributions from exciton and charge transfer configurations:<sup>2</sup>

$${}^{1}(A^{*}D) \leftrightarrow {}^{1}(AD^{*}) \leftrightarrow {}^{1}(A^{T}D^{+}). \tag{2}$$

Exciplexes are interesting not only from the physical standpoint, but also due to their potential applications for tuning the emission color<sup>3</sup> and delivering white light.<sup>4-7</sup> Several studies on exciplex formation on the organic interface have been done.<sup>8-12</sup>

Although exciplex formation may enhance the quantum yield of photophysical processes compared to excimer formation,<sup>2</sup> to our knowledge the photoluminescence (PL) quantum yield (PLQY)  $\eta_{PL}$  of an exciplex has never been reported to have a higher value than that of the emissive molecule. Hence, from the point of view of device efficiency, and particularly for blue emission, exciplexes should be avoided. To that end, two methods have been reported. The simpler and more general method is to insert a weaker electron donating

material between the donor and acceptor materials.<sup>13</sup> The other uses the exciplex-forming material as a dopant; light doping reduces the probability of exciplex formation significantly.<sup>14</sup> To obtain an efficient device, the second method requires a host for exciplex formation, normally a blue emitter. This limits its use and does not provide a general solution.

This letter describes the exciplex emission between two promising high-glass-transition-temperature materials, 4,4',4''-tris[2-naphthyl(phenyl)-amino]triphenyl-amine (2-TNATA)  $(T_g = 110^{\circ}\text{C})^{15}$  and 2,2',7,7'-tetrakis(2,2'-diphenylvinyl)spiro-9,9'-bifluorene (Spiro-DPVBi)  $(T_g = 130 \, ^{\circ}\text{C})^{16}$  2-TNATA is a starburst molecule, which has proven to be an excellent hole-transporting material for improving the thermal stability of OLEDs and reducing device operation voltage. Spiro-DPVBi is one of the most thermally stable and efficient blue-emitting materials, developed to replace the efficient but low  $T_g$  (=  $64^{\circ}\text{C}$ ) blue emitter 4,4'-bis(2,2-diphenylvinyl)biphenyl (DPVBi). This study used a combinatorial sliding shutter technique, which eliminates uncontrolled batch-to-batch variations in the fabrication conditions, to avoid this exciplex formation and identify the optimal structural parameters for 2-TNATA/Spiro-DPVBi-based OLEDs.

# II. Experimental Procedure

Figure 1 shows the molecular structures of the materials used to fabricate the multilayer devices, including 2-TNATA, N,N'-diphenyl-N,N'-bis(1-naphthylphenyl)-1,1'-biphenyl-4,4'-diamine (NPB), Spiro-DPVBi, and tris (8-hydroxy quinoline) Al (Alq<sub>3</sub>), and the device structure. The Applied Films Corp  $R_{\square} \sim 20~\Omega/\square$ , 150 - 200 nm-thick indium tin oxide (ITO) coated glass substrates were etched in diluted aquaregia to increase the ITO work function

and enhance hole injection. <sup>19</sup> The substrates were then degreased by detergent and organic solvents. The organic layers, CsF buffer layer, and Al cathode were deposited by thermal evaporation in a high-vacuum chamber installed in an Ar filled glove-box (<1 ppm O<sub>2</sub>, H<sub>2</sub>O). The base pressure for deposition was < 10<sup>-6</sup> Torr. The organic layers included 40 nm 2-TNATA (as a hole transporting layer (HTL)), and 0, 2, 5, or 10 nm of 2-TNATA:Spiro-DPVBi (50:50 wt.%). Then the substrate was rotated by 90° and different thicknesses of NPB (0, 2, 4, or 8 nm) were deposited over it. 40 nm Spiro-DPVBi and 10 nm Alq<sub>3</sub> followed as two electron transporting layers fabricated to reduce the operating voltage. By using the sliding shutter technique, all 16 variations of this OLED structure were deposited at the same time, eliminating uncontrolled variations in the batch-to-batch fabrication conditions.

The cathode consisted of ~1 nm CsF and ~150 nm Al. The deposition rate of the organic layers was ~0.1 nm/s, controlled by a calibrated quartz-crystal thickness monitor. The CsF layer was deposited at ~0.01 nm/sec. The Al was deposited at 0.5 - 0.7 nm/sec through a mask of 21×21 1.5 mm diameter holes, yielding a 21×21 matrix array of OLED pixels.<sup>17</sup>

The current density-voltage J(V) and electroluminescence (EL) intensity-voltage  $I_{EL}(V)$  curves were measured using a Keithley 2000 digital multimeter and Minolta L100 luminance meter. The EL and PL spectra were measured using an OceanOptics Chem-2000 spectrometer. The PL spectra and  $\eta_{PL}$  of the 260 nm-thick film samples were measured using an integrating sphere.<sup>20</sup> The PL was excited by the multiline UV emission at 351 + 361 nm from an Ar<sup>+</sup> laser.

## III. Results and Discussion

The PL spectra of thermally evaporated films of 2-TNATA, spiro-DPVBi, 50:50 wt.% mixture, and Alq<sub>3</sub>, are shown in Fig. 2. The PL peaks of 2-TNATA and Spiro-DPVBi are at almost the same wavelength ~460 nm; the 2-TNATA spectra exhibit a longer wavelength tail. The PL emission peak of the 1:1 weight mixture of 2-TNATA and Spiro-DPVBi at 527 nm is clearly due to an exciplex. Note that it is slightly broader than the Alq<sub>3</sub> emission band around 525 nm, and it contains a blue shoulder, due to emission from the 2-TNATA and/or Spiro-DPVBi.

The half-wave oxidation potentials ( $E^{ox}_{1/2}$ ) of 2-TNATA and NPB were measured using cyclic voltametry. They are 0.11 V and 0.51 V vs. Ag/Ag<sup>+</sup> (0.01mol cm<sup>-3</sup>), respectively. From these values and those of the absorption edges, the (LUMO, HOMO) energies of 2-TNATA, Spiro-DPVBi, and NPB are (-2.13, -5.15), (-2.50, -5.50) and (-2.43, -5.55) eV, respectively.

The empirical formula for the exciplex emission energy then yields<sup>21</sup>

$$hv_{Exciplex} = E^{ox}(2 - TNATA) - E^{red}(spiro - DPVBi) - 0.15 \pm 0.1eV$$

$$= LUMO(spiro - DPVBi) - HOMO(2 - TNATA) - 0.15 \pm 0.1eV$$

$$= (-2.50) - (-5.15) - 0.15 \pm 0.1eV = 2.50 \pm 0.1eV$$
(3)

The exciplex peak at 527 nm, corresponding to 2.36 eV, agrees well with the above expression.

Figs. 3a-3d show the evolution of the EL spectra of the 0, 2, 5, and 10 nm 50:50 wt.% TNATA-Spiro-DPVBi blend devices without an NPB buffer (Devices 1, 2, 3, and 4, respectively), biased at 4, 5, 7, and 9 V. The exciplex emission is easily seen in Figs. 3b - 3d; in Device 1, with no blend layer, the exciplex emission is a weak shoulder at low voltage. As the thickness of the blend layer increases, the exciplex emission becomes much stronger. On

the other hand, in all Devices 1 - 4, the spectra exhibit an electric field-induced blueshift due to field-induced dissociation of the exciplexes. The observed behavior is explained as follows: in Device 1, only molecules close to the sharp TNATA/Spiro-DPVBi interface can form exciplex states. As the thickness of the blend layer increases, the number of exciplex states increases rapidly, and the exciplex emission increases.

Figs. 3e and 3f show the evolution of the EL spectra devices with a 10 nm-thick blend layer, 2 nm NPB (Fig. 3e, Device 5), and 8 nm NPB (Fig. 3f, Device 6). The effect of the NPB layer on reducing the exciplex emission is clear. With 2 nm of NPB (Device 5), the emission evolves from almost pure exciplex emission at 4 V to almost pure Spiro-DPVBi emission at 9 V. With 8 nm of NPB, the emission is almost purely from Spiro-DPVBi over the entire bias range. Although not shown, the emission of Device 7 (0 nm blend, 8 nm NPB) is purely from Spiro-DPVBi.

It may be argued that the emission band around 530 nm could be due to  $Alq_3$  rather than the 2-TNATA-Spiro-DPVBi exciplex. However, by comparing Devices 1 and 2 we see that adding a thin layer of the blend does not change the I(V) curve (i.e., it does not affect the transport; see Fig. 4), so we would expect the emission zone to be unaffected as well. Yet the emission band around 530 nm is much more prominent in Device 2 than in Device 1. In addition, that band weakens with increasing bias, as expected for exciplex but not for  $Alq_3$  emission band.

Figure 4 shows the (a)  $I_{EL}(V)$  and (b) J(V) curves of Devices 1 to 6. In the device with no NPB buffer layer, adding the 2-TNATA:Spiro-DPVBi 50:50 wt.% blend, up to 10 nm thick, only shifted the J(V) slightly towards higher voltage. On the other hand, adding 8 nm of NPB led to noticeably higher driving voltage. This indicates that the J(V) curve is mainly

Device#	1	2	3	4	5	6	7
Blend	0	2	5	10	10	10	0
NPB (nm)	o	0	0	0	2	8	8

Table I. Device number and their corresponding 2-TNATA:Spiro-DPVBi blending, NPB layer thickness in the paper.

controlled by the electron and hole barriers between 2-TNATA and Spiro-DPVBi, and the blend layer has only a minor effect on the transport of electrons and holes. In the blend layer, the electrons drift in the Spiro-DPVBi LUMO band, while the holes drift in the 2-TNATA HOMO band.

Although the J(V) curves and EL spectra are different, the turn-on voltage (defined as the voltage for 1 Cd/m<sup>2</sup> emission) of all six devices is similar (3.4 - 3.8 eV).

The emission of the exciplex around ~527 nm has a much larger photopic response than that of Spiro-DPVBi around ~460 nm. Yet the maximal brightness of the devices with significant exciplex emission (7600, 7300, 5300, and 6300 Cd/m<sup>2</sup> for Device 1 to 4, respectively) is much lower than that of those with no exciplex emission (17600 and 18900 Cd/m<sup>2</sup> for Device 6 and 7, respectively). This may be due to the low PLQY of the blends: For thermally evaporated 2-TNATA, Spiro-DPVBi and their 1:1 blend films,  $\eta_{PL} = 11$ , 35, and 7.8%, respectively.

The external quantum efficiency  $\eta_{ext}$  <sup>22</sup> vs. I of all six devices are shown in Fig. 5. The devices with strongest exciplex emission (Device 3 and 4) have the lowest efficiency (~0.25%). Device 1 and 2 have maximum efficiency of ~0.5%. The devices with no exciplex emission have much higher efficiency, 2.77% for Device 7 and 1.77% for Device 6.

 $\eta_{ext}$  is given by the expression

$$\eta_{ext} = \chi \eta_{PL} \, \eta_r \, \eta_e \tag{4}$$

where  $\chi$  is the fraction of charge carrier recombination in the material resulting in singlet excitons (= 0.25%),  $\eta_r$  is the fraction of injected charge carriers that form excitons (determined by charge balance), and  $\eta_e$  is the fraction of emitted photons that are coupled out of the device. Comparing Devices 4 and 6, which have the same blend layer but different NPB layers, we note that  $\eta_{ext}$  of Device 6 is ~ 6.5 time that of Device 4, while  $\eta_{PL}$  of Spiro-DPVBi is ~4.6 time that of the blend layer. Thus the  $\eta_{PL}$  difference can account for most of the  $\eta_{ext}$  difference. Since  $\chi$  and  $\eta_e$  are the same in these two devices, the remaining difference must be due to a difference in carrier balance, which is introduced by inserting 8 nm NPB. The source of the difference between  $\eta_{ext}$  in Devices 6 and 7 may due to the remaining small amount of exciplex emission in Device 6 (see Figure 3f).

The HOMO and LUMO energies of NPB (-5.50, -2.50 eV, respectively) and Spiro-DPVBi, (-5.55, -2.43 eV, respectively) are very close. Hence there is no significant energy barrier for carriers at the interface between these materials. Consequently, the efficient Spiro-DPVBi emission is surprising. However, this can be understood by taking into account the electron blocking ability of NPB. It has a high hole mobility  $\mu_h \sim 3 \times 10^{-4}$  cm<sup>2</sup>/Vs<sup>23</sup> but much lower electron mobility. Hence the electrons at the Spiro-DPVBi layer will be blocked by NPB when its thickness is sufficiently large. By comparing the spectra at 4 V in Figs. 3d, 3e, and 3f (devices with 10 nm blend layer and 0, 2, and 8 nm NPB layer, respectively), it can be easily seen that the 8 nm-thick NPB layer blocks the electrons almost completely. Otherwise, the electrons would recombine with holes in the blend layer to give exciplex emission. Although no effective energy barriers exist, the electron blocking property of NPB results in

the formation of a well-defined emission zone and consequently efficient devices. The absence of the energy barrier, however, probably compromises the efficiency. This could be the reason that in the most efficient device  $\eta_{ext} = 2.8\%$ , while in other devices with NPB and DPVBi it can reach 3.50%.<sup>24</sup>

## IV. Summary and Conclusions

In summary, a combinatorial study of OLEDs incorporating the two thermally stable materials 2-TNATA and Spiro-DPVBi, between which exciplex emission occurs, and their 1:1 blend, was described. The thicknesses of the blend layer and an NPB layer between the blend layer and Spiro-DPVBi layer were varied systematically. The exciplex emission was found to be inefficient ( $\eta_{ext} \sim 0.25\%$ ). Adding the NPB spacer layer reduced the exciplex emission and increased the efficient blue emission, to up to  $\eta_{ext} = 2.8\%$ , with turn-on voltage of 3.8V.

## Acknowledgements

Ames Laboratory is operated by Iowa State University for the US Department of Energy under Contract W-7405-ENG-82. This work was supported by the Director for Energy Research, Office of Basic Energy Science.

#### References

- 1. C. W. Tang and S. A. VanSlyke, Appl. Phys. Lett. 51, 913 (1987).
- 2. S. A. Jenekhe and J. A. Osaheni, Science 265, 765 (1994).
- 3. H. Ogawa, R. Okuda and Y. Shirota, Appl. Phys. A 67, 599 (1998).

- 4. C.Chao, and S. Chen, Appl. Phys. Lett. 73, 426 (1998).
- 5. J. Feng, F. Li, W.Gao, S. Liu, Y. Liu and Y. Wang, Appl. Phys. Lett, 78, 3947 (2001).
- J. Thompson, R. I. R. Blyth, M. Mazzeo, M. Anni, G. Gigli, and R. Cingolani, Appl. Phys. Lett. 79, 560 (2001).
- 7. S. W. Cha and J.-I. Jin, J. Mater. Chem. 13, 479 (2003).
- 8. K. Itano, H. Ogawa, and Y. Shirota, Appl. Phys. Lett. 72, 636 (1998).
- 9. T. Noda, H. Ogawa, and Y. Shirota, Adv. Mater. 11, 283 (1999).
- 10. T. Noda, and Y. Shirota, J. Luminescence 87-89, 1168 (2000).
- 11. D.-Q. Gao, Y.-Y. Huang, C.-H. Huang, F.-Y. Li, and L. Huang, Chem. Phys. Lett. 350, 206 (2001).
- 12. L. C. Palilis, A. J. Mäkinen, M. Uchida, and Z. H. Kafafi, Appli. Phys. Lett. 82, 2209 (2003).
- 13. T. Noda, H. Ogawa, and Y. Shirota, Adv. Mater. 11, 283 (1999).
- 14. B. Chen, X. H. Zhang, X. Q. Lin, H. L. Kwong, N. B. Wong, C. S. Lee, W. A. Gaambling, and S. T. Lee, Syn. Met. 118, 193 (2001).
- 15. Y. Shirota, Y. Kuwabara, D. Okuda, R. Okuda, H. Ogawa, H. Inada, T. Wakimoto, H. Nakada, Y. Yonemoto, S. Kawami, and K. Imai, J. Luminescence 72-74, 985 (1997).
- 16. H. Spreitzer, H. Schenk, J. Salbeck, F. Weissoertel, H. Riel, and W. Reiss, in *Organic Light Emitting Materials and Devices*, edited by Z. H. Kafafi, Proc. SPIE 3797, 316 (SPIE, Bellingham, WA, 1999); F. Steuber, J. Staudigel, M. Stössel, J. Simmerer, A. Winnacker, H. Spreitzer, F. Weissörtel, and J. Salbeck, Adv. Mat. 12, 130 (2000).
- 17. C. Hosokawa, H. Higashi, H. Nakamura, and T. Kusumoto, Appl. Phys. Lett. 67, 3853 (1995).

- 18. L. Zou, V. Savvate'ev, J. Booher, C. H. Kim, and J. Shinar, Appl. Phys. Lett. 79, 2282 (2001).
- 19. F. Li, H. Tang, J. Anderegg, and J. Shinar, Appl. Phys. Lett. 70, 1233 (1997).
- 20. J.C. de Mello, H. F. Wittmann, and R.H. Friend, Adv. Mater. 9, 230 (1997).
- 21. A. Weller, in *The Exciplex*, edited by M. Gordon and W. R. Ware (Academic Press, NY, 1975) p. 23.
- D. O'Brien, A. Bleyer, D. G. Lidzey, D. D. C. Bradley, and T. Tsutsui, J. Appl. Phys. 82, 2662 (1997).
- 23. E. W. Forsythe, M. A. Abkowitz, Y. Gao, and C. W. Tang, J. Vac. Sci. Tech. A 18, 1869 (2000).
- 24. K. O. Cheon and J. Shinar, Appl. Phys. Lett. 81, 1738 (2002).

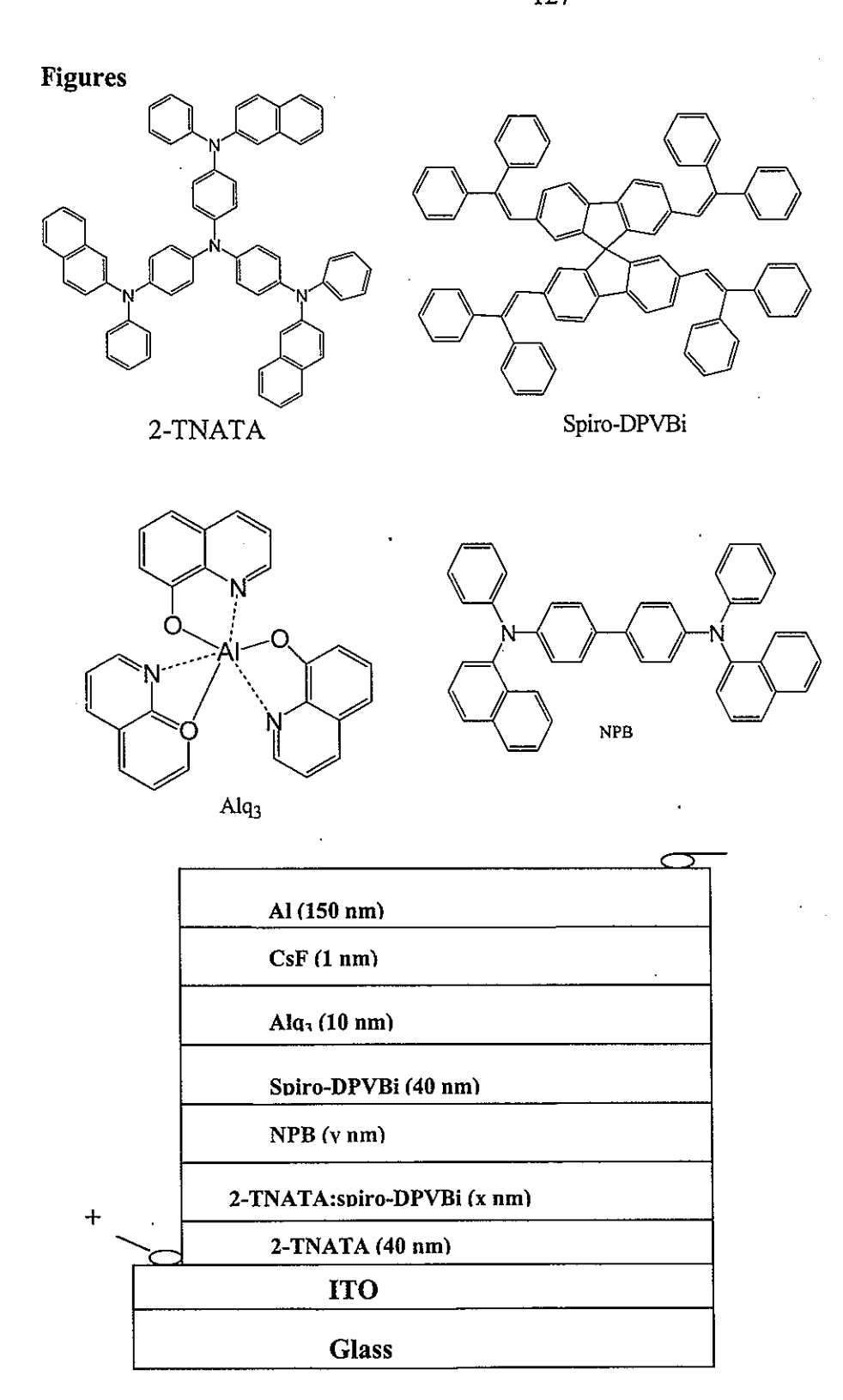


Figure 1. Molecular structures and device structure of OLEDs. x = 0, 2, 5, 10, and y = 0, 2, 4, and 8.

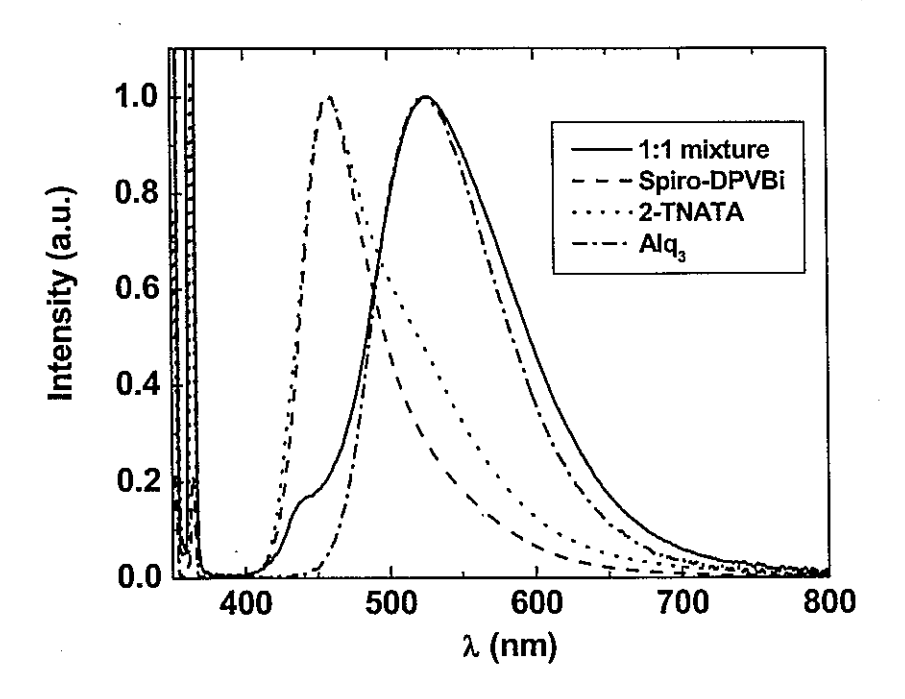


Figure 2. PL spectra of thermally evaporated films: 2-TNATA:spiro-DPVBi mixture (50:50 wt.%), spiro-DPVBi, 2-TNATA, and Alq<sub>3</sub>. The films' thickness was ~260 nm.

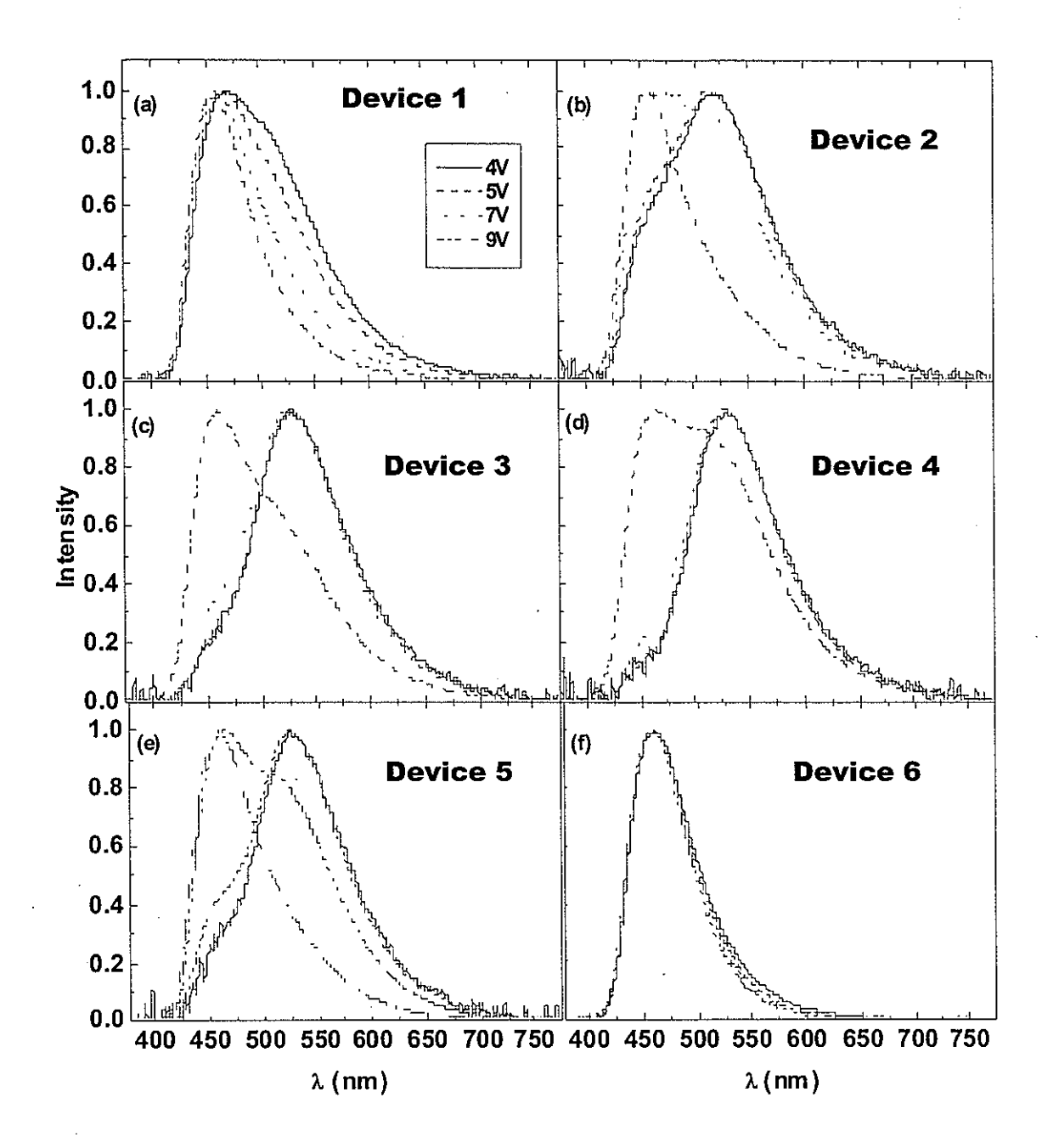


Figure 3. The EL spectra at 4, 5, 7, and 9 V. The thickness of the 50:50 wt.% blend layer and NPB layers are, (a) 0 and 0, (b) 2 and 0, (c) 5 and 0, (d) 10 and 0, (e) 10 and 2, and (f) 10 and 8 nm, respectively.

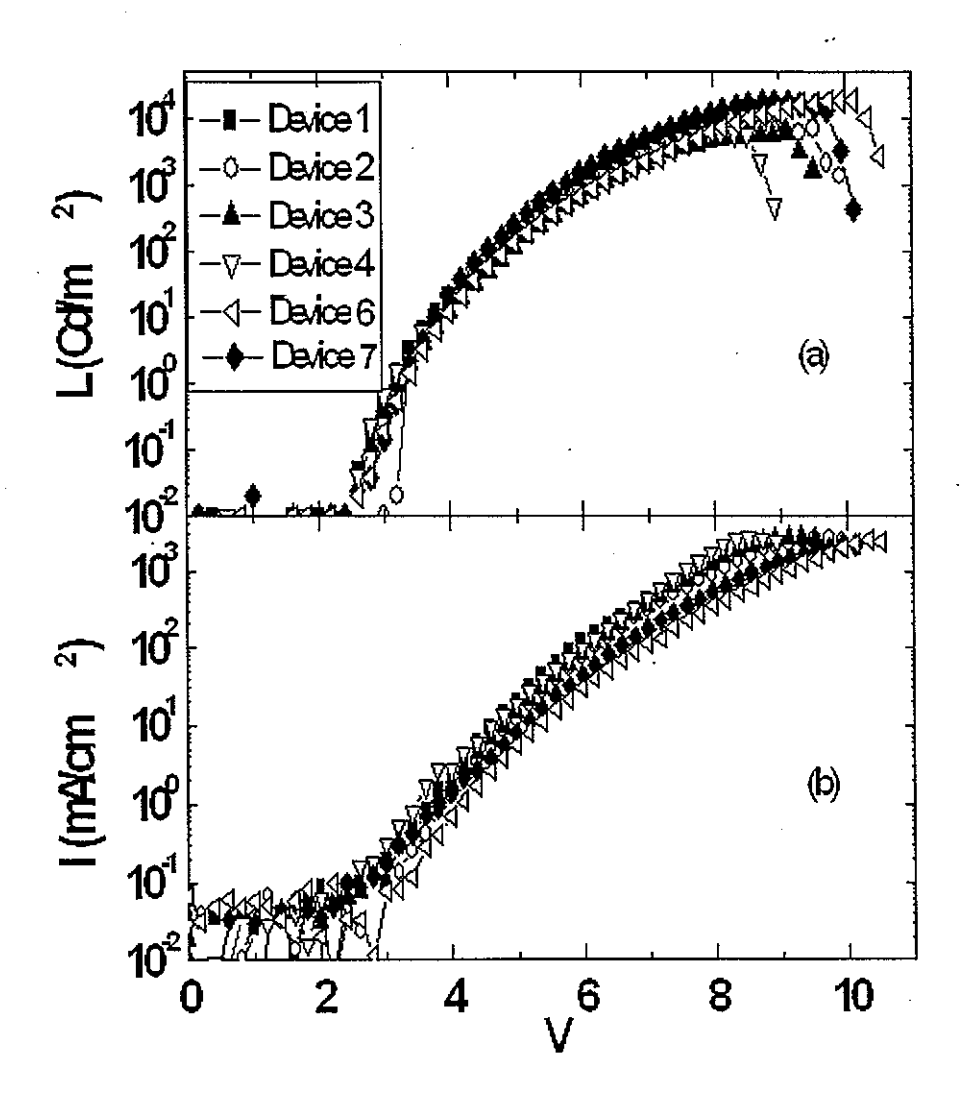


Figure 4. The (a) brightness vs. voltage and (b) current density vs. voltage curves for Devices 1 to 4, 6 and 7.

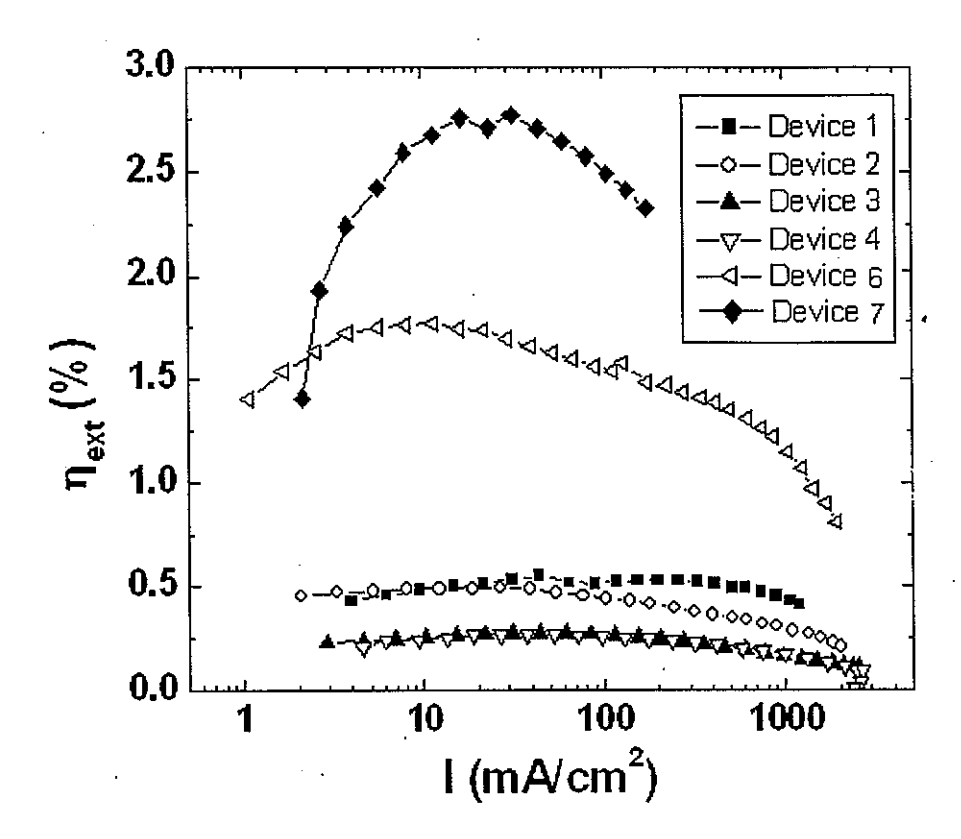


Figure 5. The external efficiency  $\eta_{ext}$  of Devices 1 to 4, 6 and 7. The addition of 8 nm of NPB layer significantly enhances the device efficiency by suppressing the inefficient exciplex emission.

## Chapter 6. General Conclusions

### I. General Discussion

There are two major parts in the work presented in this dissertation. First, ODMR was used to study the small molecular OLEDs and films. The first work (Chapter 3) is ODMR (PLDMR, ELDMR, and EDMR) studies of classical CuPc/TPD/Alq<sub>3</sub>/buffer/Al OLED, in which the buffer layers are AlOx and CsF. While this structure represents fluorescent OLED, the second ODMR work is on the CuPc/NPB/x% PtOEP:Alq<sub>3</sub>/Alq<sub>3</sub>/ CsF/Al phosphorescent OLED (Ph-OLED). The second part of work is a combinatorial study of exciplex formation at two promising high glass transition temperature organic materials.

Chapter 1 is a general introduction of OLEDs and chapter 2 is the introduction of ODMR technique. Following the two general introduction chapters, the first EL-, PL-, and EDMR studies of tris-(8-hydroxyquinoline) aluminum (Alq<sub>3</sub>)-based OLEDs and films are described in chapter 3. The OLEDs studied differ only in the buffer layer between organic and metal cathodes, which strongly affect the performance of OLEDs. At low temperatures, a spin-1/2 resonance enhances the current density J, the EL intensity  $I_{EL}$ , and the PL intensity  $I_{PL}$  ( $\Delta J/J$ ,  $\Delta I_{EL}/I_{EL}$ , and  $\Delta I_{PL}/I_{PL} > 0$ ).  $\Delta J/J$  and  $\Delta I_{EL}/I_{EL}$  are insensitive to the nature of the Alq<sub>3</sub>/cathode interface. The low temperature resonance weaken with increasing T and become unobservable above 60 K.  $\Delta I_{PL}/I_{PL}$  also decreases with T, but more slowly, and it is still observable at 250 K. The low temperature enhancing spin-1/2 resonance is attributed to the magnetic resonance reduction of polaron population, which otherwise quenches SEs. For T> 60K, a quenching spin-1/2 EL- and EDMR resonance emerges and grows with T, but not detectable in PL. This resonance is sensitive to the buffer layer between Alq<sub>3</sub> and the

cathode, and is attributed to magnetic resonance enhancement of the spin-dependent formation of negative spinless bipolarons (dianions) from spin-1/2 negative polarons at the organic/cathode interface. The results provide insight on the nature of organic interface and the impact of the interface on the device performance. The additional electric field produced by the increase of the negative charge density at the interface increases SE dissociation. This model quantitatively agrees with the quenching resonance.

Due to large exciton binding energy, a 25% upper limit exists in the internal quantum efficiency of fluorescent OLEDs. Ph-OLEDs move this limit up to 100% and thus is of great important in the field. Chapter 4 presents the ELDMR studies of PtOPE doped Alq3 based Ph-OLEDs. The doping concentration of PtOEP varies from 0% to 20%. In 1% PtOEP doped Alq<sub>3</sub> OLED, the emission consists of PtOEP phosphorescent and Alq<sub>3</sub> fluorescent emission. The ELDMR current dependence of these two emission bands is identical in both 20K (enhancing) and room temperature (quenching). The enhancing resonance is attributed to the magnetic-resonance reduction of SE quenching by a reduced population of polarons. The quenching resonance is attributed to magnetic resonance enhancement formation of dianions at the organic/cathode interface. Both low temperature enhancing and room temperature quenching resonance of PtOEP phosphorescence decrease quickly with PtOEP concentration up to 6%. The results can be explained by assuming that the ELDMR of the guest emission is due to the effect of magnetic resonance conditions on the host SEs. A rate equation model is established to explain the evolution of the ELDMR with dye concentration. In the 20 wt.%doped devices, the spin-1/2 polaron resonance is quenching at all T and both  $|\Delta I_{EL}/I_{EL}|$ , and the resonance linewidth, decrease with increasing T;  $|\Delta I_{EL}/I_{EL}|$  is weakly current-dependent at both 20 K and 295 K. The resonance is tentatively attributed to magnetic resonance

enhancement of the spin-dependent formation of dianions/dications from polarons in the bulk organic layer.

When an exciton extends on two different molecules, it is called exciplex. Exciplexes are interesting not only from the academics standpoint, but also due to their potential applications for tuning the emission color and producing white light. However, exciplex is normally not efficient and need to avoid. In Chapter 5, combinatorial matrix array technique is used to study exciplex formation in blends of two high glass-transition-temperature material: hole-transporter 2-TNATA, and electron-transporter and blue-emitter Spiro-DPVBi. The thickness of 2-TNATA:spiro-DPVBi blend layer and NPB layer are varied systematically. In devices with no NPB spacer layer, a green emission band similar Alq<sub>3</sub> increases dramatically with the blend thickness. By comparing the J-V characteristics and the driving voltage evolution of emission, the green emission was attributed to exciplex emission between 2-TNATA and spiro-DPVBi. This assignment agrees well with the energy level relationship. By inserting a NPB spacer layer between the blend and spiro-DPVBi, the exciplex can be effectively reduced. The efficiency of the device is closely related to the exciplex emission. This exciplex emission efficiency is found to be low and thus inserting NPB layer can effectively enhance the efficiency and obtain pure spiro-DPVBi blue emission.

## II. Recommendations for Future Research

This dissertation presents ODMR results on fluorescent and phosphorescent dye doped small molecular OLEDs. Fluorescent dye doped OLED is also widely used to tune the color, increase efficiency and enhance lifetime of OLEDs. The future study could be the ELDMR and EDMR study of fluorescent dye rubrene doped DPVBi and /or DPVBi only OLED with

CsF as buffer layer. DPVBi is a highly efficient blue emitter and recently a white OLED (WOLED) based on lightly rubrene doped DPVBi structure obtains record-setting brightness for WOLED and is also the most efficient fluorescent WOLED reported. In addition, rubrene's SEs energy is about twice that of TEs, which might provide interesting physics related to TE-TE annihilation.

2-TNATA also forms orange emission exciplex with Alq<sub>3</sub>. Since 2-TNATA:spiro-DPVBi emission can be tuned from green to blue, it is possible to make WOLED based on the two exciplexes. In addition, ODMR study of exciplex has not been reported, and it might also provide interesting physics.

# Acknowledgements

I would like to show my sincere thanks to my advisor Prof. Joseph Shinar for so many years of excellent advice and encouragement. Without his guidance, the research work presented in this dissertation would never be possible.

I would like to show my special thanks to my lovely wife, Wei Liu. She fills my life with deep love and makes the years of my Ph.D. study an everlasting happy time. I also thank my lovely daughter, April, who makes our life so much fun and happiness. Special thanks also to my mom and dad. Their selfless love and guidance are with me all the time and I owe them so much.

My thanks also to my peers at Prof. Shinar's research group: Chang-Hwan Kim and Lijuan Zou for many discussions of results and encouragement; Brian Leigh Uhlhorn for guiding me for ODMR experiments; Kwong-Ohk Cheon, Moon-Ky Lee, Bhaskar Choudhury, Dr. Haixing Wu, Zhaoqun Zhou and Ying Chen for friendship these years.

I would like also thanks Professor Ghassan E. Jabbour in University of Arizona for providing PtOEP and Ir(ppy)<sub>3</sub> for my ELDMR study of phosphorescent OLED, and Prof. Yasuhiko Shirota in Osaka University in Japan for providing 2-TNATA for my study on exciplex system. I also would like to thank Dr. Paul Lane for his work on the ODMR study of Alq<sub>3</sub> OLED.

This work was performed at Ames Laboratory under Contract No. W-7405-Eng-82 with the U.S. Department of Energy. The United States government has assigned the DOE Report number IS-T 2100 to this dissertation.